4,5-Diazafluorene co-oligomers as electrondeficientlight-emitting materials and selectivefluorescence sensors for mercury(II) cations

Ghosh, Sanjay; Alghunaim, Abulaziz S.; AL-Mashhadani, Mohammed; Krompiec, Michal Piotr; Hallett, Megan; Perepichka, Igor

Journal of Materials Chemistry C

DOI:
10.1039/C7TC05051H

Published: 14/04/2018

Peer reviewed version

Journal of Materials Chemistry C

4,5-Diazafluorene co-oligomers as electron-deficient light-emitting materials and selective fluorescence sensors for mercury(II) cations

Journal:	*Journal of Materials Chemistry C*
Manuscript ID	TC-ART-11-2017-005051.R1
Article Type:	Paper
Date Submitted by the Author:	n/a

Complete List of Authors:	Ghosh, Sanjay; Bangor University, School of Chemistry Alghunaim, Abdulaziz; Bangor University, School of Chemistry Al-mashhadani, Mohammed; Bangor University, School of Chemistry Krompiec, Michal; Bangor University, School of Chemistry Hallett, Megan; Bangor University, School of Chemistry Perepichka, Igor; Bangor University, School of Chemistry

Note: The following files were submitted by the author for peer review, but cannot be converted to PDF. You must view these files (e.g. movies) online.

ESI-2_FNF sensor.MOV
ESI-3_FFNFF sensor.MOV
ESI-4_FNoF sensor.MOV

4,5-Diazafluorene co-oligomers as electron-deficient light-emitting materials and selective fluorescence sensors for mercury(II) cations[†,‡]

Sanjay Ghosh, Abdulaziz S. Alghunaim, Mohammed H. Al-mashhadani, Michal P. Krompiec,[§] Megan Hallett, and Igor F. Perepichka*

School of Chemistry, Bangor University, Bangor, LL57 2UW, UK

**E-mail: i.perepichka@bangor.ac.uk; i_perepichka@yahoo.com; Tel: +44–(0)1248–382386*

Abstract. A series of 4,5-diazafluorene-based (**N**) conjugated co-oligomers with 9,9-dialkylfluorene (**F**) or electron-deficient dibenzothiophene-*S,S*-dioxide (**S**) have been synthesized by Pd-catalyzed coupling reaction (**FNF**, **FFNFF**, **FNoF**, **SNS, NSN**). Cyclic voltammetry studies reveal their improved electron affinity compared to oligofluorene. **SNS** and **NSN** co-oligomers showed a decrease of their LUMO energies by 0.37 – 0.38 eV compared to **FNF** cooligomer. Absorption/emission studies showed that all oligomers, except **FNoF**, are blue-emitting materials (λ_{PL} ~ 400 – 450 nm) with high quantum yields of their photoluminescence (Φ_{PL} = 84 – 100% in solution and 24 – 42% in the solid state). **FNoF** trimer emits in yellow region with very low Φ_{PL} ~ 1%, but the emission efficiency is substantially increased to Φ_{PL} = 10–17% in the solid state. **FNF** co-oligomer was studied as metal cation responsive colorimetric and fluorescent sensor using a series of mono- and divalent cations and showed high sensitivity and selectivity toward mercury cations. On addition of Hg^{2+}, the blue emission of **FNF** (λ_{PL} = 404 nm) was quenched and a new, bathochromically shifted (to the green region, λ_{PL} = 507 nm) emission band appears, which allows to use this compound as both "ON → OFF" and "OFF → ON" fluorescent sensor.

1 Introduction

During the past two decades, fluorene-based oligomers and polymers have extensively been studied as efficient blue light-emitting materials with good thermal and electrochemical stability, high charge mobility, and easily tunable properties through chemical modifications and co-polymerization for organic light-emitting devices (OLEDs) and other optoelectronic applications.[1,2,3,4,5]

[†] We dedicate this paper to Prof. Fred Wudl in celebration of 50 years of his contributions to the field of π-conjugated organic materials.

[‡] Electronic supplementary information (ESI) available: procedures for synthesis of the oligomers and intermediates. ^{1}H and ^{13}C NMR spectra and MS for characterized compounds; ^{13}C DEPT and COSY NMR spectra for selected compounds; additional data on UV-Vis and PL experiments (including metal cation effects) and DFT calculations. See DOI #######

[§] Present address: Merck Chemicals Ltd, Southampton, UK.

More recently, the topologically similar structure of dibenzothiophene-*S,S*-dioxide (Figure 1), which consist of an electron deficient sulfonyl (–SO_2–) group as a bridge between the benzene rings (instead of –CR_2– bridge in the fluorene) has attracted much attention for the construction of conjugated light-emitting oligomers[6,7,8] and polymers,[9,10,11,12,13,14,15,16] as well as molecular OLED materials with thermally activated delayed fluorescence (TADF).[17,18,19,20] An incorporation of dibenzothiophene-*S,S*-dioxide units into polymeric or molecular systems improved their electron affinity and electron transporting in the materials, and facilitated intramolecular charge-transfer in some specific structures.

Another electron-deficient conjugated moiety of a similar topology is 4,5-diazafluorene,[21] in which case two carbons (CH groups) in the benzene rings are substituted by more electronegative nitrogen atoms. According to DFT calculations, the LUMO (lowest unoccupied molecular orbital) energy levels of dibenzothiophene-*S,S*-dioxide (**S**) and 4,5-diazafluorene (**N**) are lower than that in fluorene (**F**) by 1.04 eV and 0.58 eV, respectively, while the HOMO–LUMO energy gaps (HOMO is highest occupied molecular orbital) are very close for all three units (Figure 1). As such, an incorporation of **N** moieties into the conjugated oligomers and polymers should substantially decrease their LUMO energy levels to afford materials with high electron affinity for using as electron transporting materials or n-type semiconductors. Some 4,5-diazafluorene derivatives are fluorescent and they have already been exploited in a few studies for design of semiconductive light-emitting materials with improved electron injection/transporting properties,[22,23,24] donor-acceptor conjugates[25,26,27,28] and conjugated co-polymers.[29]

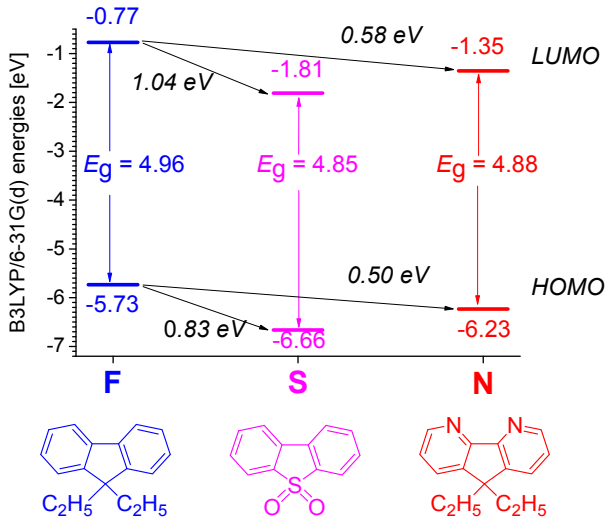

Figure 1 Frontier orbital energy levels of 9,9-diethylfluorene, dibenzothiophene-*S,S*-dioxide and 9,9-diethyl-4,5-diazafluorene, calculated by DFT/B3LYP/6-31G(d).

Apart from the improved electron deficiency (compared to fluorene), 4,5-diazafluorene can act as N^N ligand to form complexes with metal cations. Many 4,5-diazafluorene derivatives have

been studied in the past as chelating agents for transition (and some main group elements) metals.[30,31,32,33,34,35] More recently, 4,5-diazafluorene has also attracted attention for design of cationic iridium (III) complexes for light-emitting electrochemical cells (LEECs).[36,37,38,39,40]

For fluorescent ligands, coordination with metal cations can lead to a change of their fluorescence properties through different mechanisms, e.g. fluorescence resonance energy transfer (FRET), photo-induced energy transfer (PCT) or photoinduced electron transfer (PET).[41] This strategy had been used by Wong's group to demonstrate fluorescence sensing of bipolar donor-acceptor (D–A) spiro-bridged bis(diphenylamino)fluorene/4,5-diazafluorene molecules in complexation with metal cations.[25] Modulation of the emission color on protonation or on complexation with metal cations was also recently shown for 4,-5-diazafluorene copolymers by Huang's group.[29]

In this work we report a series of novel co-oligomers with an improved electron affinity based on electron-deficient **N** and **S** moieties and electron-rich **F** moiety. We demonstrate how the combination of these building blocks tune the LUMO energy levels of the co-oligomers and their ability toward n-doping, as well as how these structural variations effect on the emission characteristics of the materials. We also present the results on complexation of the trimer **FNF** with a series of metal cations (M^+ and M^{2+}), which shows remarkable sensitivity and selectivity of its fluorescence to the toxic mercury cation, Hg^{2+}, and thus can be used as selective fluorescent sensors for mercury salts in the presence of other cations.

2 Results and discussion

2.1 Synthesis

Synthesis of co-oligomers **FNF**, **FFNFF**, **FNoF**, **NSN**, and **SNS** is depicted in Scheme 1 (see ESI for details). 4,5-Diazafluorenone (**3**) was reduced into 4,5-diazafluorene by Wolf-Kizhner reaction. Its alkylation by *n*-hexyliodide and *t*-BuOK, as a base, in tetrahydrofuran (THF) or by n-octyliodide and NaOH, as a base, in dimethylsulfoxide (in the presence of tertiary ammonium salt as catalyst), gave the monomers **1** and **5** with the yields of 49% and 53% (in two steps), respectively. Palladium-catalyzed Suzuki coupling of the monomers **1** and **3** with fluorene- or bifluorene-boronic acids (**2** or **4**) gave the trimers **FNF** and **FNoF**, and the pentamer **FFNFF**. While **FNF** and **FNoF** were obtained with conventional heating, the pentamer in these conditions gave very low yield due to substantial mono-coupling of bifluorene **4** on prolonged heating and formation of mono-substituted by-product. Therefore, the reaction was performed in a microwave-assisted conditions at 150 °C affording **FFNFF** with 61% yield after column purification. Borolane derivatives of dibenzothiophene-*S,S*-dioxide **6** and **8** were synthesized from corresponding mono-/dibromo-

dibenzothiophene-*S,S*-dioxides in excellent yields (~75–85%) using Miyaura coupling with bis(pinacolato)diboron, catalyzed by $PdCl_2$(dppf) (see ESI). This procedure was found to be a much better method compared to the previously reported procedure, which gave only 26% yield of **8**.[42] Reactions of dibromo- and monobromo-diazafluorenes **5** and **7** with monoborolane **6** and diborolane **8**, respectively, gave corresponding 4,5-diazafluorene/dibenzothiophene-*S,S*-dioxide trimers **SNS** and **NSN**. Generally, Pd-catalyzed couplings worked well to give the co-oligomers with good yields of 49–71% (except **NSN**, in which case the yield was lower, 26%). All synthesized oligomers are stable light-yellow compounds, with good solubility in common organic solvents.

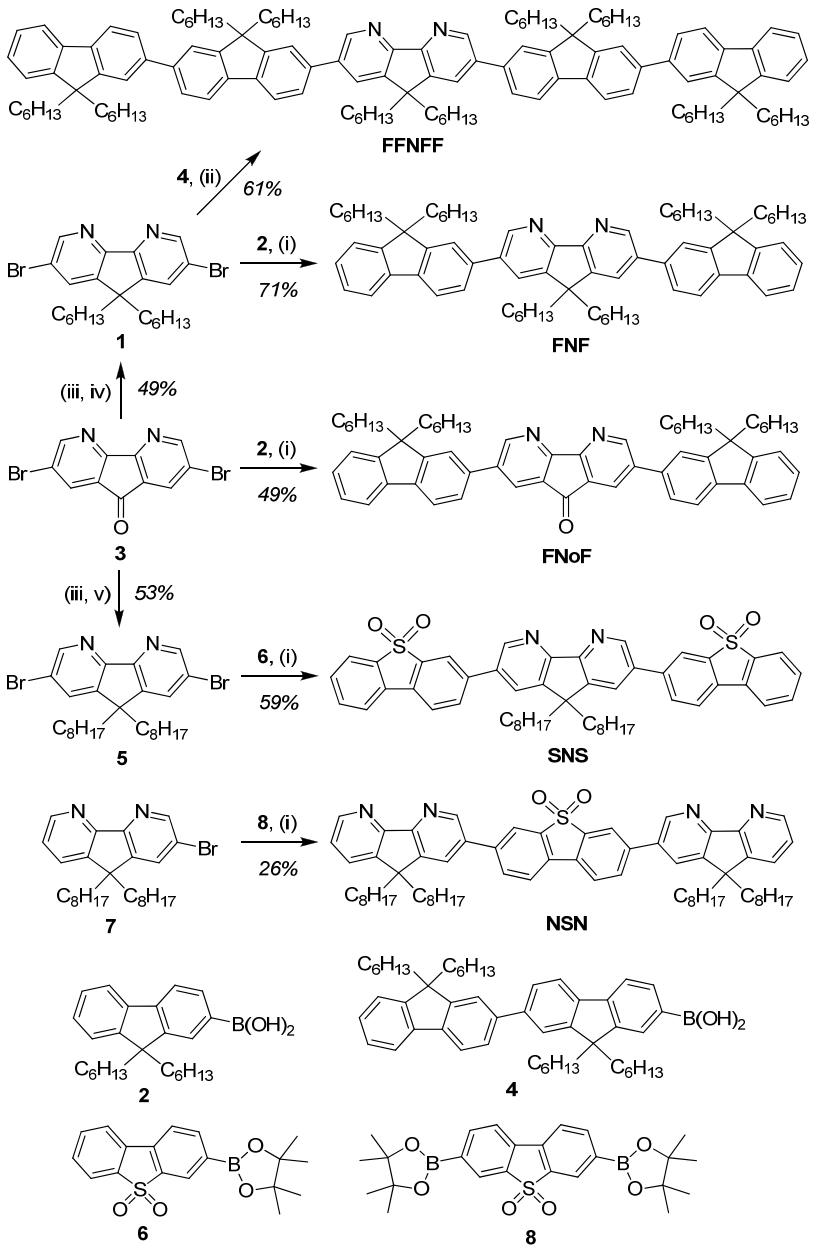

Scheme 1 Synthesis of 4,5-diazafluorene-based co-oligomers: (i) $Pd(PPh_3)_2Cl_2$, 2M K_2CO_3, dioxane or dioxane–EtOH, reflux, 24–32 h; (ii) $Pd(PPh_3)_4$, 2M K_2CO_3, toluene–EtOH, MW = 150 W, 150 ºC, 4 h; (iii) $N_2H_4{\times}H_2O$, AcOH (cat.), ethylene glycol, 135–140 ºC, 20 h (71%); (iv) $C_6H_{13}I$, *t*-BuOK, THF, –5…+25 ºC, 32 h (69%); (v) $C_8H_{17}I$, 50% NaOH, $[BzNEt_3]^+Cl^-$ (cat.), DMSO, r.t., 23 h (75%).

2.2 Absorption and emission spectra

The absorption and emission spectra of all the co-oligomers have been studied both in solution (degassed dichloromethane, DCM) and in the solid state (spin-coated films on quartz windows) at room temperature (Figure 2 and Table 1). UV-Vis spectra of all oligomers, both in solution and in films (Figures 2a,c) showed characteristic absorption bands between 300 nm to 400 nm attributed to the spin allowed π–π^* transition. **FNoF**, apart of an absorption in the UV region, also showed additional broad low intense band in the visible region (400–500 nm, peaked at ~450 nm) attributed to spin forbidden n–π^* transition on the carbonyl group of 4,5-diazafluorenone. All the trimers showed only minor changes in their absorption maxima (in the range of 7.5 nm and 13 nm, in DCM and in films, respectively). Compared to **FNF**, more electron deficient **SNS** and **NSN** demonstrated some hypsochromic shifts of their absorption spectra (by ~4–5.5 nm in DCM and ~9.5–15 nm in films), and an elongation of the conjugation in **FFNFF** pentamers resulted in bathochromic shifts by 7–11.5 nm. The optical energy gaps of the oligomers determined from the red absorption edge of the spin-coated films were in the range of E_g^{opt} ~ 2.92–3.09 eV, except of **FNoF** whose E_g^{opt} = 2.44 eV.

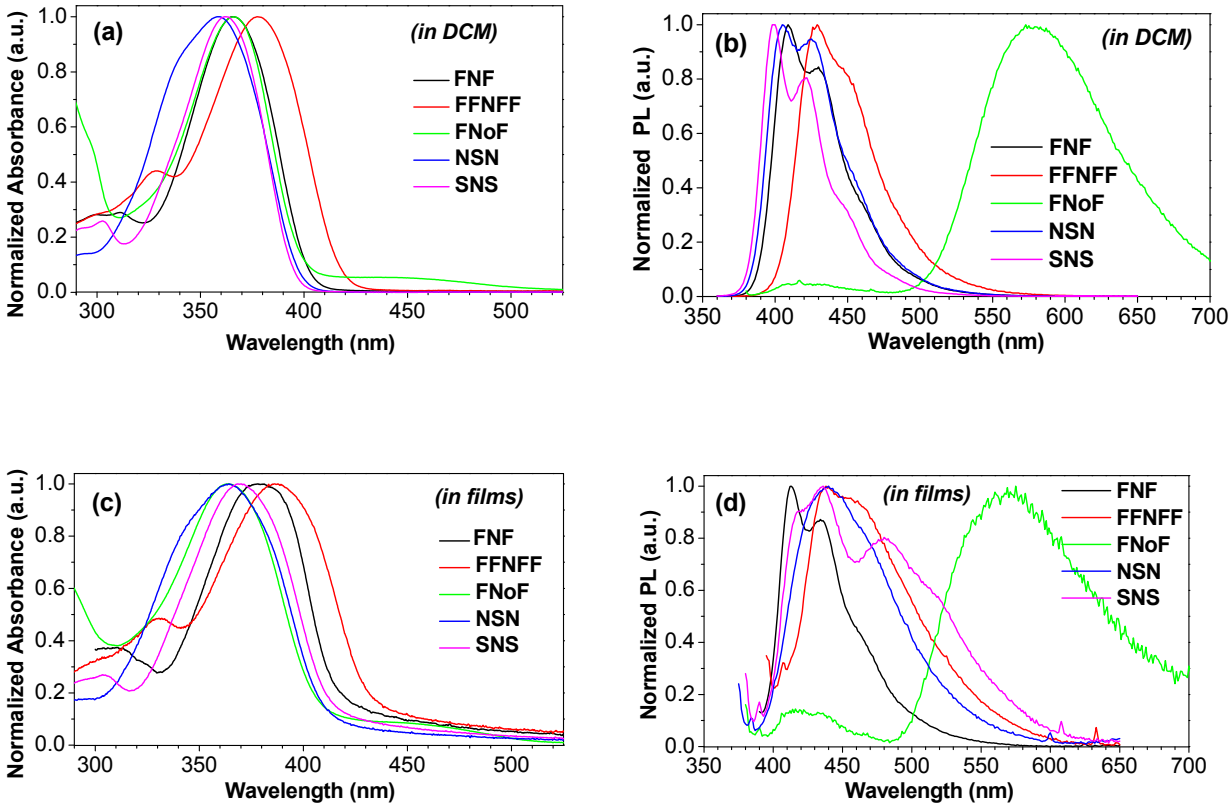

Figure 2 Normalized UV-Vis absorption (a,c) and photoluminescence (b,d) spectra of 4,5-diazafluorene co-oligomers in DCM solution (a,b) and in films (c,d). For PL spectra, λ_{ex} are shown in the Table 1.

Table 1 Absorption and photoluminescence maxima of 4,5-diazafluorene-based co-oligomers in solution and in the solid-state, their photoluminescence quantum yields and optical energy gaps.

Comp.	λ_{abs} (nm)[a] DCM	λ_{abs} (nm)[a] Film	λ_{PL} (nm)[a] DCM	λ_{PL} (nm)[a] Film	Φ_{PL} (%), [λ_{ex} (nm)],[b] DCM	Φ_{PL} (%), [λ_{ex} (nm)],[c] Film	E_g^{opt} (eV)[d]
FNF	**366**	310, **379**	**409**, 430sh	**413**, 434	93 [350]	35 [370]	3.09
FFNFF	328, **378**	330, **386**	**429**, 447sh	**438**, 460sh	84 [350]	42 [385]	2.92
FNoF	**366**, 440sh	**364**, 440sh	416, **575**	416, **570**	1 [370] 1 [370][e]	10.5 [370][e,f] 14.4–17.3 [370][e,g]	2.44
NSN	340sh,[h] **358.5**	345sh, **364**	**405**, 425	**440**	89 [350]	24 [365]	3.02
SNS	303, **362**	305, **369.5**	**399**, 421	418sh, **435**, 480	101 [350]	30 [370]	2.99

[a] The strongest peaks are shown in bold. [b]Photoluminescence quantum yields (PLQYs) in solution estimated using 9,10-diphenylanthracene as a reference (Φ_{PL} = 0.90 in degassed cyclohexane);[43] (excitation wavelengths in nm are shown in brackets). [c]Absolute PLQYs in the solid state determined using an integrating sphere for spin coated films on quartz substrates. [d]Optical energy gaps determined by the red edge of absorption spectra for spin coated films on quartz substrates. [e]Absolute PLQY, measured on an integrating sphere. [f]For powder sample. [g]For films (slight increase of PLQY was observed on thermal annealing the films at 80 – 130 °C, see Figure S5 in the ESI). [h]sh – shoulder.

Oligomers **FNF**, **FFNFF**, **NSN** and **SNS** are highly emissive materials which fluoresce in the blue region with a typical vibronic structure of their emission spectra, characteristic for rigid-rod conjugated systems (Figures 2b,d). They showed high photoluminescence quantum yields (PLQY, Φ_{PL}) of their emission of 84–100% in solution (vs 9,10-diphenylanthracene standard) and 24–42% in the solid state (absolute PLQY), the values which are similar to that commonly observed in oligofluorenes.[6,44,45,46,47,48,49] Due to intramolecular donor-acceptor interaction, the local excited state (LE) emission in **FNoF** in the blue region was almost completely quenched and a new broad intramolecular charge transfer (ICT) emission band in the yellow region at 570 – 575 nm appeared. while the PLQY of this emission in solution is rather low (Φ_{PL} ~ 1% (DCM), Figures 2b, Table 1). Fluorene–fluorenone–fluorene trimer, **FFoF**, as an analog of **FNoF** showed similar spectral changes and substantial quenching the emission (in DCM: λ_{PL} = 584 nm, Φ_{PL} = 4%).[50] Also, quenching the oligo/polyfluorene emission by "fluorenone defects" in the main chain[51] with an appearance new band in the green region was subject of numerous studies.[52,53,54,55,56]

Often, the emission of luminescent materials in the solid state is decreased compared to the solution because the excited states of the aggregates decay *via* non-radiative pathways. Surprisingly, the PLQY of **FNoF** was drastically increased in the solid state (as powder or spin-coated films) to ca. 10 – 17% (Table 1). Thermal annealing of the films at 80 – 100 °C does not change the shape of the emission, but leads to some increase of PLQY (from 14.4 to 17.3%; Figure S5 in the ESI). This

indicates that intramolecular interactions inhibit non-radiative pathways of the excited state decay. We did not studied the details of the photophysical processes responsive for stronger quenching the emission in solution compared to the solid state, but there are several examples in the literature on an improved solid-state emission. One widely studied phenomenon is an aggregation-induced emission (AIE) due to restriction of intramolecular rotations in a condensed phase.[57] Other possibilities include e.g. conformation planarization and twisted/planarized intramolecular charge transfer (TICT/PICT). Also, tuning the triplet energy levels by solid state effect might be responsible for the difference between the solution and solid-state PLQY. Thus, rigid molecules of anthracene and perylene showed substantially higher PLQY in a single crystal state (Φ_{PL} = 64% and 31%, respectively) compared to their solutions (Φ_{PL} = 0.28 % and 0.02%, respectively).[58] This was explained by low-lying second triplet energy level in solutions (E_{T2} = 3.24 eV), which is lower than the energy level of the singlet excited state (E_{S1} = 3.29 eV), thus facilitating the singlet-triplet inter-system crossing and quenching the emission (in the solid state, the second triplet state energy, E_{T2} = 3.51 eV, is higher than the energy level of the singlet excited state E_{S1} = 3.11 eV).

Solvent effect. Solvent polarity effect on the absorption and emission spectra was carried out for the oligomer **FNF** (Figure 3a). In our previous studies on fluorene/dibenzothiophene-*S,S*-dioxide co-oligomer (**FSF**), we observed very little effect of the solvent polarity on the absorption spectra [$\Delta\lambda_{abs}$(EtOH–hexane) = 5 nm] but more pronounced effect on the PL spectra [$\Delta\lambda_{PL}$(EtOH–hexane) = 41 nm].[7] Detailed photophysical studies of **FSF** have shown that only weak D–A interaction occurs in **FSF** in its ground state, but the excited state of the molecule is highly polar, with twisted intramolecular charge transfer (TICT). Polar solvents stabilize the excited ICT state, so depending on the solvent polarity, the emission occurs from either LE (in non-polar solvents) or ICT state (in polar solvents), or from both (dual LE/ICT emission[9,10]). The **N** moiety is somewhat weaker as an acceptor compared to **S** (Figure 1). On the other hand, the nitrogen atoms in **N** are part of the π-cloud of the main oligomer chain. So, **FNF** showed positive solvatochromic effect in both absorption and emission spectra, while the shift in the emission is less pronounced compared to **FSF** [Figure 3a: $\Delta\lambda_{abs}$(EtOH–hexane) = 8.5 nm, $\Delta\lambda_{PL}$(EtOH–hexane) = 17 nm; see also Figure S6 in the ESI]. Similar positive solvatochromism was observed for **FFNFF** and **FNoF**, in which cases the influence of the solvent polarity on the emission wavelength are even more pronounced (**FFNFF**: $\Delta\lambda_{PL}$(EtOH–hexane) = 32.5 nm; **FNoF**: $\Delta\lambda_{PL}$(ACN–hexane) = 77 nm; Figures 3b,c and Table S3 in the ESI). These spectral changes of **FNoF** ressemble well the emission of its fluorene–fluorenone–fluorene analog (**FFoF**), which showed substantial solvatochromism of its emission (λ_{PL} = 507 nm (methylcyclohexane), 584 nm ($CHCl_3$), 543 nm (films)).[59]

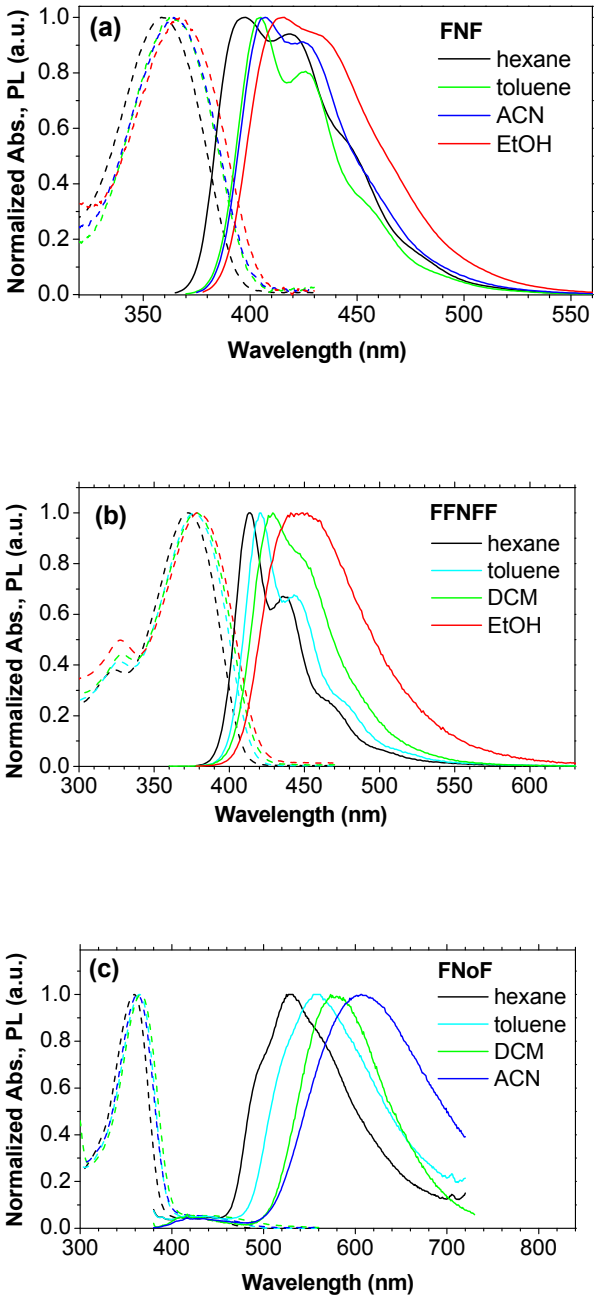

Figure 3 Effect of the solvent polarity on the absorption (solid lines) and emission spectra (dotted lines; excited at the absorption maxima) of (a) **FNF**, (b) **FFNFF** and (c) **FNoF** oligomers.

Response to protic acid. The pyridine nitrogen atom of azaaromatic compounds, including 4,5-diazafluorene can be protonated, which should cause changes of their absorption and emission spectra.29[60] Titration of **FNF** solution [~ 0.01 mM] in THF with methanesulfonic acid (0.05 – 0.5 mM; an excess 5 – 50 times) results in some decrease of the intensity of **FNF** absorption at 365 nm and an appearance of a shoulder absorption at the red edge of the spectrum, with an isobestic point at 386 nm (Figure 4a). At higher concentrations of the acid (1 – 40 mM), **FNF** absorption band vanished and new band corresponding to the protonated form(s) of the oligomer appears at ~ 410

nm (deviation from the isobestic point at higher concentration might be due to partial protonation of both pyridine rings). Similar changes are observed in photoluminescence spectra, i.e. disappearance of vibronic emission of **FNF** in the blue region and an appearance of green emission of the protonated **FNF** at 510 nm (Figure 4b and Figure S7c in the ESI). These changes in a emission color are obvious under illumination by UV lamp (365nm) and clear seen by naked eyes (an insert in Figures S7d,e in the ESI) illustrating promising light-emitting properties of the oligomer in its protonated form.

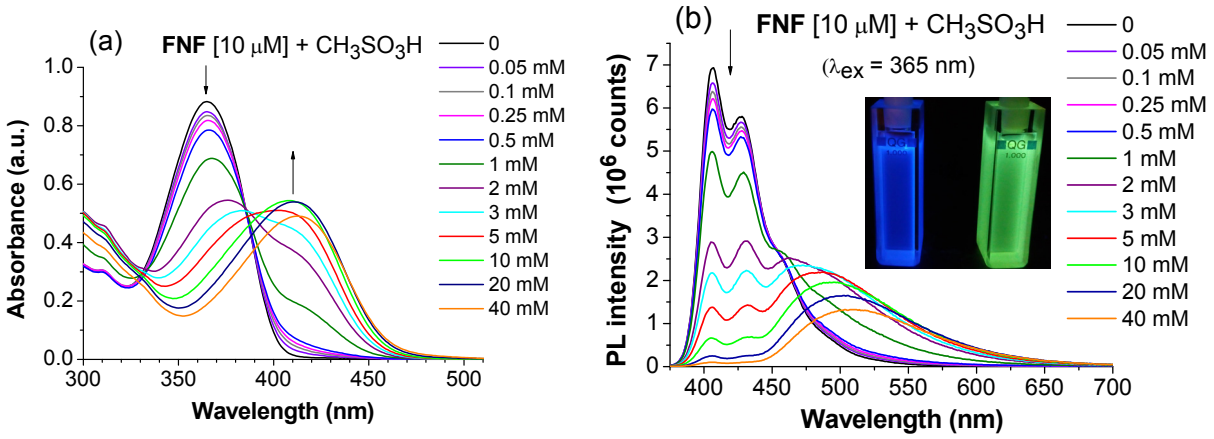

Figure 4 Changes in UV-Vis absorption (a) and photoluminescence (b) spectra of **FNF** [~10 μM] in THF at various concentrations of methanesulfonic acid (0.05 – 40 mM). For PL spectra corrected to the differences in the absorption at the excitation wavelength (λ_{ex} = 365 nm) see Figure S7c in the ESI. Inset photos show the colors of the emission under hand-held UV lamp (365 nm)

2.3 Cyclic voltammetry study

To evaluate the redox properties in n-doping and p-doping processes, synthesized co-oligomers were studied by cyclic voltammetry method (CV) (Figure 5). Due to the presence of electron-deficient **N** and **S** moieties, an oxidation of oligomers occurs at high potentials (onset oxidation potentials E_{onset}^{ox} = 0.64–0.98 V vs Fc/Fc^+ couple; Table 2) and is electrochemically irreversible (quasi-reversible for **FNF**). The reversibility of the reduction process is better (quasi-reversible or reversible for all trimers), allowing to estimate their half-wave potential $E_{1/2}^{red}$. Thus, replacement of fluorene moiety in **FNF** ($E_{1/2}^{red}$ = –2.35 V) by more electron deficient **S** moiety (**SNS**) results in pronounced positive shift of the reduction wave by 0.38 V to $E_{1/2}^{red}$ = –1.96 V (similar potential of –1.97 V was observed for **NSN** oligomer). These results are in line with the computed LUMO energy levels for **F**, **N** and **S** (Figure 1).

Cyclic voltammetry data have been used to estimate the HOMO and LUMO energies of the oligomers and their HOMO–LUMO gaps (E_g^{CV}, Table 2). Qualitatively the results on the HOMO–LUMO gaps from CV experiments are in agreement with that obtained from electron absorption spectroscopy data. When considering their numerical differences, it should be taken into account

that optical and electrochemical measurements have deal with different physical processes. The use of different solvents can also contribute to the not ideal coincidence of the estimations of the energy levels by these methods.

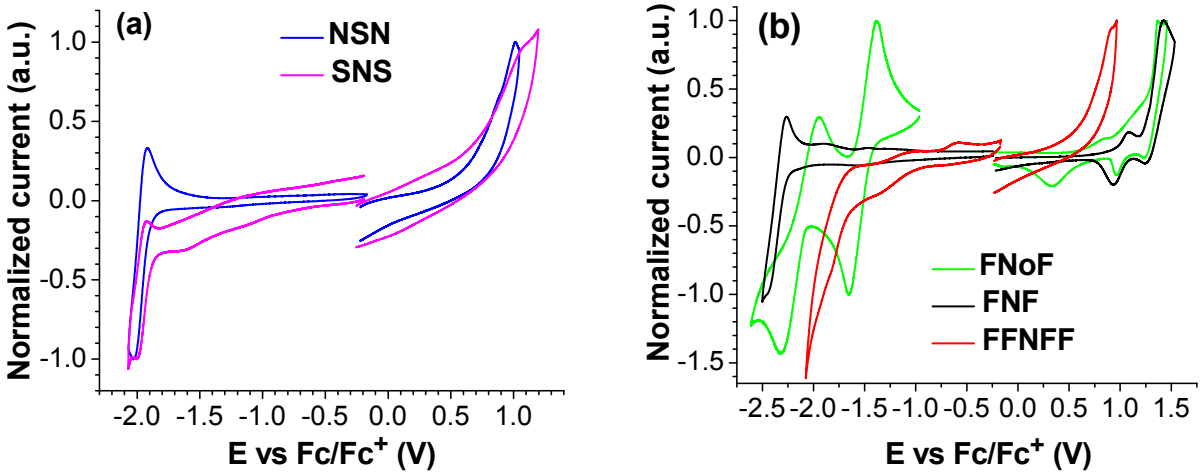

Figure 5 Cyclic voltammograms of (a) **N/S** co-oligomers (b) **F/N** co-oligomers. Reduction and oxidation scans were performed in THF and in DCM, respectively, with 0.2 M Bu_4NPF_6 as supporting electrolyte at room temperature. Scan rate is 100 mV/s. Ag/Ag^+ was used as the reference electrode and the CV were calibrated with Fc/Fc^+ as an internal reference.

Table 2 Redox potentials of oligomers determined by cyclic voltammetry, HOMO and LUMO energy levels and the HOMO–LUMO gaps from CV data and from DFT/B3LYP/6-31G(d) calculations.[a]

Samples	E_{onset}^{ox} (V)[a]	$E_{1/2}^{red}$ (V)[a]	E_{HOMO}^{CV} (eV)[b]	E_{LUMO}^{CV} (eV)[b]	E_g^{CV} (eV)[b]	E_{HOMO}^{DFT} (eV)	E_{LUMO}^{DFT} (eV)	E_g^{DFT} (eV)
FNF	0.98[c]	–2.35	–5.78	–2.45	3.33	–5.45	–1.69	3.76
FFNFF	0.64	–1.72	–5.44	–3.08	2.36	–5.25	–1.77	3.48
FNoF	0.81	–1.51, –2.14[d]	–5.61	–3.29	2.32	–5.65	–2.56	3.09
NSN	0.66	–1.97	–5.46	–2.83	2.63	–6.02	–2.26	3.76
SNS	0.70	–1.96	–5.50	–2.84	2.66	–6.10	–2.34	3.76

[a]CV potentials are given vs Fc/Fc^+ couple as an internal reference (the average $E_{1/2}$ potentials for Fc/Fc^+ vs used Ag/Ag^+ reference electrode were 0.20–0.22 V in DCM and 0.19 – 0.21 V in THF). Oxidation and reduction potentials were measured in DCM and THF, respectively, with 0.2 M Bu_4NPF_6 as supporting electrolyte at scan rate of 100 mV/s. E_{onset}^{ox} and $E_{1/2}^{red}$ are onset oxidation and half-wave reduction potentials, respectively (oxidation processes are irreversible, so the onset potentials have been estimated from the CV traces). [b]$E_{HOMO}^{CV} = -(E_{onset}^{ox} + 4.8)$, $E_{LUMO}^{CV} = -(E_{1/2}^{red} + 4.8)$. [c]Half-wave oxidation, $E_{1/2}^{ox}$ (this value was used for estimation of HOMO of **FNF**). [d]Second reduction potential, $E_{1/2}^{red2}$.

2.4 Computational study

To estimate the frontier energy levels and distribution of the HOMO/LUMO orbitals in the synthesized co-oligomers, we performed DFT calculations at the B3LYP/6-31G(d) level of theory

using Gaussian09 package of programs (Figure 6 and Figures S1 – S4 in the ESI).[61] Compared to **FNF** oligomer, oligomers **SNS** and **NSN** consisting electron-deficient **S** moiety, showed substantial stabilization of their LUMO orbital (by 0.65 eV and 0.57 eV, respectively), which is in good agreement with CV data (E_{LUMO}^{CV} are decreased by 0.38 and 0.39 eV, respectively; Table 2). Yet, the HOMO–LUMO gaps for all three co-oligomers remain almost unchanged.

For all three c both HOMO and LUMO are delocalized along the whole molecules. Even for **FNF**, no substantially increased localization of LUMO on electron-deficient central **N** moiety (or HOMO on the end fluorene moieties) were observed, indicating on the very weak charge transfer character in the molecule. This is in good agreement with absorption/emission measurements, which showed only weak solvatochromic effect. In contrast to that, the HOMO in **FNoF** is delocalized over the whole π-system of the trimer, whereas the LUMO is fully localized on the central 4,5-diazafluorenone moiety assuming the strong intramolecular charge transfer in this molecule. Indeed, its HOMO–LUMO gap is much lower than that for other oligomers and spectroscopic studies of **FNoF** showed substantially distinctive absorption and especially emission spectra for this trimer (Figures 2, 3 and Table S3 in the ESI). As expected, an elongated conjugation in **FFNFF** pentamer compared to trimer **FNF** led to a decrease of its LUMO and an increase of its HOMO energy levels (and as such HOMO–LUMO gap contraction), and somewhat more pronounced localization of its LUMO on the central part of the molecule.

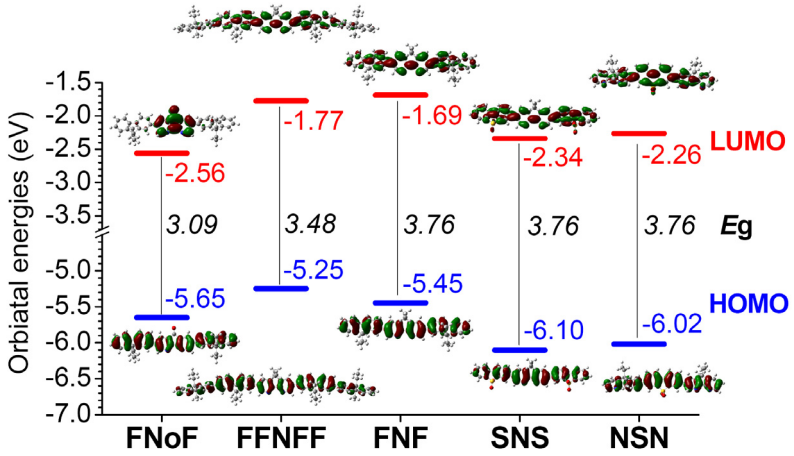

Figure 6 HOMO/LUMO energy levels, HOMO–LUMO gaps and localization of the frontier orbital coefficients for co-oligomers **FNoF**, **FFNFF**, **FNF, SNS**, and **SNS** by DFT B3LYP/6-31G(d) calculations in a gas phase.

Modelling the solvent effect (acetonitrile) by PCM method (polarizable continuum model) using 6-31G or 6-311G basis sets shows that the solvent polarity mainly effect on the LUMO energy levels of the co-oligomers whereas the effect on the HOMO is less pronounced (Figure S4 in the ESI). For 4,5-diazafluorene co-oligomers with electron-donating fluorene (**FNF**, **FFNFF** and

FNoF), the solvation by a polar acetonitrile leads to some contraction of the HOMO–LUMO energy gaps, E_g^{DFT}. These results are in line with a positive solvatochromism for these co-oligomers as demonstrated by spectroscopic studies (Figure 3). In the case of **SNS**, and **SNS**, however, polar acetinitrile has negligible effect on HOMO, LUMO and E_g^{DFT} (Figure S4 in the ESI).

2.5 FNF co-oligomer as selective fluorescent sensor for mercury cations

The co-oligomer **FNF** has been used to study the ability of the 4,5-diazafluorene moiety to act as chelating N^N ligand to form complexes with metal cations. **FNF** itself showed only weak charge-transfer character (according to DFT calculations and its very weak solvatochromism). The complexation of the central **N** moiety with positively charged cations should increase the intramolecular charge transfer from the end fluorene group onto the central 4,5-diazafluorene moiety.[62] This is what was actually observed in the case of **FNoF** with the central electron-deficient 4,5-diazafluorenone moiety, in which case pronounced ICT, accompanied by drastic changes in the emission characteristics were observed (Figures 2b,d and 3c).

For these studies we used a series of monovalent and divalent metal salts ($LiClO_4$, $NaClO_4$, $AgClO_4$, $Mg(ClO_4)_2$, $Ba(ClO_4)_2$, $Cu(BF_4)_2$, $Ni(NO_3)_2$, $Pb(ClO_4)_2$ and $Hg(ClO_4)_2$) to look at the metal ion sensing properties of **FNF** by electron absorption and fluorescence spectroscopies. In THF solution, **FNF** absorbs at λ_{abs} = 365 nm and emits at λ_{PL} = 404 nm (Figures 7a,b). Initial experiments with ~1.4 μM **FNF** and 10-fold concentrations of metal salts (~14 μM) in THF solution showed no or only weak effect of Li^+, Na^+, Ag^+, Cu^{2+}, Mg^{2+} and Ba^{2+} cations on both absorption and emission spectra compared to the cation-free solution of **FNF** (Figure 7). Indeed, only small decrease in the intensities of absorption and emission bands was observed in these cases, with no spectral shifts or changes in the width of the spectra. In the case of Ni^{2+} and Pb^{2+}, the decrease of absorption intensity was larger, with some bathochromic shifts of the bands (to 371 and 378 nm, respectively) and an appearance of shoulders on the red edges of their absorption spectra (Figure 7c). However, the emission spectra did not shift or change their shape, but only a decrease of the fluorescence intensity was observed (Figure 7d). In contrast to that, in the presence of Hg^{2+}, the absorption spectrum was drastically changed, showing more pronounced bathochromic shift, with two new bands at 387 and 405 nm. The blue emission of **FNF** was almost completely quenched and a new greenish emission band appeared at 507 nm (Figure 7d; see also Figures S8 and S12 in the ESI for changes in the color space and the absorption/emission colors). The process of complexation of **FNF** with Hg^{2+} cations is reversible as has been proven by dilution of {**FNF** + $Hg(ClO_4)_2$} with cation-free **FNF** solutions of the same concentration (Figure S9 in the ESI).

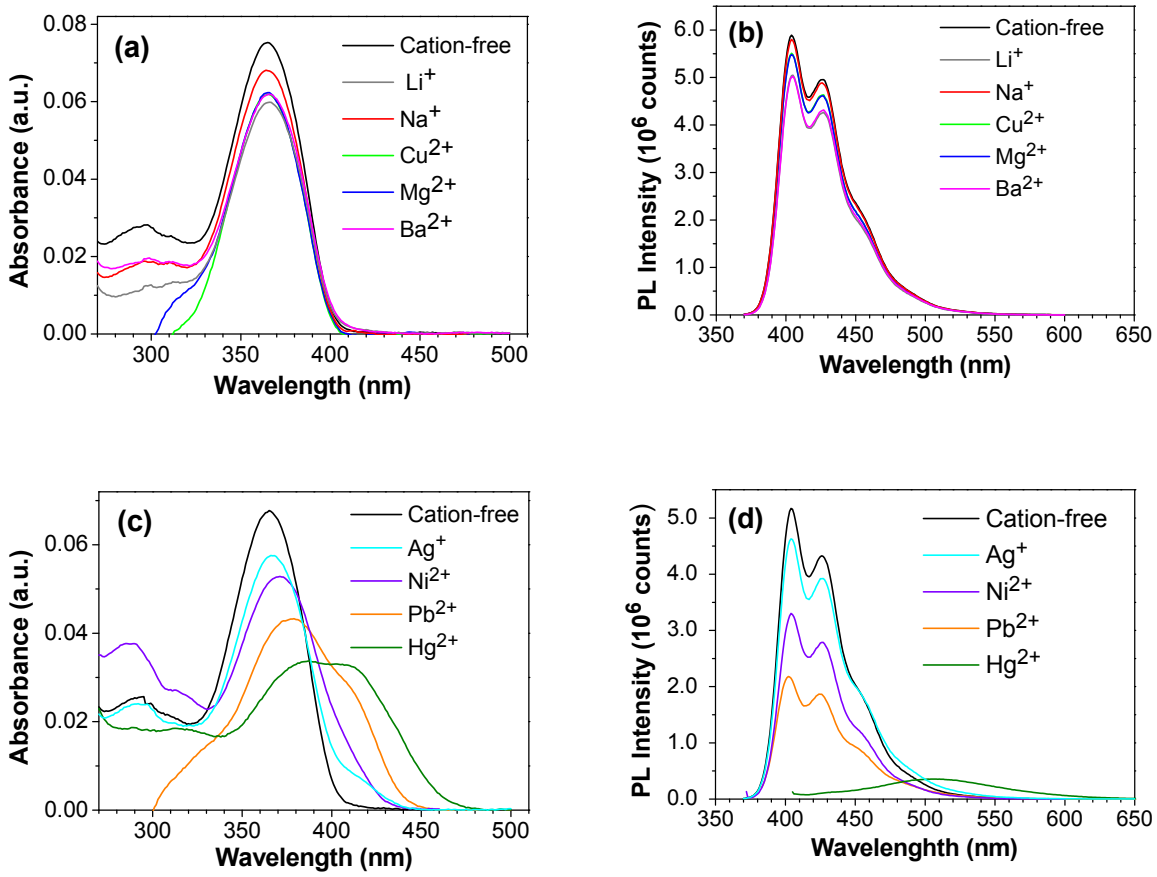

Figure 7 The effect of metal cations on the absorption (a,c) and emission (b,d) spectra of co-oligomer **FNF** in THF solutions. Concentration of **FNF** is ~1.4 μM, concentration of metal salts is ~14 μM. For PL spectra, excitations are at the wavelengths close to the absorption maxima: λ_{ex} = 365 nm (cation-free, Li^+, Na^+, Cu^{2+}, Mg^{2+}, Ba^{2+}), 367 nm (Ag^+), 371 nm (Ni^{2+}), 379 nm (Pb^{2+}), 395 nm (Hg^{2+}).

Thus, the **FNF** oligomer showed good metal ion responsive properties towards Hg^{2+} compared to other cations. Mercury is a highly toxic metal and the development of sensitive and selective sensors for Hg^{2+}, which causes environment, water pollution and living organisms intoxication is a very challenging task.[63] A large number of different classes of materials (organic, inorganic/hybrids, nanoparticles, biomolecules) and methods (colorimetric, fluorescent, electrochemical, field-effect transistors etc) have been developed for Hg^{2+} detection. Among them, the detection based on changes of the fluorescence is one of the promising and widely used method due to its high sensitivity, good selectivity (in some cases) and simplicity of the method. Both "ON → OFF" (quenching the fluorescence)[64,65,66,67,68,69,70,71,72,73,74,75] and "OFF → ON" (growing the fluorescence)[76,77,78] modes of the detection have been exploited. In more rare cases, the detection based on the changes of PL spectra, potentially allowing dual-mode detection, was used.[79,80] While visually spectral changes of the emission are obvious in this case, the problem of full separation of

the emissions of free fluorescent ligands and their complexes with Hg^{2+} might be an issue for quantitative monitoring at two different wavelengths. Different approaches have been used to decrease the detection limit of Hg^{2+}, e.g. sensors based on Hg^{2+} mediated folding of fluorophore labelled DNA (detection limit 3.2 nM),[81] signal amplification by oligonucleotide–conjugated polymer intercalates (detection limit 0.27 nM),[82] polymerase assisted fluorescence amplification (detection limit 40 pM),[83] fluorescence polarization enhancement of DNA-fluorophore by gold nanoparticles (detection limit 0.2 ppb).[84] The detection limits for simple organic molecules as chromophores/fluorophores is higher (~0.1 – 10 μM), but they have an advantage of relatively easy and cheap synthesis of materials, and simple method of analysis/detection.

As complexation of **FNF** with Hg^{2+} leads to disappearance of the oligomer emission in blue reagion and an appearance of green emission of the complex (Figure 7d), we estimated the relative intensities of the emissions of **FNF** in the presence of different cations (versus cation-free **FNF** solution) by monitoring at two wavelengths, 416 and 507 nm. Figure 8a clearly demonstrates high selectivity of **FNF** toward Hg^{2+} compared to other studied cations in both "ON → OFF" (quenching the fluorescence at 416 nm) and "OFF → ON" (growing the fluorescence at 507 nm) modes of sensing. Absorption spectra of **FNF** also showed some changes on addition of metal cations. For Li^{+}, Na^{+}, Mg^{2+}, Ca^{2+} and Ba^{2+}, only decreasing the absorption intensities are observed, whereas Ag^{+}, Ni^{2+} and Pb^{2+} show some bathochromic shifts of **FNF** absorption and an appearance of new long wavelength band (Figures 7a,c). This shift and an intensity of a new long-wavelength band is much more pronounced in the case of Hg^{2+}. Comparison of the absorption intensities of **FNF** in the presence of various metal cations, monitored at two wavelengths, i.e. at 366 nm (**FNF** absorption) and at 440 nm, demonstrates that Hg^{2+} can be selectively detected by a colorimetric method as well (Figure 8b).

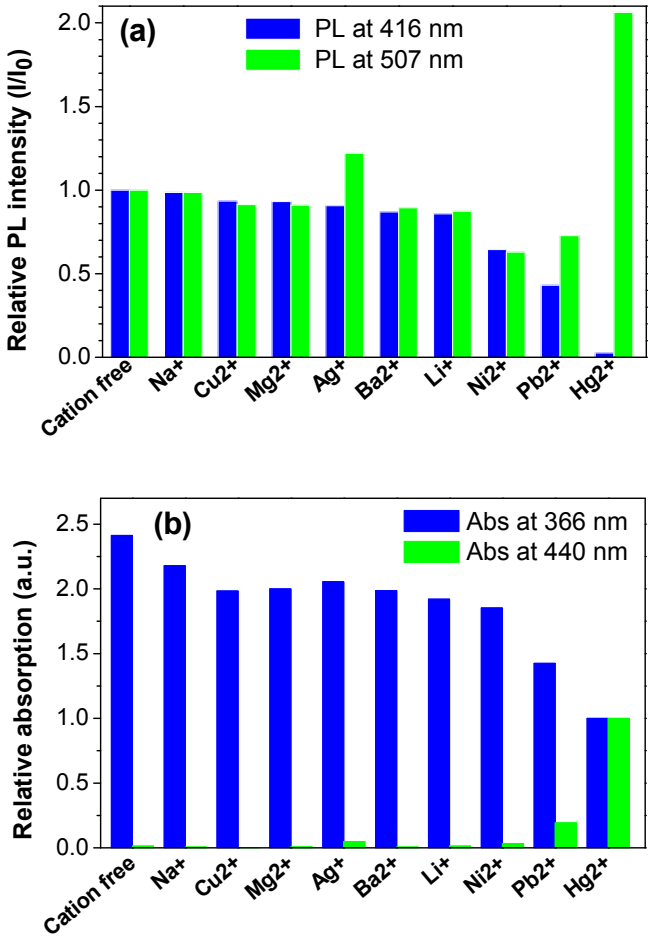

Figure 8 (a) Relative fluorescence intensities of **FNF** solutions in THF in the presence of metal cations (I) versus cation-free **FNF** solution (I_0) monitored at λ_{PL} = 416 nm (blue bars) and 507 nm (green bars). (b) Absorption intensities of **FNF** solutions in THF in the presence of metal cations and for cation-free solution normalized to the absorption intensities in the presence of Hg^{2+} cations, monitored at λ_{abs} = 366 nm (blue bars) and 440 nm (green bars). The values of absorption and PL intensities have been taken from Figure 7.

Complexation of **FNF** with Hg^{2+} led to bathochromic shift of its absorption (Figure 9a), quenching the emission in the blue region and an appearance of new emission band in the green region (Figure 9b). These changes are attributed to changes in the electronic structure of **FNF** on complexation. As evidenced from the absorption/emission and DFT studies, donor-acceptor interaction between the fluorene and 4,5-diazafluorene units in **FNF** is rather weak and its emission occurs solely from the LE state. Complexation of **N** with Hg^{2+} increases the electron acceptor character of the central moiety facilitating the ICT in the ground state and the bathochromically-shifted emission from the ICT excited state (Figure 9).

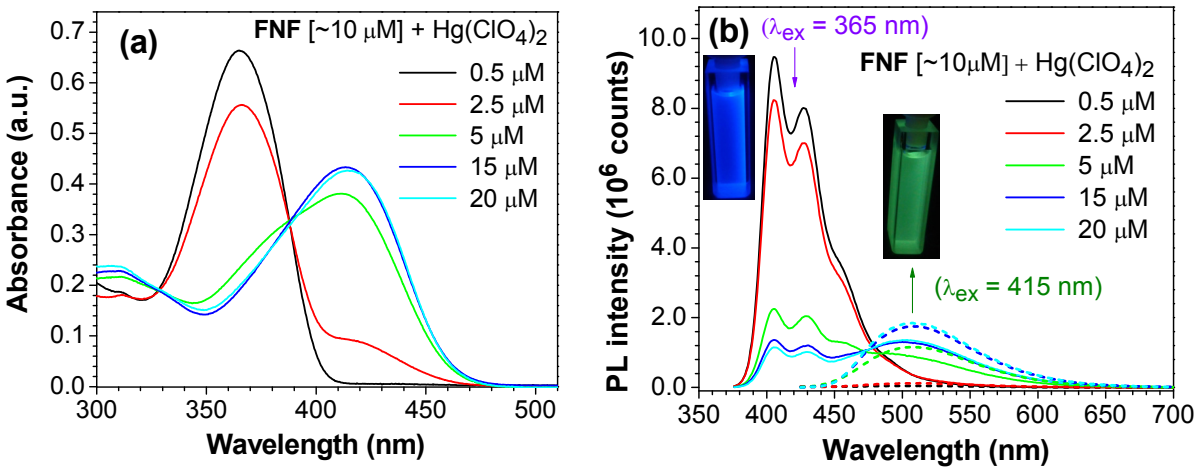

Figure 9 The absorption (a) and PL spectra (b) of **FNF** (~10 μM) in THF with an increased concentration of $Hg(ClO_4)_2$. For PL spectra (b), the THF solutions were excited at 365 nm (solid lines) and 415 nm (dashed lines), respectively. Inset photos show the colors of the emission under hand-held UV lamp (365 nm)

To look at the stoichiometry of this complexation, we performed titration of **FNF** solution (20 μM) with $Hg(ClO_4)_2$, monitoring their absorption and emission spectra (Figure S10 in the ESI). Job's plots for both absorption and fluorescence intensities revealed the formation of a 2:1 complex, 2[**FNF**]:[Hg^{2+}] (Figures S11 and S12 in the ESI). Titration of 10 μM **FNF** solution with $Hg(ClO_4)_2$ also showed the maximum fluorescence at 2:1 ratio [**FNF**]:[Hg^{2+}]. From the linear dependence of **FNF** fluorescence intensity at 510 nm at low Hg^{2+} concentrations, we estimated the detection limit of Hg^{2+} in these conditions of ~0.15 μM (Figure S13 in the ESI).

Changes in absorption/emission spectra of **FNF** in the presence of metal cations is based on its complexation as N^N ligand, so the efficiency of the process depends on the equilibrium constants and tuning the energies of the optical transition. The process is especially efficient for Hg^{2+} cations, while it can compete with complexation of other metal cations. To look at the interference of Hg^{2+} detection by other metal cations we have studied the absorption and emission spectra of {**FNF** [10 μM] + $Hg(ClO_4)_2$ [5 μM]} solutions in THF in the presence of other metal salts (Figures S14 and S15 in the ESI). In the case of Na^+, Cu^{2+} and Ba^{2+}, no changes in the emission wavelengths or their intensities have been observed even at high concentrations (20 μM) of these cations (Figure S14 in the ESI). On the other hand, some changes in the intensities and/or wavelengths of the absorption/emission spectra have been observed in the case of Mg^2, Ag^+ and Ni^{2+} cations, which might interfere at some extent in quantitative detection of Hg^{2+} in solutions (Figure S15 in the ESI). This can be partly minimized by a proper choice of the excitation wavelength (close to the isobestic points of the absorption spectra) and two-wavelengths detection (in ON → OFF and OFF → ON

modes, at shorter and longer wavelengths, respectively). We should also mention that the changes of the emission color in the presence of Hg^{2+} cations are pronounced and can be easily detected by naked eyes. Qualitatively, there is no observable interference in the emission color of {**FNF** + $Hg(ClO_4)_2$} solutions under hand-held UV lamp (365 nm) irradiation by other metal cations (see movies in the ESI).

FNF is not a unique compound with this respect as a selective sensor for Hg^{2+}. Other oligomers also show similar bathochromic shifts in their absorption/emission spectra and changes of the color of their emission in the presence of Hg^{2+} cations. Thus, upon addition $Hg(ClO_4)_2$, the emission of **FFNFF** solution is changed from blue to yellowish-green (λ_{PL}: 423, 443 nm → 538 nm) and the emission of **FNoF** solution is changed from yellow to orange (λ_{PL}: 569 nm → 617 nm) (Figure S16 in the ESI). Other studied cations do not change the emission colors of **FFNFF** and **FNoF** solutions (see movies in the ESI).

Further optimization of the conditions (concentration of 4,5-diazfluorene conjugated ligand, solvent, two-wavelength monitoring, as well as new molecular design to separate the LE emission if a free molecule and ICT emission in the complex) can further improve the sensitivity and the selectivity of this type of fluorescent sensors toward mercury cations.

3 Conclusion

A series of 4,5-diazafluorene (**N**) co-oligomers with fluorene (**F**) and dibenzothiophene-*S,S*-dioxide (**S**) have been synthesized, i.e. **FNF**, **FFNFF**, **FNoF**, **SNS**, and **NSN** (**No** is 4,5-diazafluorenone). Electrochemical studies reveal that incorporation of electron-deficient **N** unit decreases the LUMO energy levels compared to corresponding oligofluorenes. Combination of **N** moiety with the other electron-deficient building block **S** results in the oligomers (**SNS** and **NSN**) with substantially improved electron affinities (by 0.37 – 0.38 eV from cyclic voltammetry measurements, 0.57 – 0.65 eV from DFT calculations). **FNF**, **FFNFF**, **SNS**, and **NSN** oligomers are strongly fluorescent materials emitting in the blue region (~400 – 450 nm) with high photoluminescence quantum yields both in solution (Φ_{PL} = 84 – 100%) and in the solid state (Φ_{PL} = 24 – 32%). **FNoF** possesses lower HOMO–LUMO gap compared to other oligomers due to its charge-transfer character and shows a shift of the emission to the green region (λ_{PL} = 570 – 575 nm) and substantial quenching the emission in solution down to Φ_{PL} = 1%. In the solid state, however, its emission is unexpectedly increased to 10–17%.

Studies of the ion sensing properties of **FNF** in solution with a series of metal cations (Li^+, Na^+, Ag^+, Cu^{2+}, Mg^{2+}, Ba^{2+}, Ni^{2+}, Pb^{2+} and Hg^{2+}) showed high sensitivity of its absorption and emission spectra toward Hg^{2+} cations. In contrast to other cations, which showed no or very small effect on the absorption and fluorescence spectra of **FNF**, an addition of mercury salt strongly

quenches the blue emission (λ_{PL} = 404 nm) of **FNF** and results in an appearance of the other, bathochromically shifted emission band at λ_{PL} = 507 nm. Thus, monitoring the fluorescence of **FNF** at these two wavelengths [ON → OFF (in blue region) and OFF → ON (in green region)] allows selectively recognize Hg^{2+}. It has been demonstrated that an interaction of **FNF** with Hg^{2+} leads to formation of 2:1 complex whose emission is bathochromically shifted due to an increased intramolecular charge transfer character in the molecule. As such, 4,5-diazafluorene-based conjugates represent promising class of ON → OFF // OFF → ON fluorescent sensors for selective detection of toxic mercury cations. Our work on the design of more sensitive and selective fluorescent sensors for Hg^{2+} based on 4,5-diazafluorene oligomers and polymers is in progress.

Acknowledgement

We thank the LCRI (Low Carbon Research Institute) programme for funding (Welsh European Funding Office, Grant WEFO-80366). S.G. thanks to Bangor University for a 125 Anniversary Scholarship. M.H.A. thanks to The Higher Committee for Education Development in Iraq (HCED) for a Scholarship to do his PhD studies at Bangor University. M.P.K. thanks LCRI and Bangor University for a postdoctoral fellowship.

References

1 A.C Grimsdale and K Müllen, *Adv. Polym. Sci*., 2006, **199**, 1–82.
2 W. Y. Wang, *Coord. Chem. Rev*., 2005, **249**, 971–997.
3 U. Scherf and D. Neher (Eds.), *Polyfluorenes. Advances in Polymer Science – Vol. 212*, Springer–Verlag, Berlin, 2008, pp. 145–180.
4 D. F. Perepichka, I. F. Perepichka, H. Meng and F. Wudl, in Book: *Organic Light-Emitting Materials and Devices*, Z. R. Li and H. Meng (Eds.), CRC Press, Boca Raton, FL, 2006, Chapter 2, pp. 45–293 (2nd Edition, 2015, pp. 41–308).
5 A. L. Kanibolotsky, I. F. Perepichka and P. J. Skabara, *Chem. Soc. Rev.,* 2010, **39**, 2695–2728.
6 I. I. Perepichka, I. F. Perepichka, M. R. Bryce, and L.-O. Pålsson, *Chem. Commun.,* 2005, 3397–3399.
7 F. B. Dias, S. Pollock, G. Hedley, L. Pålsson, A. Monkman, I. I. Perepichka, I. F. Perepichka, M. Tavasli and M. R. Bryce, *J. Phys. Chem. B,* 2006, **110**, 19329–19339.
8 J. Zhang, S. Dong, K. Zhang, A. Liang, X. Yang, F. Huang and Y. Cao, *Chem. Commun.,* 2014, **50**, 8227–8230.
9 F. B. Dias, S. King, A. P. Monkman, I. I. Perepichka, M. A. Kryuchkov, I. F. Perepichka and M. R. Bryce, *J. Phys. Chem. B*, 2008, **112**, 6557–6566.
10 S. M. King, I. I. Perepichka, I. F. Perepichka, F. B. Dias, M. R. Bryce and A. P. Monkman, *Adv. Funct. Mater.,* 2009, **19**, 586–591.
11 K. T. Kamtekar, H. L. Vaughan, B. P. Lyons, A. P. Monkman, S. U. Pandya and M. R. Bryce, *Macromolecules*, 2010, **43**, 4481–4488.
12 J. H. Cook, J. Santos, H. Li, H. A. Al-Attar, M. R. Bryce and A. P. Monkman, *J. Mater. Chem. C*, 2014, **2**, 5587–5592.
13 L. Yu, J. Liu, S. Hu, R. He, W. Yang, H. Wu, J. Peng, R. Xia and D. D. C. Bradley, *Adv. Funct. Mater.*, 2013, **23**, 4366–4376.
14 R. He, J. Xu, Y. Xue, D. Chen, L. Ying, W. Yang and Y. Cao, *J. Mater. Chem. C*, 2014, **2**, 7881–7890.
15 J. Yang, L. Zhao, X. Wang, S. Wang, J. Ding, L. Wang, X. Jing and F. Wang, *Macromol. Chem. Phys.*, 2014, **215**, 1107−1115.
16 L. Hu, Y. Yang, J. Xu, J. Liang, T. Guo, B. Zhang, W. Yang and Y. Cao, *J. Mater. Chem. C,* 2016, **4**, 1305–1312.
17 F. B. Dias, K. N. Bourdakos, V. Jankus, K. C. Moss, K. T. Kamtekar, V. Bhalla, J. Santos, M. R. Bryce and A. P. Monkman, *Adv. Mater.*, 2013, **25**, 3707–3714.

18 V. Jankus, P. Data, D. Graves, C. McGuinness, J. Santos, M. R. Bryce, F. B. Dias and A. P. Monkman, *Adv. Funct. Mater.*, 2014, **24**, 6178–6186.
19 R. S. Nobuyasu, Z. Ren, G. C. Griffiths, A. S. Batsanov, P. Data, S. Yan, A. P. Monkman, M. R. Bryce and F. B. Dias, *Adv. Opt. Mater*., 2016, **4**, 597–607.
20 J. S. Ward, R. S. Nobuyasu, A. S. Batsanov, P. Data, A. P. Monkman, F. B. Dias and Martin R. Bryce, *Chem. Commun.,* 2016, **52**, 2612–2615.
21 K. Ono and K. Saito, *Heterocycles*, 2008, **75**, 2381–2413.
22 K.-T. Wong, R.-T. Chen, F.-C. Fang, C.-C. Wu and Y.-T. Lin, *Org. Lett.*, 2005, **7**, 1979–1982.
23 C.-C. Chi, C.-L. Chiang, S.-W. Liu, H. Yueh, C.-T. Chen and C.-T. Chen, *J. Mater. Chem.*, 2009, **19**, 5561–5571.
24 H.-F. Chen, T.-C. Wang, W.-Y. Hung, H.-C. Chiu, C. Yunc and K.-T. Wong, *J. Mater. Chem.*, 2012, **22**, 9658–9664.
25 K.-T. Wong, H.-F. Chen, and F.-C. Fang, *Org. Lett.*, 2006, **8**, 3501–3504.
26 W.-J. Li, H.-M. Wu, Y.-B. Li, C.-P. Hu, M.-D. Yi, L.-H. Xie, L. Chen, J.-F. Zhao, X.-H. Zhao, N.-E. Shi, Y. Qian, C. Wang, W. Wei and W. Huang, *Tetrahedron*, 2012, **68**, 8216–8221.
27 C.-J. Zheng, J. Ye, M.-F. Lo, M.-K. Fung, X.-M. Ou, X.-H. Zhang and C.-S. Lee, *Chem. Mater.*, 2012, **24**, 643−650.
28 Z. Fan, H. Zhao, N. Li, Y. Quan, Q. Chen, S. Ye, S. Li, Y. Wang, Q. Fan and W. Huang, *ACS Appl. Mater. Interf.*, 2015, **7**, 9445−9452.
29 W.-J. Li, B. Liu, Y. Qian, L.-H. Xie, J. Wang, S.-B. Li and W. Huang, *Polym. Chem.*, 2013, **4**, 1796–1802.
30 Y. Wang, W. J. Perez, G. Y. Zheng, D. P. Rillema and C. L. Huber, *Inorg. Chem.*, 1998, **37**, 2227–2234.
31 H. J. Eppley, S. M. Lato, A. D. Ellington and J. M. Zaleski, *Chem. Commun.*, 1999, 2405–2406.
32 Q.-Y. Zhu, J. Dai, D.-X. Jia, L.-H. Cao and H.-H. Lin, *Eur. J. Inorg. Chem.*, 2004, 4789–4794.
33 W.-Y. Wong, *Coord. Chem. Rev.*, 2005, **249**, 971–997.
34 H. Jiang, E. Stepowska and D. Song, *Eur. J. Inorg. Chem.*, 2009, 2083–2089.
35 V. T. Annibale, D. A. Dalessandro and D. Song, *J. Am. Chem. Soc.*, 2013, **135**, 16175−16183.
36 H.-C. Su, F.-C. Fang, T.-Y. Hwu, H.-H. Hsieh, H.-F. Chen, G.-H. Lee, S.-M. Peng, K.-Tsung Wong and C.-C. Wu, *Adv. Funct. Mater.*, 2007, **17**, 1019–1027.
37 H.-C. Su, H.-F. Chen, C.-C. Wu and K.-T. Wong, *Chem. Asian J.*, 2008, **3**, 1922–1928.
38 H.-C. Su, H.-F. Chen, F.-C. Fang, C.-C. Liu, C.-C. Wu, K.-T. Wong, Y.-H. Liu and S.-M. Peng, *J. Am. Chem. Soc.*, 2008, **130**, 3413–3419.
39 C. Ulbricht, B. Beyer, C. Friebe, A. Winter and U. S. Schubert, *Adv. Mater.,* 2009, **21**, 4418–4441.
40 H.-F. Chen, W.-Y. Hung, S.-W. Chen, T.-C. Wang, S.-W. Lin, S.-H. Chou, C.-T. Liao, H.-C. Su, H.-A. Pan, P.-T. Chou, Y.-H. Liu and K.-T. Wong, *Inorg. Chem.*, 2012, **51**, 12114−12121.
41 Z. Liu, W. He and Z. Guo, *Chem. Soc. Rev*., 2013, **42**, 1568–1600.
42 K. C. Moss, K. N. Bourdakos, V. Bhalla, K. T. Kamatekar, M. R. Bryce, M. A. Fox, H. L. Vaughan, F. B. Dias and A. P. Monkman, *J. Org. Chem.*, 2010, **75**, 6771–6781.
43 S. Hamai and F. Hirayama, *J. Phys. Chem.,* 1983, **87**, 83–89.
44 K.-T. Wong, Y.-Y. Chien, R.-T. Chen, C.-F. Wang, Y.-T. Lin, H.-H. Chiang, P.-Y. Hsieh, C.-C. Wu, C. H. Chou, Y. O. Su, G.-H. Lee and S.-M. Peng, *J. Am. Chem. Soc.*, 2002, **124**, 11576–11577.
45 Y. Geng, A. Trajkovska, S. W. Culligan, J. J. Ou, H. M. P. Chen, D. Katsis and S. H. Chen, *J. Am. Chem. Soc.*, 2003, **125**, 14032–14038.
46 Y. Geng, A. C. A. Chen, J. J. Ou and S. H. Chen, *Chem. Mater.*, 2003, **15**, 4352–4360.
47 X.-H. Zhou, J.-C. Yan and J. Pei, *Org. Lett.*, 2003, **5**, 3543–3546.
48 A. L. Kanibolotsky, R. Berridge, P. J. Skabara, I. F. Perepichka, D. D. C. Bradley and M. Koeberg, *J. Am. Chem. Soc.*, 2004, **126**, 13695–13702.
49 T.-C. Chao, Y.-T. Lin, C.-Y. Yang, T. S. Hung, H.-C. Chou, C.-C. Wu and K.-T. Wong, *Adv. Mater.*, 2005, **17**, 992–996.
50 P. Robert, A. Bolduc and W. G. Skene, *J. Phys. Chem. A*, 2012, **116**, 9305–9314.
51 P. Robert, A. Bolduc and W. G. Skene, *J. Phys. Chem. A*, 2012, **116**, 9305–9314.
52 C. Chi, C. Im, V. Enkelmann, A. Ziegler, G. Lieser and G. Wegner, *Chem. Eur. J.*, 2005, **11**, 6833–6845.
53 X. Gong, P. K. Iyer, D. Moses, G. C. Bazan, A. J. Heeger and X. S. Xiao, *Adv. Funct. Mater.*, 2003, **13**, 325–330.
54 L. Romaner, A. Pogantsch, P. S. de Freitas, U. Scherf, M. Gaal, E. Zojet and E. J. W. List, *Adv. Funct. Mater.*, 2003, **13**, 597–601.
55 M. Sims, D.D.C. Bradley, M. Ariu, M. Koeberg, A. Asimakis, M. Grell and D. G. Lidzey, *Adv. Funct. Mater.*, 2004, **14**, 765–781.
56 A. P. Kulkarni, X. Kong and S. A. Jenekhe, *J. Phys. Chem. B*, 2004, **108**, 8689–8701.
57 Y. Hong, J. W. Y. Lam and B. Z. Tang, *Chem. Commun.*, 2009, 4332–4353.
58 R. Katoh, K. Suzuki, A. Furube, M. Kotani and K. Tokumaru, *J. Phys. Chem. C*, 2009**, 113**, 2961–2965.
59 C. Chi, C. Im, V. Enkelmann, A. Ziegler, G. Lieser and G. Wegner, *Chem. Eur. J.*, 2005, **11**, 6833–6845.

60 Y. Chen, F. Li and Z. Bo, *Macromolecules*, 2010, **43**, 1349–1355.

61 Gaussian 09, Revision A02, M. J. Frisch, G. W. Trucks, H. B. Schlegel, G. E. Scuseria, M. A. Robb, J. R. Cheeseman, G. Scalmani, V. Barone, B. Mennucci, G. A. Petersson, H. Nakatsuji, M. Caricato, X. Li, H. P. Hratchian, A. F. Izmaylov, J. Bloino, G. Zheng, J. L. Sonnenberg, M. Hada, M. Ehara, K. Toyota, R. Fukuda, J. Hasegawa, M. Ishida, T. Nakajima, Y. Honda, O. Kitao, H. Nakai, T. Vreven, J. A. Montgomery Jr., J. E. Peralta, F. Ogliaro, M. J. Bearpark, J. Heyd, E. N. Brothers, K. N. Kudin, V. N. Staroverov, R. Kobayashi, J. Normand, K. Raghavachari, A. P. Rendell, J. C. Burant, S. S. Iyengar, J. Tomasi, M. Cossi, N. Rega, N. J. Millam, M. Klene, J. E. Knox, J. B. Cross, V. Bakken, C. Adamo, J. Jaramillo, R. Gomperts, R. E. Stratmann, O. Yazyev, A. J. Austin, R. Cammi, C. Pomelli, J. W. Ochterski, R. L. Martin, K. Morokuma, V. G. Zakrzewski, G. A. Voth, P. Salvador, J. J. Dannenberg, S. Dapprich, A. D. Daniels, Ö. Farkas, J. B. Foresman, J. V. Ortiz, J. Cioslowski and D. J. Fox, Gaussian, Inc., Wallingford CT, 2009.

62 J.-H. Huang, W.-H. Wen, Y.-Y. Sun, P.-T. Chou and J.-M. Fang, *J. Org. Chem.*, 2005, **70**, 5827–5832.

63 H. N. Kim, W. X. Ren, J. S. Kim and J. Yoon, *Chem. Soc. Rev.,* 2012, **41**, 3210–3244.

64 L. Prodi, C. Bargossi, M. Montalti, N. Zaccheroni, N. Su, J. S. Bradshaw, R. M. Izatt and P. B. Savage, *J. Am. Chem. Soc.*, 2000, **122**, 6769–6770.

65 S. Voutsadaki, G. K. Tsikalas, E. Klontzas, G. E. Froudakis and H. E. Katerinopoulos, *Chem. Commun.*, 2010, **46**, 3292–3294.

66 J. Li, Y. Wu, F. Song, G. Wei, Y. Cheng and C. Zhu, *J. Mater. Chem.*, 2012, **22**, 478–482.

67 J. Liu, K. Vellaisamy, G. Yang, C.-H. Leung and D.-L. Ma, *Sci. Reports*, 2017, **7**, 3620.

68 M. Vedamalai, D. Kedaria, R. Vasita, S. Moric and I. Gupta, *Dalton Trans.*, 2016, **45**, 2700–2708.

69 H. Lee, H.-S. Lee, J. H. Reibenspies and R. D. Hancock, *Inorg. Chem.*, 2012, **51**, 10904−10915.

70 Y. Zhao, Z. Lin, C. He, H. Wu and C. Duan, *Inorg. Chem.*, 2006, **45**, 10013–10016.

71 Y. Mao, and M. Hong, A, Liu and D. Xu, *J. Fluorescence*, 2015, **25**, 755–761.

72 Y. Yang, R. Shen, Y.-Z. Wang, F.-Z. Qiu, Y. Feng, X.-L. Tang, D.-C. Bai, G.-L. Zhang and W.-S. Liu, *Sensors Actuators B*, 2018, **255**, 3479–3487.

73 T.-B. Wei, G.-Y. Gao, W.-J. Qu, B.-B. Shi, Q. Lin, H. Yao and Y.-M. Zhang, *Sensors Actuators B*, 2014, **199,** 142–147.

74 H.-W. Li, B. Wang, Y.-Q. Dang, L. Li, Y. Wu, *Sensors Actuators B*, 2010, **148**, 49–53.

75 H.-F. Wang and S.-P. Wu, *Tetrahedron*, 2013, **69,** 1965–1969.

76 J. H. Hu, J. B. Li, J. Qi and J. J. Chen, *New J. Chem.,* 2015, **39**, 843–848.

77 M.-H. Ha-Thi, M. Penhoat, V. Michelet and I. Leray, *Org. Lett.*, 2007, **9**, 1133–1136.

78 J. Wang and X. Qian, *Org. Lett.*, 2006, **8**, 3721–3724.

79 Z. Fang, K.-Y. Pu and B. Liu, *Macromolecules*, 2008, **41**, 8380–8387.

80 J. Wang, X. Qian and J. Cui, *J. Org. Chem.*, 2006, **71**, 4308–4311.

81 Z. Wang, J. H. Lee and Y. Lu, *Chem. Commun.*, 2008, 6005–6007.

82 X. Ren and Q.-H. Xu, *Langmuir*, 2009, **25**, 29–31.

83 X. Zhu, X. Zhou, D. Xing, *Biosensors Bioelectronics*, 2011, **26**, 2666–2669.

84 B.-C. Ye and B.-C. Yin, *Angew. Chem. Int. Ed.*, 2008, **47**, 8386 –8389.

Table of Contents Entry

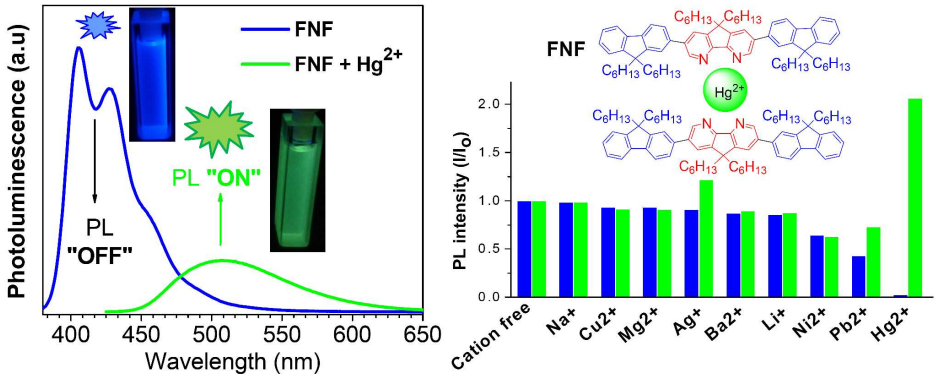

4,5-Diazafluorene co-oligomers combine improved electron affinity with strong fluorescence and can be used as electron transporting and light-emitting materials, as well as fluorescent sensors for Hg^{2+} cations in a dual ON → OFF and OFF → ON mode.

Electronic Supplementary Information (ESI)

4,5-Diazafluorene co-oligomers as electron-deficient light-emitting materials and selective fluorescence sensors for mercury(II) cations

Sanjay Ghosh, Abdulaziz S. Alghunaim, Mohammed H. Al-mashhadani, Michal P. Krompiec, Megan Hallett, and Igor F. Perepichka*

School of Chemistry, Bangor University, Bangor, LL57 2UW, UK

**E-mail: i.perepichka@bangor.ac.uk; i_perepichka@yahoo.com; Tel: +44–(0)1248–382386*

Materials and Instrumentations

All chemicals and solvents were purchased from either Aldrich, Alfa Aesar or Fischer Scientific and were used without further purification unless stated otherwise. Tetrahydrofuran (THF) was refluxed over sodium benzophenone ketyl (sodium metal + benzophenone) under argon and distilled off directly prior using the solvent for cyclic voltammetry and absorption/emission spectral measurements. Manual purification of the products was performed by column chromatography silica gel LC60 (40–60 μM). Some products were purified using Telydyne Isco automatic flash chromatograph, model Combiflash Rf 200 using Biotage disposable PTFE columns, hand-filled with silica gel LC60 (40–60 μM). For monitoring the progress of the reactions and control the products, thin layer chromatography (TLC) on pre-coated silica gel (Merck, 20 × 20 cm, Silica gel 60 F_{254}) was used.

^{1}H NMR, ^{13}C NMR and DEPT-135 C NMR spectra were recorded either on a Bruker Avance 400 MHz or Bruker Avance 500 MHz in $CDCl_3$ or DMSO-d_6. Chemical shifts are reported in ppm, relative to tetramethylsilane (TMS) reference (δ = 0.00 ppm). The following abbreviations were used to assign NMR spectra: s = singlet, d = doublet, t = triplet, dd = doublet of doublet, td = doublet of triplet. Mass spectra were recorded on GC-MS 5890 (Hewlett Packard Series II) or microTOF LC Bruker Daltonics mass spectrometers. Microwave assisted reactions were performed on a CEM Discover SP microwave reactor. Spin-coated films were prepared using spin coater from Laurel Technologies, Model WS-650Mz-23NPP/LITE.

Absorption and emission spectra, and the photoluminescence quantum yields

Shimadzu UV-3600 UV-Vis-NIR spectrophotometer and Horiba Yvon Fluromax-4 spectrofluorometer were used for recording absorption and photoluminescence spectra at room temperature. Absorption and emission spectra in solutions were measured using HPLC grade solvents in 10 mm path length quartz cells. Solid state measurements were performed for spin-coated films deposited on 12.5 mm circular quartz windows. The films were prepared by spin coating from oligomer solutions (1–3 mg per 1 mL of DCM) at 3000-4000 rpm. Photoluminescence quantum yields (PLQY, Φ_{PL}) in solutions for all oligomers were measured in HPLC grade dichloromethane (DCM) at room temperature according to the described method.[1] The values of Φ_{PL} were calculated according to the following formula:

$$\Phi_{PL} = \Phi_r \times (A/A_r) \times (OD_r/OD) \times (n^2/n_r^2)$$

where Φ_{PL} is a photoluminescence quantum yield, A is an integral intensity of the emission, OD is an optical density, and n is a refractive index of the used solvent. The subscript *r* refers to the reference fluorophore of known quantum yield [9,10-diphenylanthracene (DPA), diluted solution in cyclohexane, Φ_r = 90%). The solutions were deoxygenated by bubbling with argon for about 10 minutes before the measurements. Corrected emission and absorption spectrum was used to

calculate the quantum yields. Absolute Φ_{PL} in solutions and in the solid state were measured for spin-coated films on quartz substrates using calibrated integrating sphere Horiba F-3018 on Horiba Jobin Yvon Fluromax-4 spectrofluorometer at room temperature, and calculated by Horiba Yvon quantum yield calculator software. CIE 1931 color space have been calculated using OSRAM Color Calculator v. 7.23.

Table S1 Determination of photoluminescence quantum yields (PLQY, Φ_{PL}) of oligomers in degassed DCM.

Compound	Integral intensity of the emission A (λ_{ex} = 350 nm)	Optical density OD (a.u.)	PLQY, Φ_{PL} (%)
9,10-DPA[a]	7.53×10^7	0.05	(90)
FNoF [b]	9.75×10^5	0.05	1
FFNFF	1.04×10^8	0.07	84
FNF	1.13×10^8	0.07	93
SNS	1.21×10^8	0.07	101
NSN	8.54×10^7	0.05	89

[a] Diluted solution of DPA in degassed cyclohexane (Φ_r = 90%) was used as fluorophore standards.[2]
[b] λ_{ex} = 370 nm

Experimental procedure for the metal cations sensing study of FNF.
The metal salts used in these studies $LiClO_4$, $NaClO_4$, $AgClO_4$, $Mg(ClO_4)_2$, $Ba(ClO_4)_2$, $Cu(BF_4)_2$, $Ni(NO_3)_2$, $Pb(ClO_4)_2$ and $Hg(ClO_4)_2$ were dried under high vacuum (10^{-3} mbar) for at least 24 hours prior to using them for preparation of solutions in dry THF [hygroscopic salts were preliminary dried in an oven at 170 ºC for several hours]. The stoichiometry of the coordination complex with Hg^{2+} was determined using Job's method.[3,4] The absorption and photoluminescence spectra for titration of **FNF** with $HgClO_4$ are shown in Figure S10. The corresponding Job's plot using both fluorescence and absorption intensity (Figure S11) reveal 2:1 (**FNF**:Hg^{2+}, mole ratio) stoichiometry for the [**FNF**-Hg^{2+}] adduct. The corresponding structure of the possible complex formation is shown on Figure S12.
Measurements of known concentraions of 2[**FNF**]**:**Hg^{2+} complex emission intensity can be used to determine the unknown concentration of Hg^{2+} in a given sample by plotting calibration graph of the emission intensity *vs* concentration. Photoluminescence titration of **FNF** with Hg^{2+} ions showed that an intensity of the long wavelength emission band at 507 nm of **FNF**-Hg^{2+} complex gradually increased with an increase of Hg^{2+} ions up to certain limit that corresponds to the 2:1 ratio (Figure S13b). Linear increase in the fluorescence intensity with an increase of Hg^{2+} concentration added to the **FNF** solution in THF is observed in the range of ca. 0 – 2.5 μM that allowed to estimate the detection limit to be ca. $1.5–2 \times 10^{-7}$ M.

Cyclic voltammetry
Cyclic voltammetry experiments were conducted in a standard three-electrode configuration, using Metrohm Autolab PGSTAT-302N potentiostat/galvanostat, with iR drop compensation. Platinum disk electrode (d = 1.5 or 2 mm) and platinum wire (d = 0.2 mm) were used as the working and counter electrodes, respectively. The reference electrode was Ag/Ag^+ (silver wire immersed in a mixture of 0.01 M $AgNO_3$ and 0.1 M Bu_4NPF_6 in acetonitrile, separated from the solution by a Vycor frit). Potentials are referenced to half-wave potential ($E_{1/2}$) of ferrocene, which was used as an internal standard. The average potentials of Fc/Fc^+ vs Ag/Ag^+ in our conditions were $E_{1/2}$ = 0.20–0.22 V (in DCM) and 0.19–0.21 V (in THF). Oxidation scans were performed in DCM containing 0.2 M Bu_4NPF_6, reduction scans were carried out in a freshly distilled THF containing 0.2 M Bu_4NPF_6, under argon. The CV were recorded at the scan rate of 100 mV/s.

Computational studies

All the computational studies were performed with Gaussian 09 package of programs[5] using the density functional theory method (DFT). The hybrid functional B3LYP, which combines Becke's exchange[6] and Lee, Yang, Paar's correlation functional[7] with 6-31G or 6-311G basis sets supplemented by (d) or (d,p) polarization functions were used for calculations. The calculations were performed either in a gas phase or in acetonitrile (using polarizable continuum model, PCM). The restricted Hartree-Fock formalism was used. No constraints were used and all structures were free to optimize. The force constants and vibrational frequency for stationary points have been calculated after optimizations to check that they are true minima. To decrease the computation time, all the oligomers geometries were optimized with ethyl substituents at the positions 9,9- of fluorene and 4,5-diazafluorene (instead of longer hexyl or octyl substituents in experimental work). This was shown have no effect on the HOMO/LUMO energy levels of the co-oligomers. The visualization of the orbital coefficients was performed with GaussView 5.0 software.

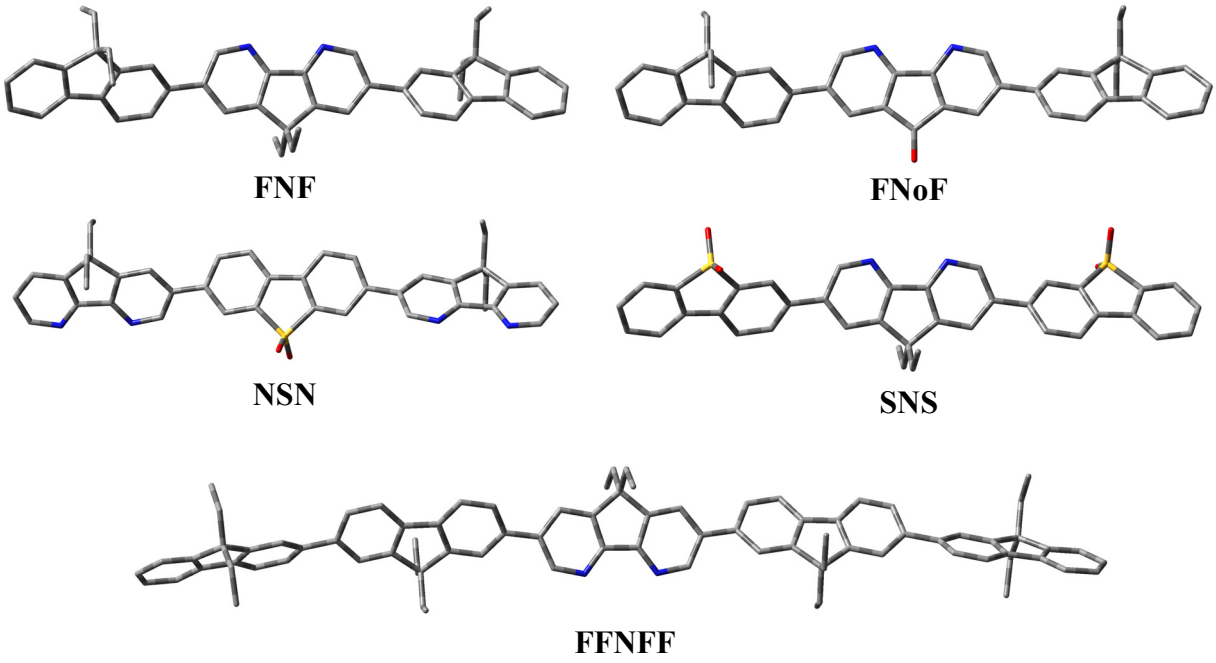

Figure S1. Optimized structures of conjugated oligomers calculated at DFT/B3LYP/6-31G(d) level. For simplicity, H atoms are omitted and tube framework used with colors blue = nitrogen, red = oxygen, and yellow = sulphur atoms using GaussView 05 software.

Table S2. Dipole moments of the optimized geometries of studied co-oligomers calculated by DFT/B3LYP using different basis sets in a gas phase and in ACN.

Compound	6-31G(d) gas phasese	6-31G(d,p) ACN	6-311G(d,p) gas phase	6-311G(d,p) ACN
FNoF	0.02	0.16	0.07	0.10
FFNFF	3.50	5.43	3.47	5.38
FNF	3.44	5.06	3.43	5.01
SNS	12.54	17.44	12.76	18.23
NSN	11.51	18.88	11.51	17.08

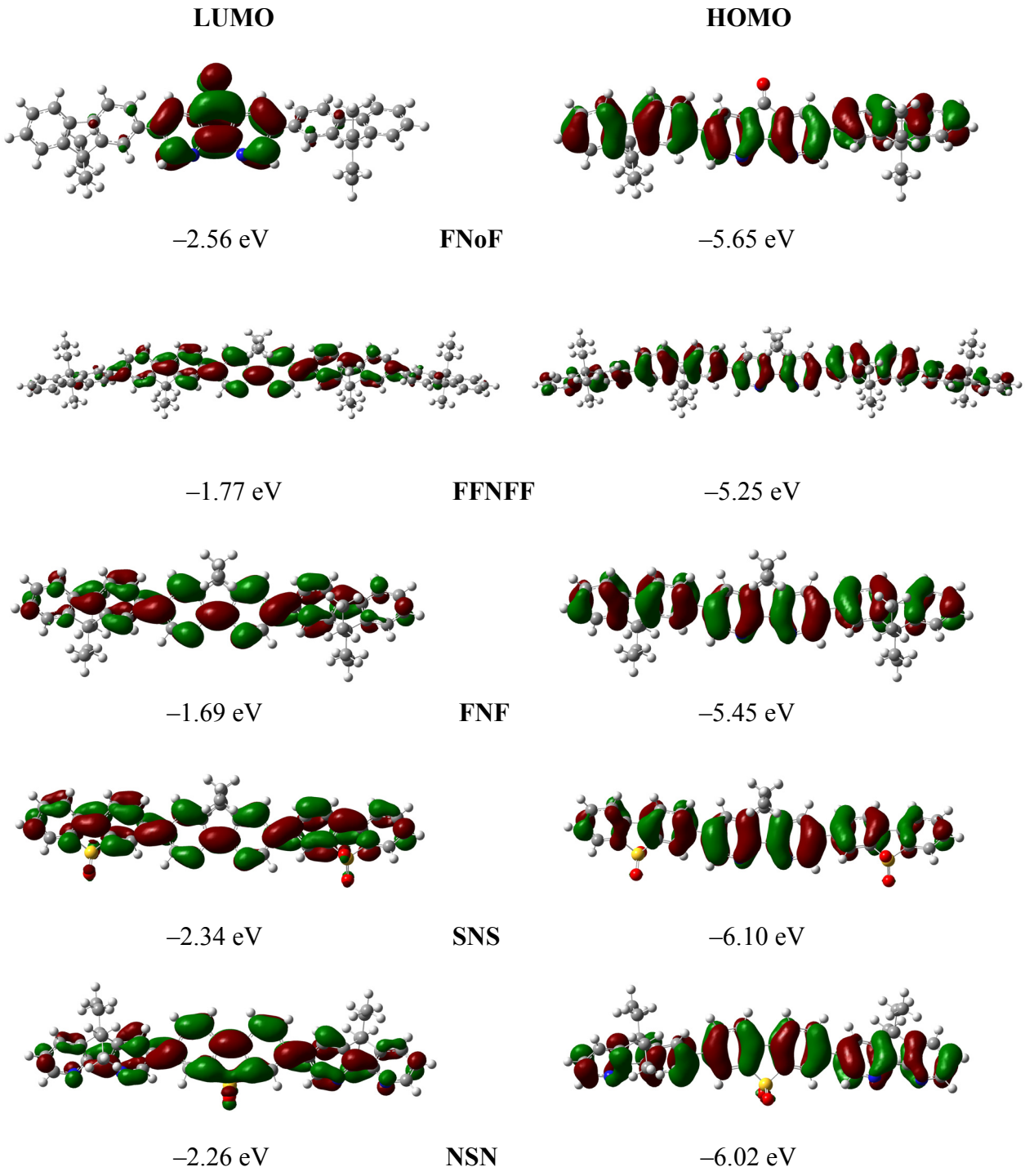

Figure S2. HOMO and LUMO orbital coefficients of 4,5-diazafluorene co-oligomers **FNoF**, **FFNFF**, **FNF**, **SNS, and NSN** by DFT/B3LYP/6-31G(d) calculations in a gas phase (surface isovalue = 0.02).

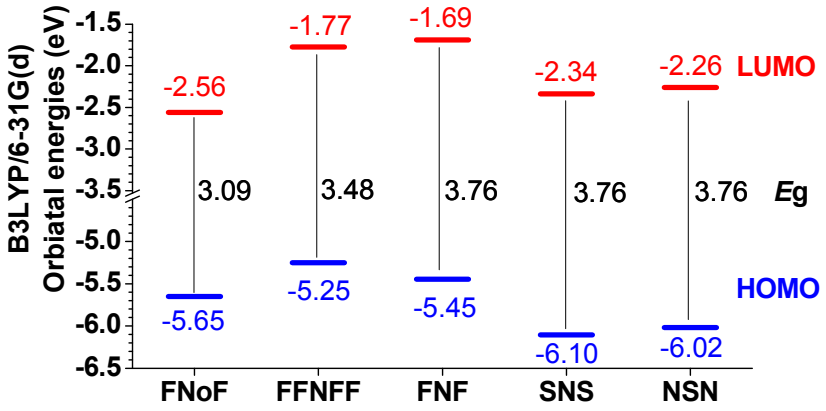

Figure S3 Frontier orbitals energy levels of 4,5-diazafluorene co-oligomers by DFT/B3LYP/6-31G(d) calculations in a gas phase.

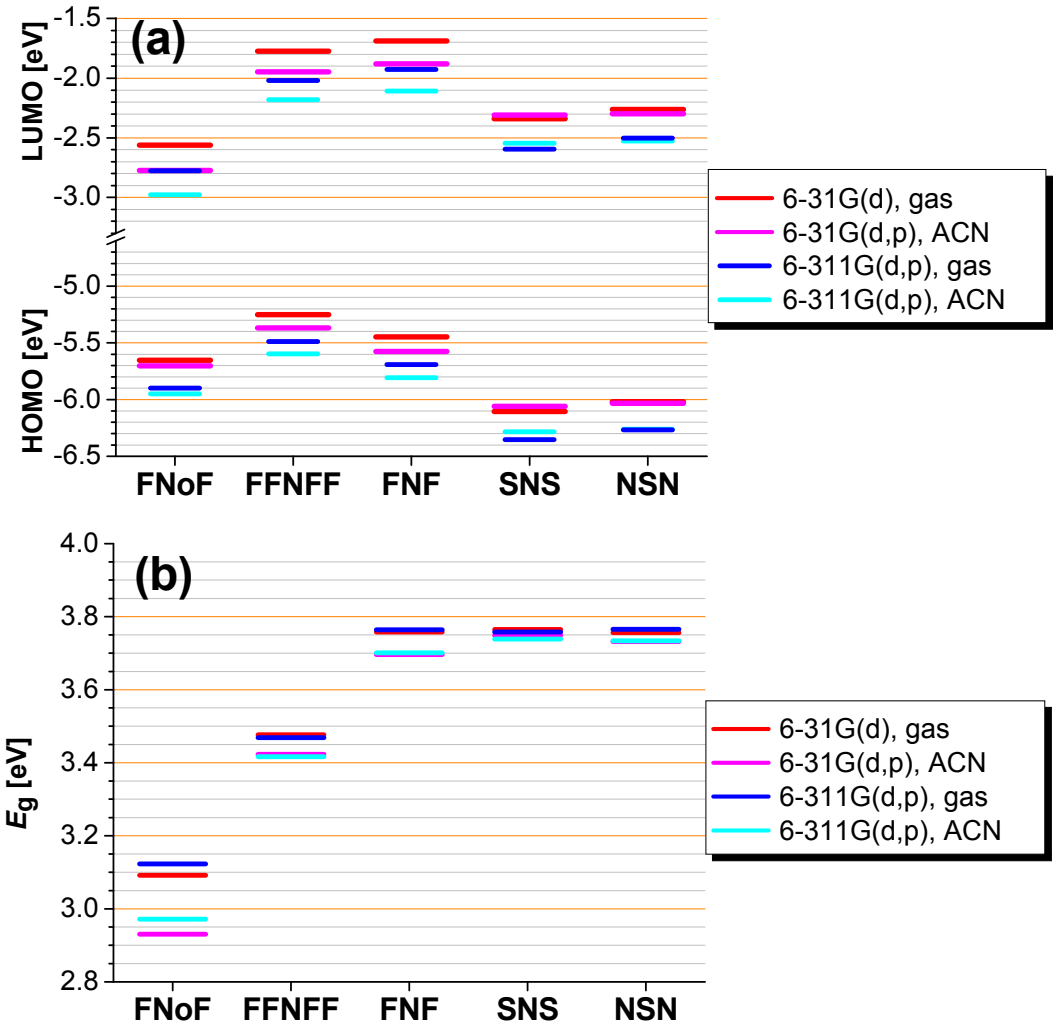

Figure S4 HOMO, LUMO (a) and HOMO–LUMO gaps, E_g (b) of 4,5-diazafluorene co-oligomers calculated by DFT/B3LYP using different basis sets and polarization functions [6-31G(d), 6-31G(d,p) and 6-311G(d,p)] in a gas phase and in acetonitrile, ACN (by PCM model).

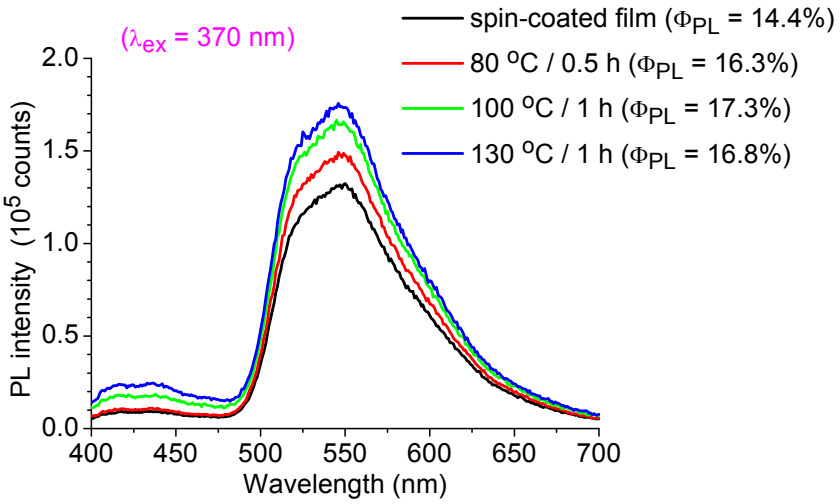

Figure S5 Photoluminescence spectra of **FNF** in the solid state (spin-coated-films from chloroform solution) before and after thermal annealing on an air. The measurements have been performed on an integrating sphere (the shown spectra have not corrected on the sphere background).

Table S3 Absorption and photoluminescence maxima of **FNF**, **FFNFF** and **FNoF** co-oligomers in different solvents.[a]

	FNF		**FFNFF**		**FNoF**	
Solvent	λ_{abs} (nm)	λ_{PL} (nm)	λ_{abs} (nm)	λ_{PL} (nm)	λ_{abs} (nm)	λ_{PL} (nm)
Hexane	**358.5**	**398**, 418, 445sh	324, **372**	**413.5**, 436	**359**, 417sh	500sh, **529**, 560sh
Toluene	**363**	**404.5**, 426, 450sh	326, **377**	**420.5**, 443	**364.5**, 422sh	**558**
DCM	**366**	**409**, 430sh	328, **378**	**429**, 446sh	**366**, 440sh	**575**
THF	**365**	**404**, 426, 450sh	–	–	–	–
ACN	**364**	**407**, 424, 450sh	–	–	**363**, 427sh	**606**
EtOH	**367**	**415**, 430sh	327, **379**	**446**	–	–

[a] The data are from the spectra shown on Figures 2a,b, 3a-c and 6a,b.

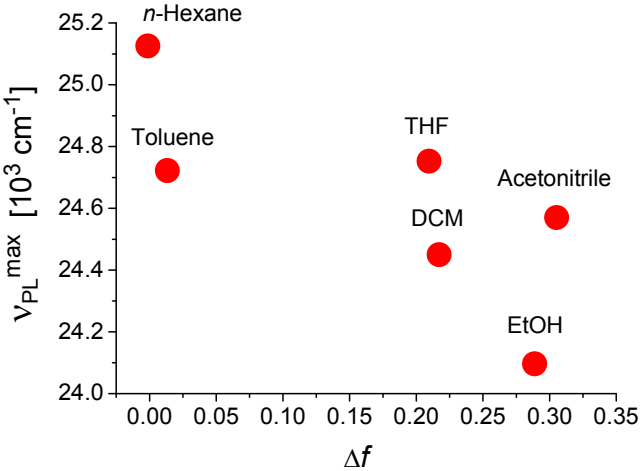

Figure S6. Solvatochromic shifts of the emission maxima ($\nu_{PL}^{max} = 1/\lambda_{PL}^{max}$) for **FNF** against the solvent polarity parameter [Lippert-Mataga equation, $\Delta f = (\varepsilon - 1)/(2\varepsilon + 1) - (n^2 - 1)/(n^2 + 1)$, where ε is a dielectric permittivity and n is a refractive index of a solvent].

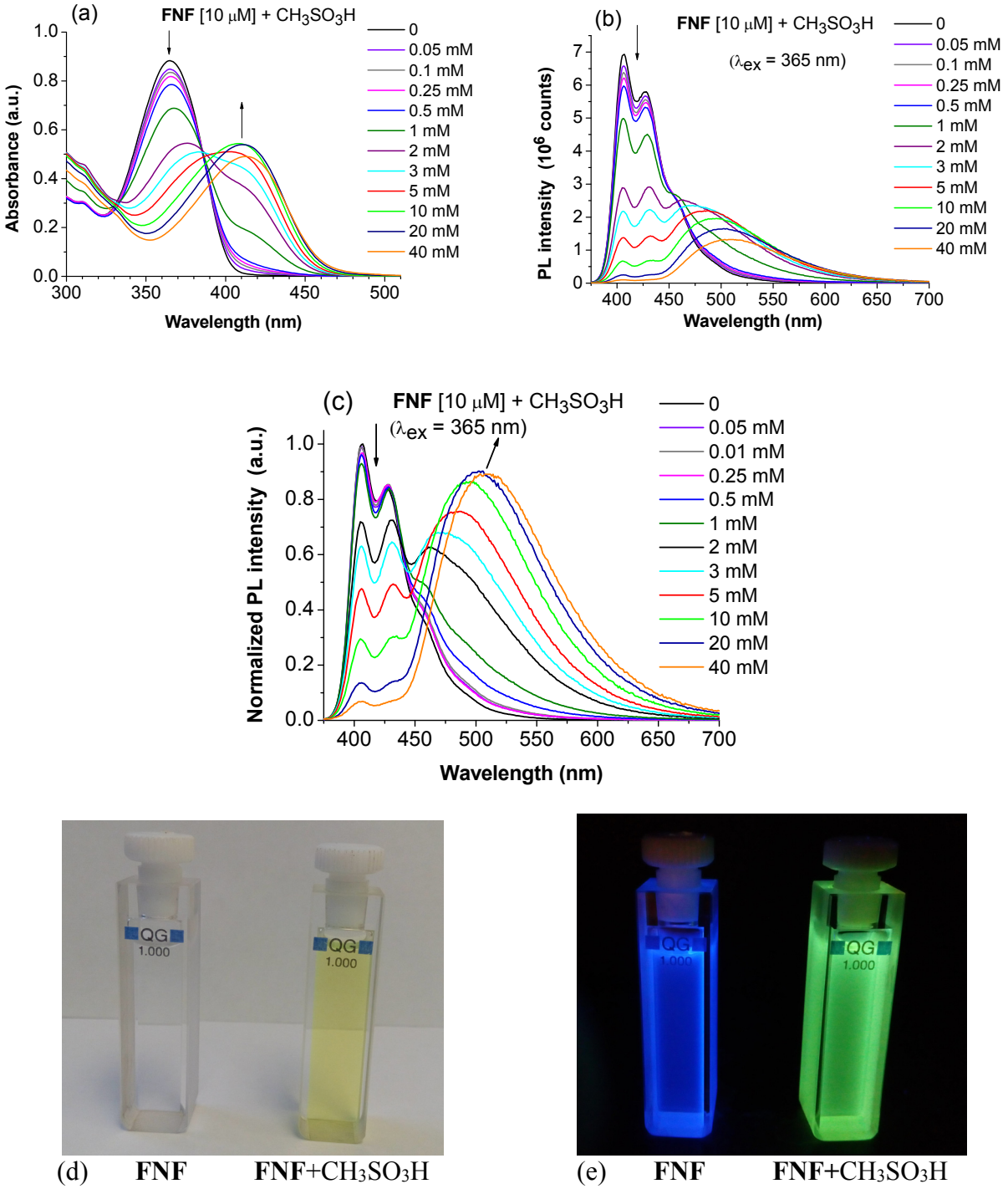

Figure S7 Changes in UV-Vis absorption (a) and photoluminescence (b) spectra of **FNF** [~10 μM] in THF at various concentrations of methanesulfonic acid (0.05 – 40 mM).

(c) As seen in Figure S7b, the intensity of PL (at λ_{PL} = 510 nm) of the protonated **FNF** is lower than PL intensity of the neutral **FNF** (λ_{PL} ~ 410 nm). This is, partially, because the absorption of **FNF** at the excitation wavelength (λ_{ex} = 365 nm) is decreased on protonation (see Figure S7a). Therefore, on the graph (c) we have corrected PL spectra to their absorption intensities at 365 nm: the intensities of PL have been multiplied by [Abs^{365}(**FNF**+CH_3SO_3H)/Abs^{365}(**FNF**)] and normalized to PL intensity of **FNF**.

(d,e) The bottom photographs show changes of the color of **FNF** solution in THF upon addition of a large excess of CH_3SO_3H: (e) under day light illumination [from colorless to light yellow] and (f) under 366 nm UV-lamp irradiation [from deep blue to green fluorescence].

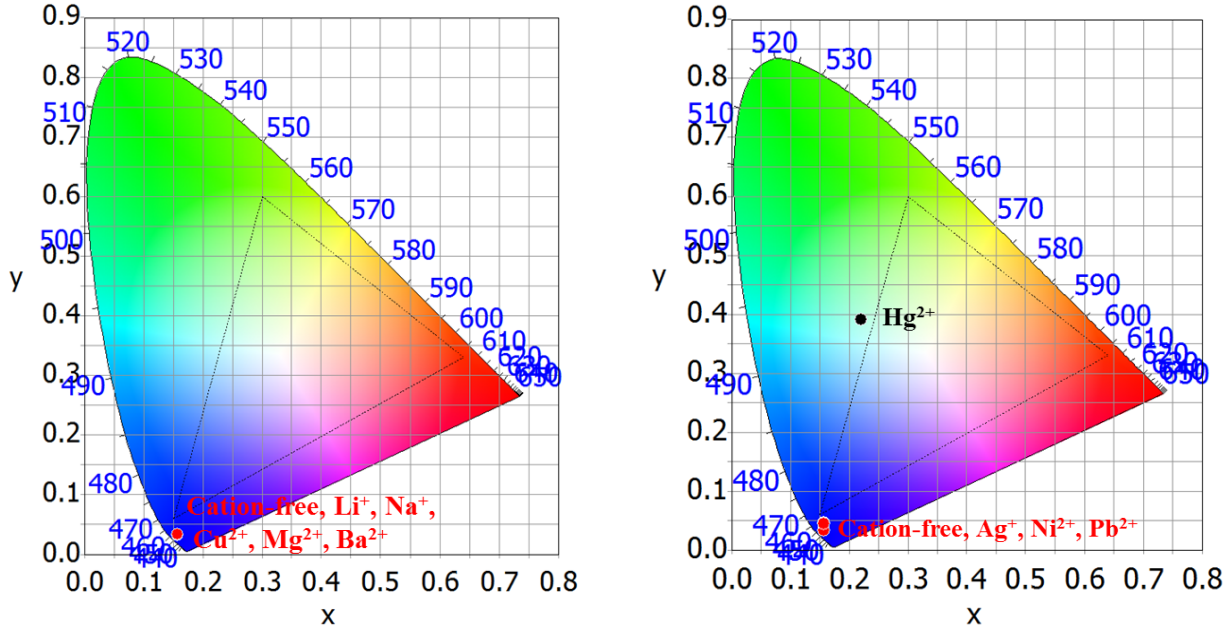

Figure S8. CIE 1931 color space diagrams of the emission spectra of **FNF** [~1.4 μM] solutions in THF in presence of various metal cations [~14 μM]. The PL spectra have been taken from Figures 7b (left diagram) and Figure 7d (right diagram). Triangle corresponds to sRGB gamut.
For PL spectra, excitations are at the wavelengths close to the absorption maxima: λ_{ex} = 365 nm (cation-free, Li^+, Na^+, Cu^{2+}, Mg^{2+}, Ba^{2+}), 367 nm (Ag^+), 371 nm (Ni^{2+}), 379 nm (Pb^{2+}), 395 nm (Hg^{2+}).

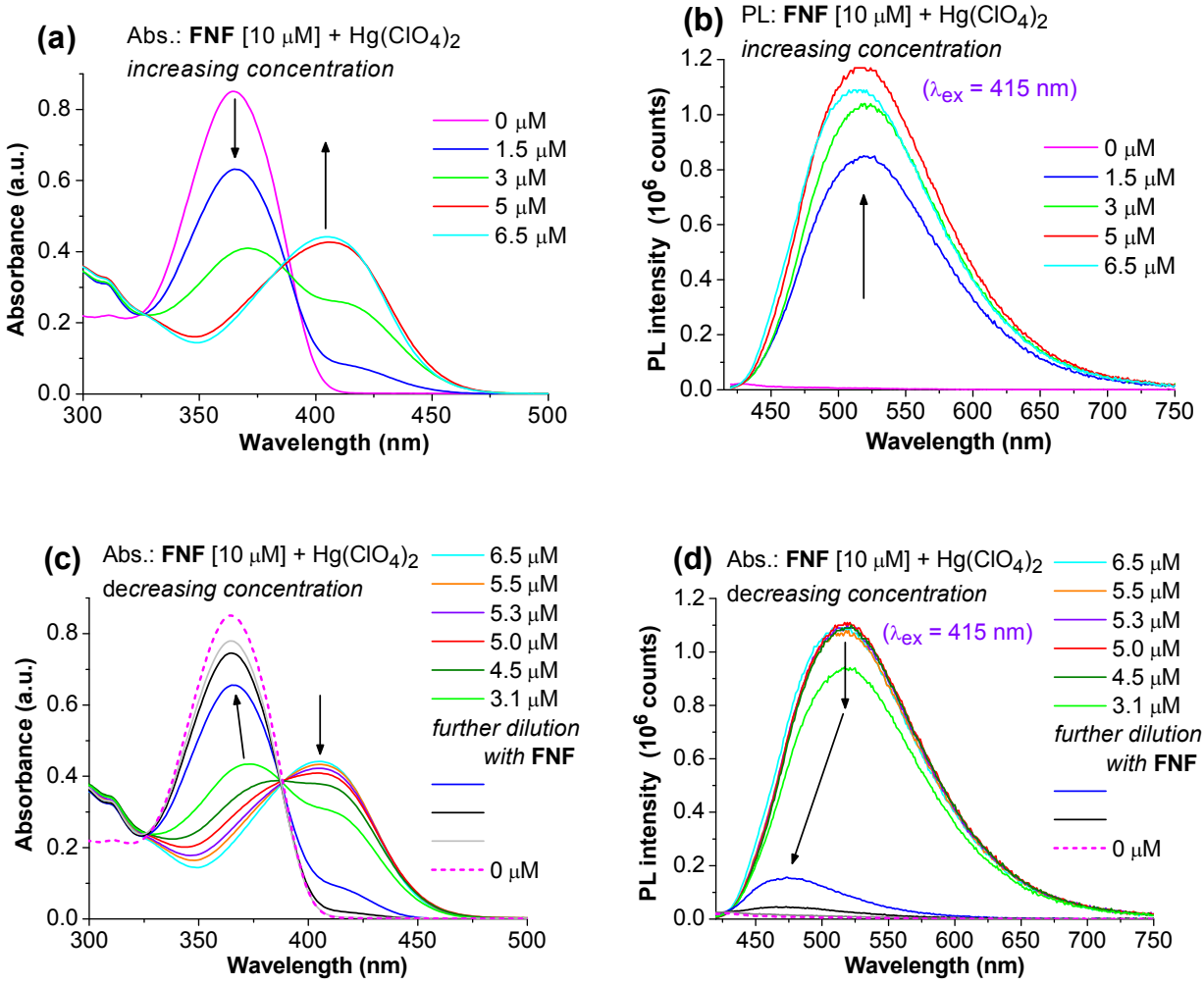

Figure S9. Changes in the absorption (a,c) and photolumionescence (b,d) spectra of **FNF** [~10 μM] solutions in THF in presence of $Hg(ClO_4)_2$ to demonstrate the reversibility of complexation.

(a,b) Concentration of $Hg(ClO_4)_2$ was increased for 0 to 6.5 μM:

(a) an absorption of **FNF** at 365 nm disappear on the cost of an appearance of red-shifted absorption of the complex **FNF**/Hg^{2+} at 405 nm;

(b) no emission is observed for an excitation of **FNF** 415 nm; and addition of $Hg(ClO_4)_2$ results in an appearance of emission at ~515 nm (OFF → ON).

(c,d) The {**FNF** [~10 μM] + $Hg(ClO_4)_2$ [6.5 μM]} from experiments (a,b) was diluted with a solution of **FNF** [~10 μM]. This kept the concentration of **FNF** constand, but the concentration of $Hg(ClO_4)_2$ was decreased from 6.5 μM to <1 μM:

(c) long-wavelength absorption of the complex **FNF**/Hg^{2+} is decreased and an absorption of free **FNF** is growing;

(d) on decrease of the concentration of $Hg(ClO_4)_2$, the emission of the complex is decereased and then disappear.

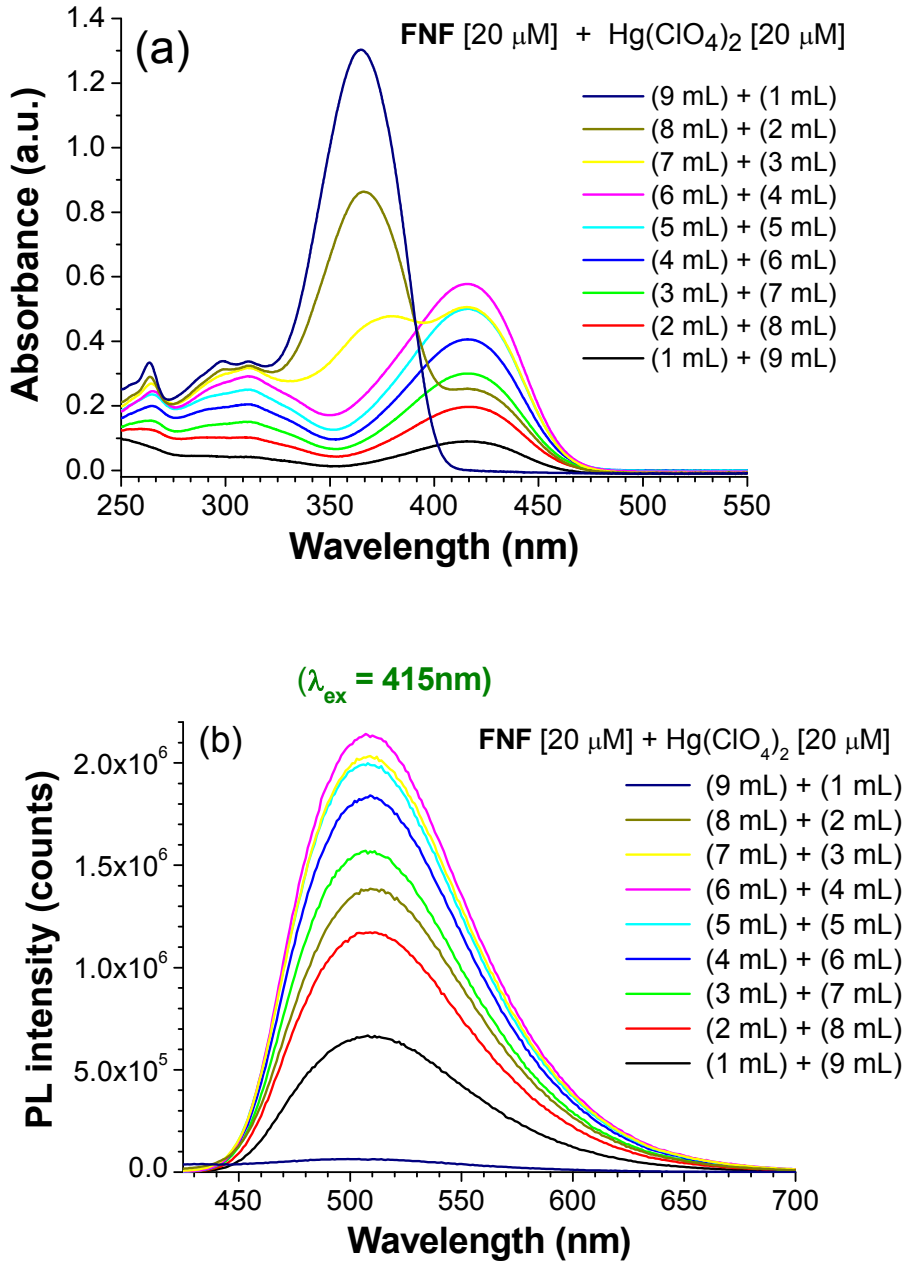

Figure S10. (a) UV-Vis absorption and (b) emission spectra of mixtures of equal concentrations (20 μM each) of **FNF** and $Hg(ClO_4)_2$ in different ratios (in THF) keeping the total volume of the solution
$V_{FNF} + V_{Hg(ClO4)2} = 10$ mL; $\lambda_{ex} = 415$ nm.

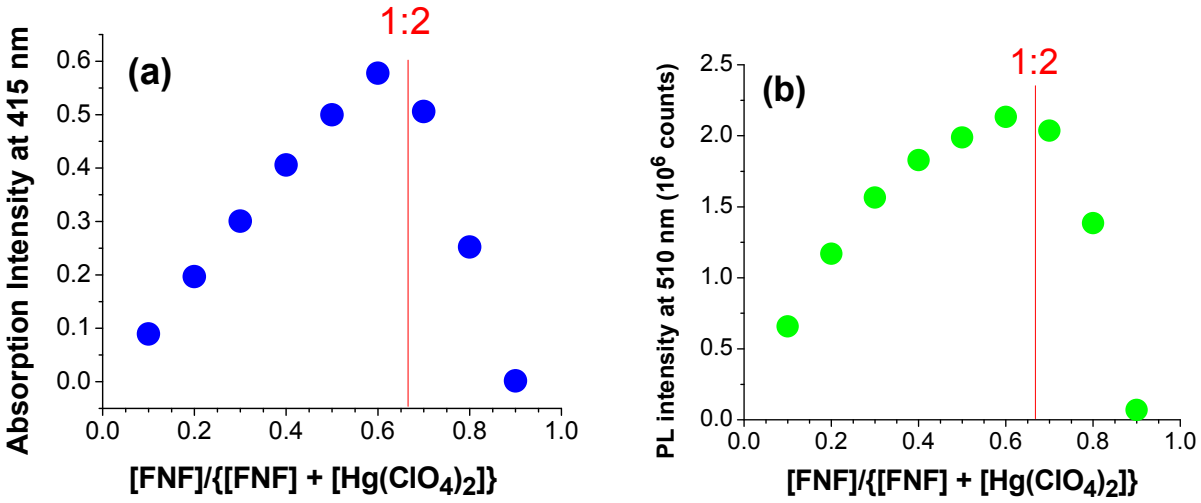

Figure S11. Job's plots for the mixtures of **FNF** (20 μM) and $Hg(ClO_4)_2$ (20 μM) at different ratios in THF: (a) absorption intensities at 415 nm; (b) PL intensities at 510 nm (λ_{ex} = 415 nm). The values have been taken from the data in Figure S5a,b.

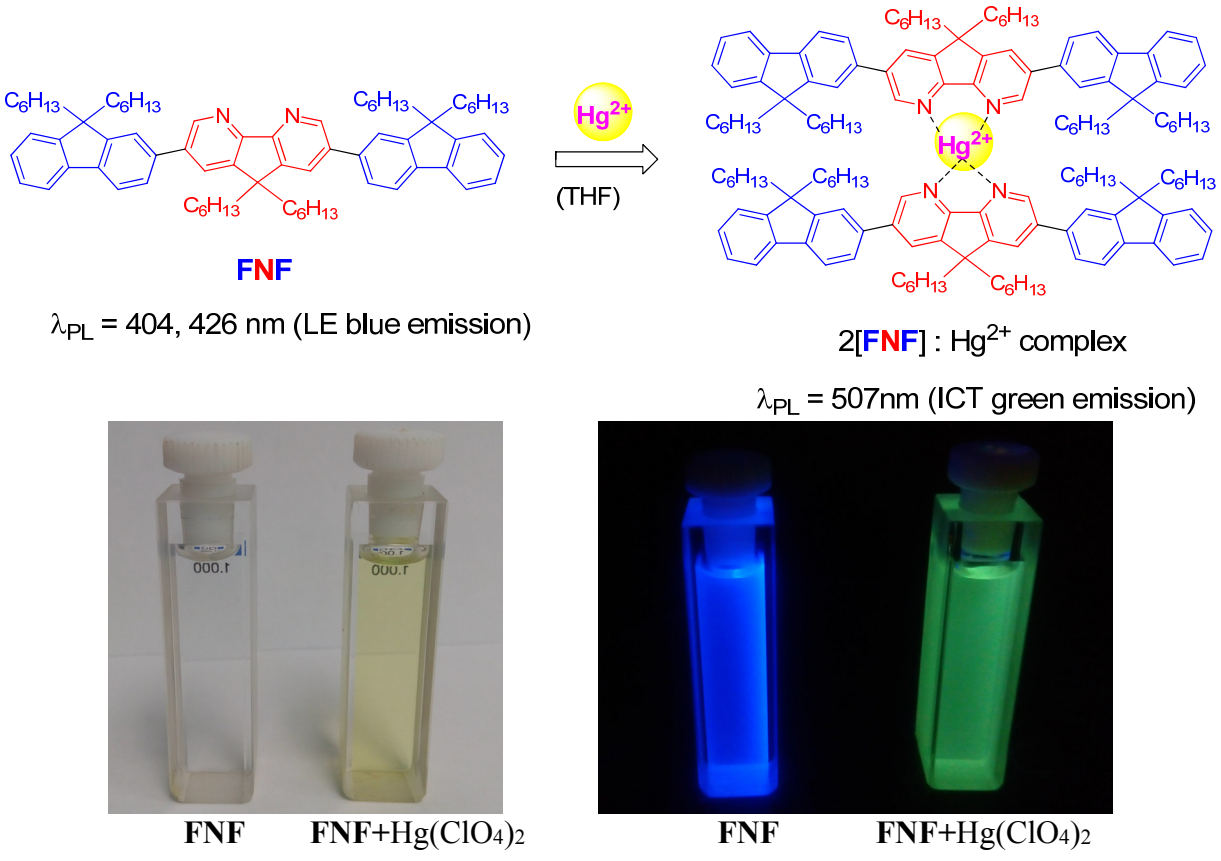

Figure S12. (Top) The reaction scheme of 2[**FNF**]:Hg^{2+} complex formation. (Bottom) The photographs show changes of the color of **FNF** solution in THF upon addition of $Hg(ClO_4)_2$: (left) under day light illumination [from colorless to light yellow] and (right) under 365 nm UV-lamp irradiation [from deep blue to green fluorescence].

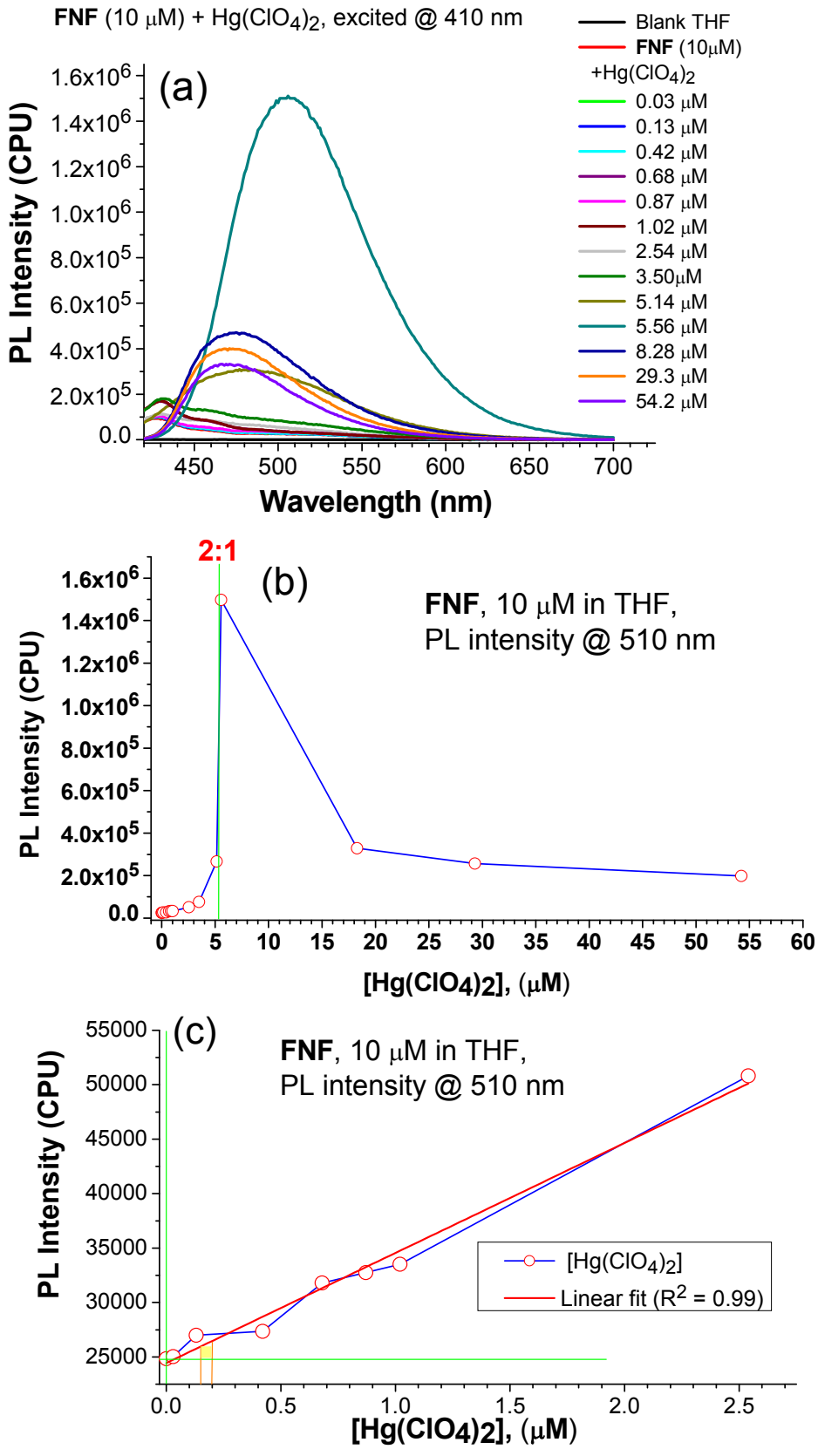

Figure S13 (a) Changes in the photoluminescence spectra of **FNF** (10μM) on titration with $Hg(ClO_4)_2$ (0 - 54.2 μM) in THF (excited at 410 nm). (b) PL intensity measured at 510 nm versus concentration of $Hg(ClO_4)_2$ (0-54.25 μM), (PL_{max} is observed at [**FNF**]:[$Hg(ClO_4)_2$] ~2:1). (c) Linear dependence of the intensity of PL measured at 510 nm versus [$Hg(ClO_4)_2$] at low concentrations of 0 - 2.54 μM.

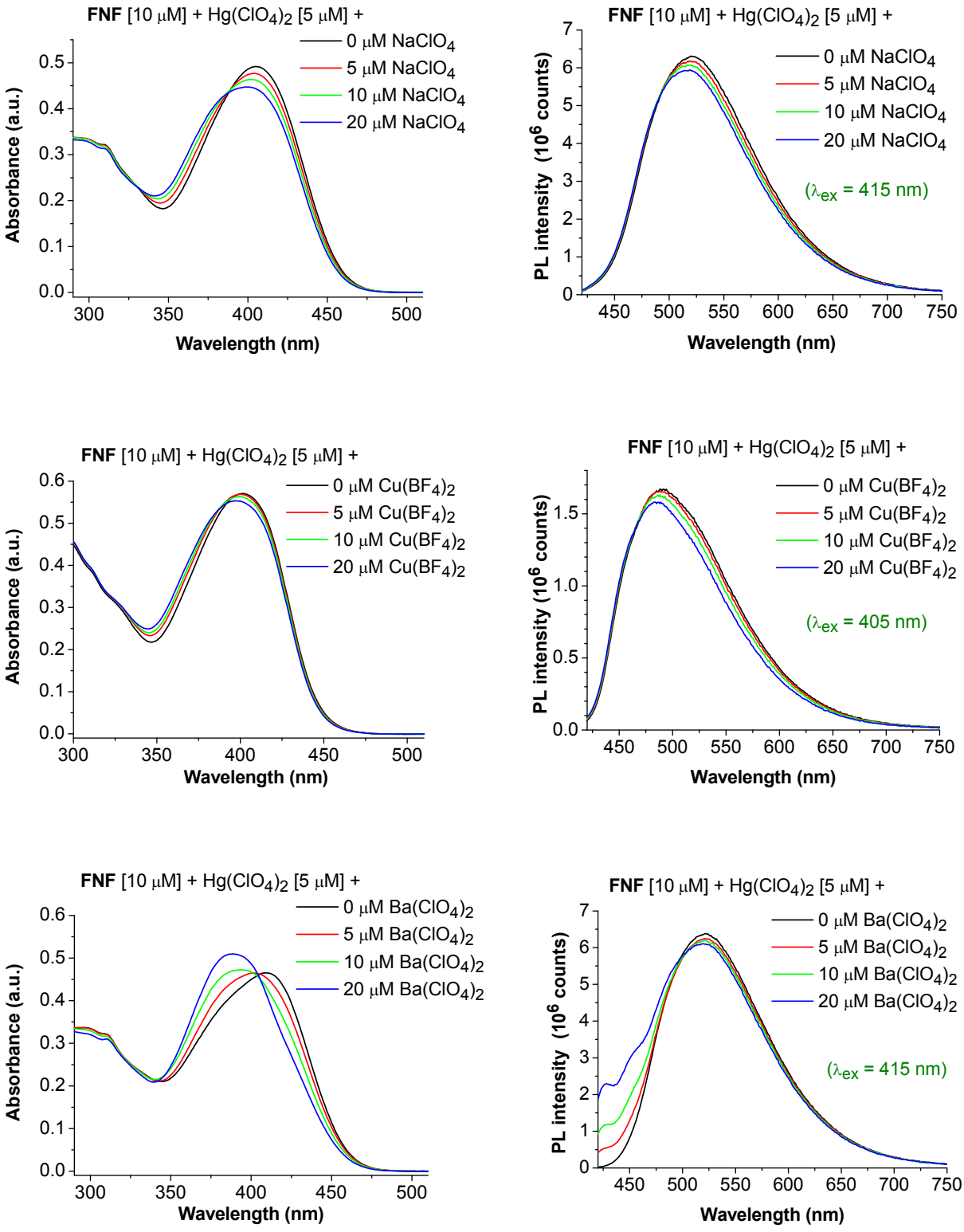

Figure S14 Absorption and photoluminescence spectra of THF solutions of **FNF** [~10 μM] and $Hg(ClO_4)_2$ [~5 μM]} in presence of $NaClO_4$, $Cu(BF_4)_2$ and $Ba(ClO_4)_2$ salts to show the interference of Hg^{2+} detection by other cations (Na^+, Cu^{2+} and Ba^{2+}).

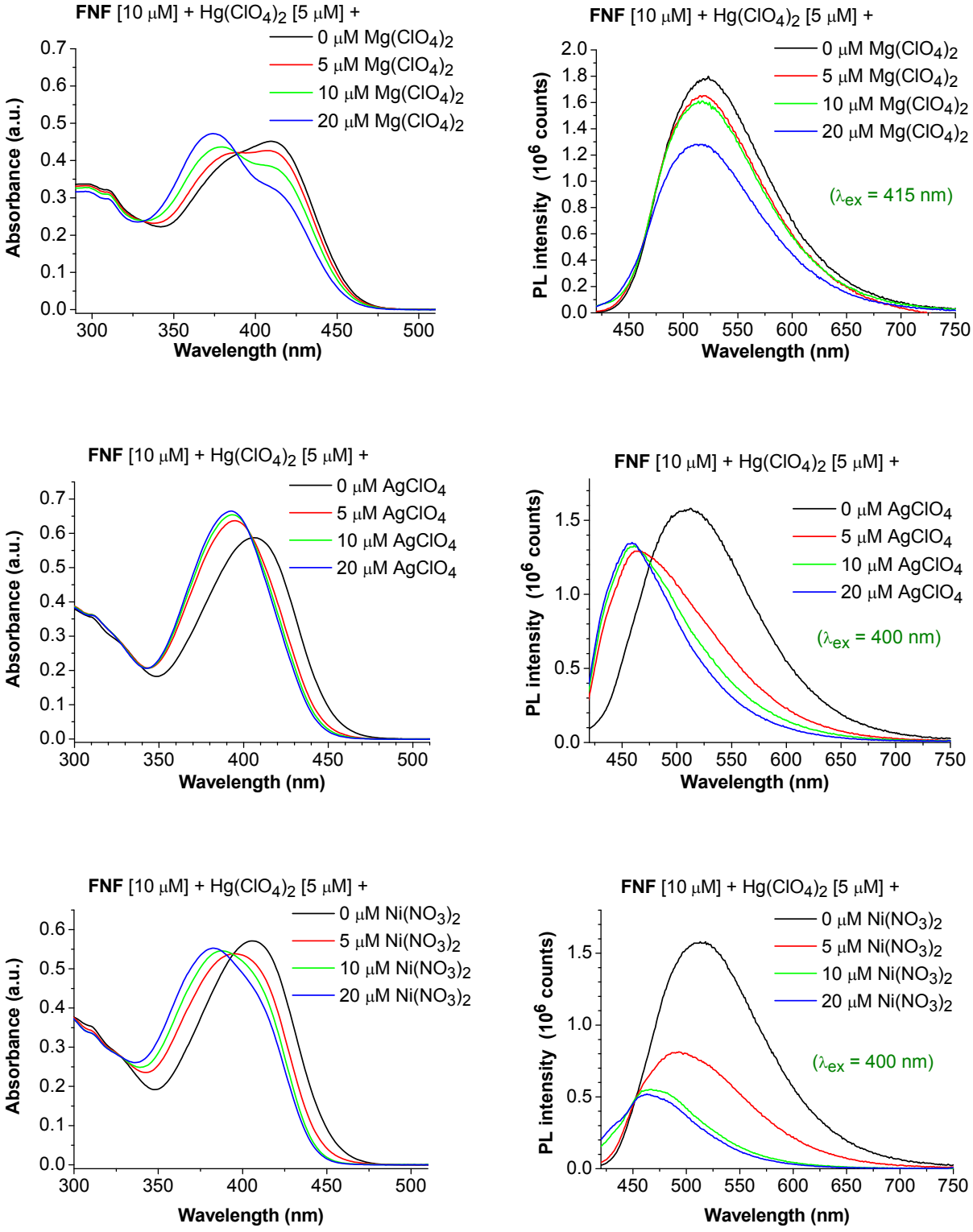

Figure S15 Absorption and photoluminescence spectra of THF solutions of **FNF** [~10 μM] and $Hg(ClO_4)_2$ [~5 μM]} in presence of $Mg(ClO_4)_2$, $AgClO_4$ and $Ni(NO_3)_2$ salts to show the interference of Hg^{2+} detection by other cations (Mg^{2+}, Ag^{+} and Ni^{2+}).

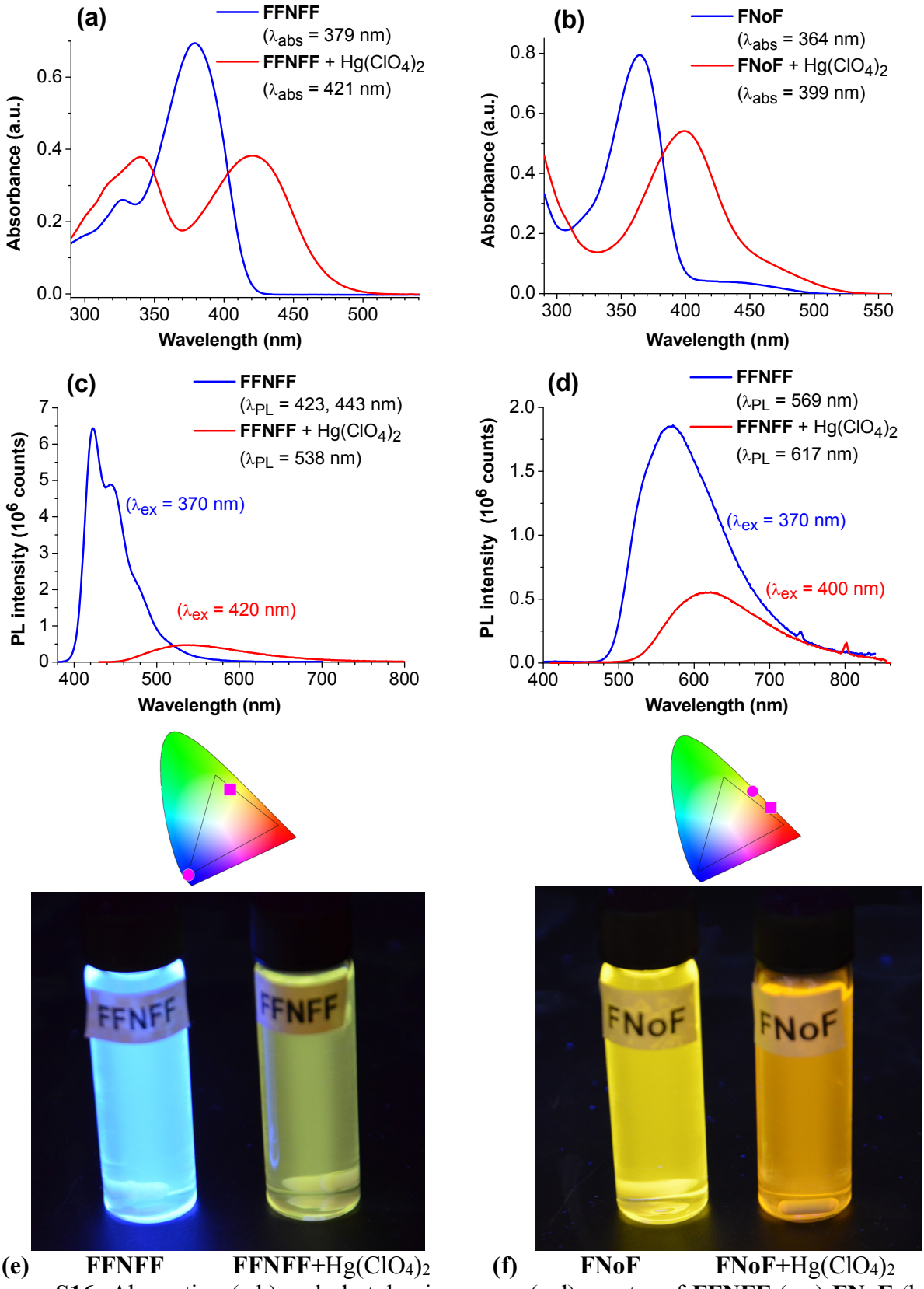

(e) **FFNFF** **FFNFF**+$Hg(ClO_4)_2$ **(f)** **FNoF** **FNoF**+$Hg(ClO_4)_2$

Figure S16 Absorption (a,b) and photoluminescence (c,d) spectra of **FFNFF** (a,c) **FNoF** (b,d) in THF in cation-free solutions and in presence of $Hg(ClO_4)_2$.
The photographs of **FFNFF** (e) and **FNoF** (f) solutions in THF under 365 nm UV-lamp irradiation before (left photographs) and after (right photographs) addition of $Hg(ClO_4)_2$. CIE 1931 color space diagrams on the top of the photographs show the changes of the emission colors (calculated from Figures S16c,d) of **FFNFF** and **FNoF** (circles) upon addition of $Hg(ClO_4)_2$ (squares).

Synthesis

Synthesis of intermediate compounds 1 – 8. 9,9-Dihexylfluoren-2-yl boronic acid **2**,[8] 2,7-dibromo-4,5-diazafluoren-9-one **3**[9], compounds **4,**[8] **5,**[8] and **7**[8] were obtained as described previously. Synthesis of compound **6** and **8** was performed similar to literature procedure[10] with slight modification described below.

2,7-Dibromo-9,9-dihexyfluorene-4,5-diazafluorene (1)

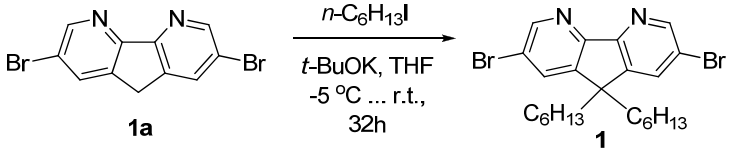

Under nitrogen, to a stirred solution of of 2,7-dibromo-4,5-diazafluorene (**1a**) (1.00 g, 3.06 mmol) in dry THF (20 mL), *n*-iodohexane (0.95 mL, 6.44 mmol) was added at -5 °C. Afterthat, a solution of potassium *tert*-butoxide (720 mg, 6.44 mmol) in dry THF (15 mL) was added over a period of 50 min keeping the temperature at -5 °C. The reaction mixture was allowed to warm up slowly to room temperature and stirred at room temperature for 32 hours. The solvent was removed on rotary evaporator and the residue was purified by column chromatography on silica gel (column size = 2 × 20 cm) eluting with isooctane:ethyl acetate(EA) = 10:1, v/v to afford the crude product (1.21 g) as a yellow solid. The crude product was further purified by recrystallization from a mixture of isopropanol:water, 5:1 (25 mL) to yield compound **1** (1.04g, 69%) as a light yellow solid.

^{1}H NMR (400 MHz, $CDCl_3$): δ (ppm) 8.75 (2H, d, J = 2.0 Hz), 7.84 (2H, d, J = 2.0 Hz), 2.06–1.87 (4H, m, $CH_2C_5H_{11}$), 1.22–0.97 (12H, m, $C_2H_4(CH_2)_3CH_3$), 0.79 (6H, t, J = 7.1 Hz, $C_5H_{10}CH_3$), 0.73–0.60 (4H, m, $CH_2CH_2C_4H_9$).

^{13}C NMR (101 MHz, $CDCl_3$): δ (ppm) 155.93, 150.93, 146.59, 133.50, 120.79, 51.56, 39.01, 31.35, 29.45, 24.01, 22.49, 13.93.

DEPT-135 ^{13}C NMR (101 MHz, $CDCl_3$): δ (ppm) 156.04, 150.93 (CH), 146.59, 133.50 (CH), 120.79, 51.70 (C-9), 39.01 ($CH_2C_5H_{11}$), 31.35 ($C_2H_4CH_2C_3H_7$), 29.45($C_3H_6CH_2C_2H_5$), 24.01 ($CH_2CH_2C_4H_9$), 22.49 ($C_4H_8CH_2CH_3$), 13.93 ($C_5H_{10}CH_3$).

MS (ESI$^+$) *m/z*: 491.97 ([M+H]$^+$, 50%, ^{79}Br/ ^{79}Br), 494.00 ([M+H]$^+$, 100%, ^{79}Br/ ^{81}Br), 495.92 ([M+H]$^+$, 51%, ^{81}Br, ^{81}Br). Calcd. for $C_{23}H_{30}Br_2N_2$: 492.08.

3-(4,4,5,5-Tetramethyl-1,3,2-dioxaborolan-2-yl)dibenzothiophenes-*S,S*-dioxide (6)

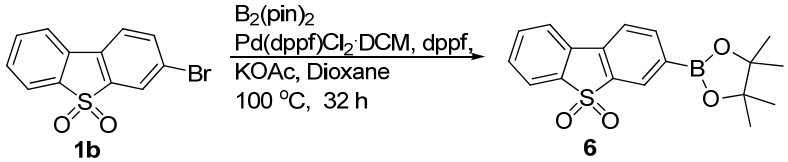

Under argon, a two-necked flask (100 mL) was charged with 3-bromodibenzothiophene-*S,S*-dioxide (**1b**) (1.01 g, 3.39 mmol), bis(pinacolato)diboron (1.29 g, 5.08 mmol), anhydrous KOAc (1.25 g, 12.73 mmol), 1,1′-bis(diphenylphosphino)ferrocene (dppf) (70 mg, 0.13 mmol) and dry dioxane (50 mL). The mixture was degassed by bubbling with argon for 15 minutes before $Pd(dppf)Cl_2 \cdot DCM$ (104 mg, 3 mol%) was added and the mixture was degassed for another 15 minutes. The mixture was heated at 100 °C for 32 hours under argon atmosphere. After cooling to room temperature, the solvent was removed under reduced pressure and the residue was diluted with water (50 mL). The aqueous solution was then extracted with DCM (2 × 50 mL), washed with water (2 × 20 mL) and dried over anhydrous $MgSO_4$. The DCM solution (dark color) was then passed through a short silica gel bed eluting with DCM (100 mL) to give a clear solution which was concentrated to afford the product **6** as an off white solid (1.05 g, 91%). According to ^{1}H NMR, the purity of the sample is >80%, with the main other component being the unreacted excess of bis(pinacolato)diboron. The product was used in the next reaction step without further purification.

^{1}H NMR (400 MHz, $CDCl_3$): δ (ppm) 8.28 (1 H, s), 8.05 (1 H, dd, *J* = 7.7, 0.7 Hz), 7.80 (3 H, m), 7.64 (1 H, td, *J* = 7.7, 1.0 Hz), 7.54 (1H, td, *J* = 7.6, 0.8 Hz), 1.36 (12 H, s).
^{13}C NMR (101 MHz, $CDCl_3$): δ (ppm) 140.12, 138.10, 137.13, 133.81, 133.80, 132.03(br.), 131.54, 130.75, 128.34, 122.16, 121.93, 120.75, 84.56, 24.87.
DEPT-135 ^{13}C NMR (101 MHz, $CDCl_3$): δ (ppm) 140.12(CH), 138.10, 137.13, 133.81(CH), 131.54, 130.75(CH), 128.35(CH), 122.17(CH), 121.93(CH), 120.75(CH), 83.50, 24.87(CH_3).
MS (EI^+) *m/z*: 341.99 ([M]$^+$, 100%). Calcd. for $C_{18}H_{19}BO_4S$: 342.11.

3,7-Bis(4,4,5,5-tetramethyl-1,3,2-dioxaborolan-2-yl)dibenzothiophene-*S,S*-dioxide (8)

Under nitrogen, a two-necked flask (100 mL) was charged with 3,8-dibromodibenzothiophene-*S,S*-dioxide (**1c**)[8] (1.01 g, 2.70 mmol), bis(pinacolato)diboron (1.49 g, 5.88 mmol), anhydrous KOAc (1.57 g, 15.99 mmol), dppf (89 mg, 0.16 mmol) and dry dioxane (50 mL) and degassed with argon for 15 min. Pd(dppf)Cl_2·DCM (131 mg, 0.16 mmol) was added and the mixture was degassed for another 15 min. The mixture was heated at 100 °C for 32 hours under argon atmosphere. After cooling to room temperature, the solvent was removed under reduced pressure and the residue was diluted with water (50 mL). The aqueous solution was extracted with DCM (2 × 50 mL), washed with water (2 × 20 mL) and dried with anhydrous $MgSO_4$. The DCM solution (dark color) was then passed through a short silica gel bed eluting with dichloromethane (100 mL) to give a clear solution which was concentrated to afford the product **8** as an off white solid (1.01 g, 85%).
^{1}H NMR (400 MHz, $CDCl_3$):δ (ppm) 8.28 (1H, s), 8.05 (1H, d, *J* = 8.1 Hz), 7.80 (1H, d, *J* = 7.7 Hz), 1.36 (12H, s).
^{13}C NMR (101 MHz, $CDCl_3$): δ (ppm) 140.05 (CH), 137.50, 133.73, 132.37 (br.), 128.33 (CH), 121.09 (CH), 84.56, 24.87 (CH_3).
DEPT-135 ^{13}C NMR (101 MHz, $CDCl_3$):δ (ppm) (101 MHz, $CDCl_3$) 140.05 (CH), 137.49 , 133.73, 128.33 (CH), 121.09 (CH), 84.56, 24.87 (CH_3).
MS (EI^+) *m/z*: 468.12 ([M]$^+$, 100%). Calcd. for $C_{24}H_{30}B_2O_6S$: 468.19.

Synthesis of the oligomers. *General procedure of Pd-catalyzed C–C coupling in the synthesis of conjugated oligomers: under inert atmosphere, flame heated three-neck flask fitted with argon (or nitrogen inlet) was charged with aryl boronic acid (or ester), arylbromide, base and degassed solvents. The mixture was degassed with argon for 15 minutes before adding Pd catalyst and degassed again for another 15–20 minutes. The degassed mixture was stirred under reflux for a required time. After cooling, the solvent was removed under reduced pressure on a rotary evaporator. The residue was dissolved in EA/DCM, washed with water, dried over $MgSO_4$, and evaporated to afford the crude product, which was then purified by flash/column chromatography on silica gel eluting with appropriate solvents.*

3,7-Bis(9,9-dihexylfluoren-2-yl)-9,9-dihexyl-4,5-diazafluorene (FNF)

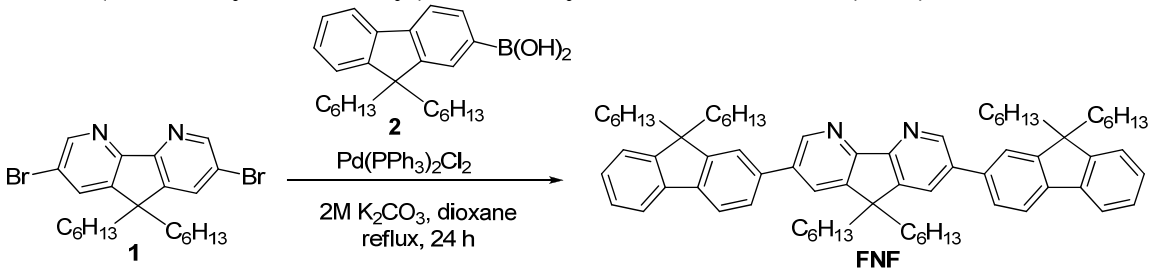

Under nitrogen, to a mixture of 2,7-dibromo-9,9-dihexy-4,5-diazafluorene (**1**) (245 mg, 0.49 mmol), 9,9-dihexylfluorene-2-boronic acid (**2**)[8] (382 mg, 1.01 mmol) and $Pd(PPh_3)_2Cl_2$ (7 mg, 2 mol%), degassed 2M aqueous K_2CO_3 (4 mL, 8 mmol) and 1,4-dioxane (10 mL) were added via syringe. The mixture was stirred under nitrogen with heating at 110 °C (oil bath) for 24 hours with protection from the sunlight. The mixture was cooled down to room temperature and the resulting slurry was poured into 5% NaCl aqueous solution (50 mL). The precipitate was collected by filtration, washed with water (3 × 20 mL), dried *in vacuo* to afford the crude product (448 mg, 88%) as a brown solid. The crude product was purified by column chromatography on silica gel, eluting first with PE to remove byproducts and then with PE:EA mixture, with gradual increase of EA contents from 2% to 6%, to yield product **FNF** (353 mg, 70.5%) as a light yellow solid.

^{1}H NMR (500 MHz, $CDCl_3$): δ (ppm) 9.01 (2H, d, J = 1.9 Hz), 7.93 (2H, d, J = 2.0 Hz), 7.83 (2H, d, J = 7.8 Hz),7.78-7.76 (2H, m), 7.67–7.63 (4H, m), 7.40–7.34 (6H, m), 2.16–2.12 (4H, m), 2.08–2.03 (8H, m), 1.24–1.01 (36H, m), 0.89–0.82 (4H, m) 0.81–0.64 (26H, m).

^{13}C NMR (100 MHz, $CDCl_3$): δ (ppm) 151.92, 151.07, 148.38 (CH), 145.72, 141.47 (× 2), 140.37 (× 2), 136.78, 128.93 (CH), 127.45 (CH), 126.91 (CH), 126.32 (CH), 123.01 (CH), 121.53 (CH), 120.26 (CH), 119.96 (CH), 55.33, 51.63, 40.29, 39.23, 31.44, 31.35, 29.62, 29.52, 24.13, 23.77, 22.52, 22.45, 13.97, 13.93.

DEPT-135 ^{13}C NMR (100MHz, $CDCl_3$): δ (ppm) 151.87, 151.05, 148.72 (CH), 145.42, 141.32, 140.42, 137.05, 136.52, 128.66 (CH), 127.40 (CH), 126.90 (CH), 126.32 (CH), 123.01 (CH), 121.48 (CH), 120.23 (CH), 119.94 (CH), 55.31 (C-9), 40.30, 39.29, 31.46, 31.39, 29.64, 29.56, 24.13, 23.77, 22.54, 22.48, [14.00, 13.96 (CH_3)].

MS (ESI$^+$) *m/z*: 1001.76 ([M + H]$^+$, 100%). Calcd. for $C_{73}H_{96}N_2$: 1000.76.

9,9-Dihexyl-2,7-bis(9,9,9',9'-tetrahexyl-9H,9'H-[2,2'-bifluoren]-7-yl)-*9H*-4,5-diazafluorene (FFNFF)

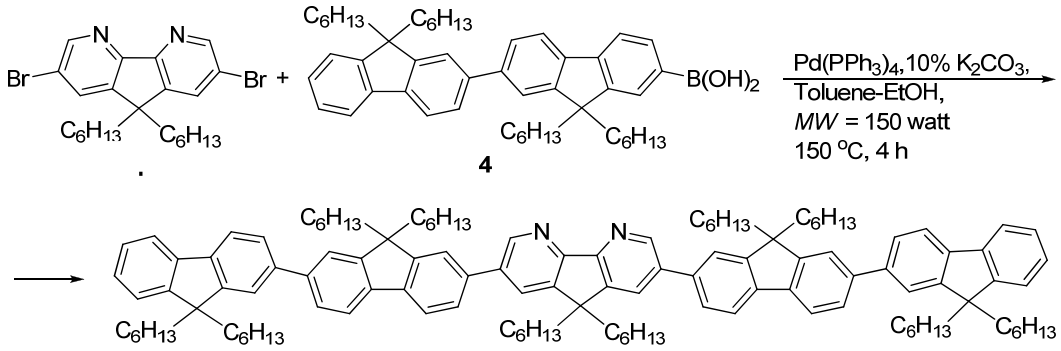

Under nitrogen, to a 35 mL thick-wall glass microwave reaction tube, 2,7-dibromo-9,9-dihexyl-4,5-diazafluorene (**1**) (10 mg, 0.02 mmol), 9,9,9',9'-tetrahexyl-2,2'-bifluoren-7-yl-boronic acid (**4**) (41 mg, 0.057 mmol), $Pd(PPh_3)_4$ (3 mg, 10 mol%), 10% K_2CO_3 aqueous solution (0.5 mL, 0.4 mmol), ethanol (0.5 mL) and toluene (3 mL) were added. The reaction mixture was degassed for 15 minutes with argon and then irradiated with microwave (150 W) keeping the temperature at 150 °C in a microwave reactor for 4 hours. The reaction mixture was cooled down to room temperature and the solvent was evaporated. The residual slurry was poured into 5% NaCl aqueous solution, the product was extracted with chloroform (2 × 15 mL), the combined organic layers were washed with water until pH = 7, dried over anhydrous $MgSO_4$ and the solvent was evaporated to afford the crude product (45 mg) as a yellowish solid. The crude product was purified by flash chromatography on silica gel, eluting first with PE, then with gradient increase to PE:EA, 4:1 to yield pure product **FFNFF** (21 mg, 61%) as a light yellow solid.

^{1}H NMR (400 MHz, $CDCl_3$): δ (ppm) 9.04 (2H, d, J = 1.8 Hz), 7.96 (2H, d, J = 1.8 Hz), 7.89–7.63 (20H, m), 7.39–7.29 (6H, m), 2.18–1.98 (20H, m), 1.22–1.02 (60H, m), 0.92–0.64 (50H, m).

^{13}C NMR (101 MHz, $CDCl_3$): δ 157.22, 152.20, 151.84, 151.52, 151.02, 148.73, 145.55, 141.05, 141.01, 140.76, 140.45, 140.37, 139.57, 137.02, 136.55, 128.68, 127.05, 126.81, 126.44, 126.28, 126.07, 122.95, 121.61, 121.59, 121.46, 120.32, 120.20, 119.92, 119.75, 55.48, 55.19, 51.51, 40.38, 40.29, 39.32, 31.48, 31.44, 31.41, 29.70, 29.61, 29.58, 24.16, 23.85, 23.79, 22.57, 22.54, 22.50, 14.02, 13.98.
DEPT-135 ^{13}C NMR (101 MHz, $CDCl_3$): δ 157.21, 152.20, 151.84, 151.52, 151.02, 148.73 (CH), 145.55, 141.05, 141.01, 140.76, 140.45, 140.37, 139.57, 137.02, 136.55, 128.6 8 (CH), 127.05 (CH), 126.81 (CH), 126.44 (CH), 126.27 (CH), 126.07 (CH), 122.95 (CH), 121.60 (CH), 121.59 (CH), 121.46 (CH), 120.32 (CH), 120.20 (CH), 119.92 (CH), 119.75 (CH), [55.48, 55.19 (C-9)], 51.51 (CH_2) [40.38, 40.29, 39.32 (CH_2)], [31.48, 31.44, 31.41 (CH_2)], [29.70, 29.61, 29.58 (CH_2)],[24.16, 23.85, 23.79 (CH_2)], [22.57, 22.54, 22.50 (CH_2)], [14.02, 13.98 (CH_3)].
MS (MALDI TOF) *m/z*: 1666.81 ([M + H]$^+$, 100%). Calcd. for $C_{123}H_{160}N_2$: 1665.26.

3,7-Bis(9,9-dihexylfluoren-2-yl)-4,5-diazafluoren-9-one (FNoF)

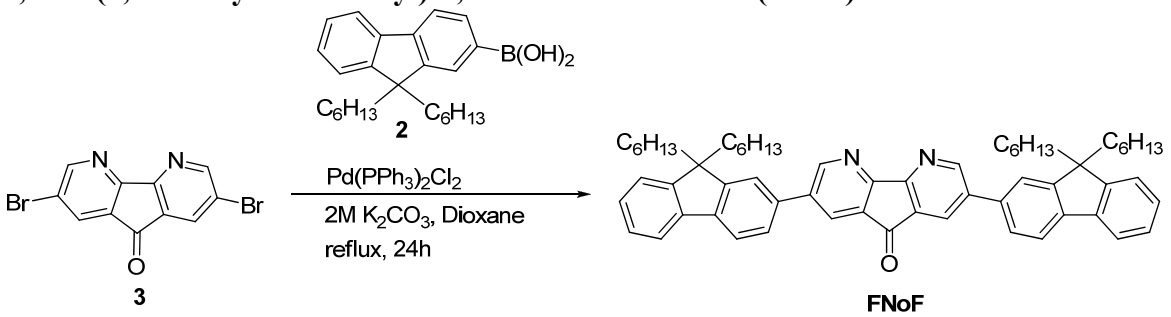

Under nitrogen, to a three-necked flask containing 2,7-dibromo-4,5-diazafluoren-9-one (**3**) (201 mg, 0.581 mmol), 9,9-dihexylfluoren-2-boronic acid (**2**)[8] (453 mg, 1.20 mmol) and $Pd(PPh_3)_2Cl_2$ (9 mg, 2 mol%), degassed 2M aqueous K_2CO_3 (4 mL, 8 mmol) and 1,4-dioxane (10 mL) were added via a syringe. The reaction mixture was stirred under reflux (oil bath, 110 °C) for 24 hours under nitrogen, with protection from the sunlight. The reaction mixture was cooled down to room temperature and the resulting slurry was poured into 5% NaCl aqueous solution. The product was extracted with DCM (2 × 25 mL), the combined organic layer was washed with water until pH = 7, dried over anhydrous $MgSO_4$, filtered off and the solvent was evaporated to afford the crude product (405 mg, 79%) as a yellow solid. The crude product was purified by flash chromatography on silica gel, eluting first with PE and then with PE:DCM mixture (gradient from 1:1 to 1:4 v/v ratio) to yield pure product **FNoF** (252 mg, 49%) as a yellow solid.
^{1}H NMR (400 MHz, $CDCl_3$): δ (ppm) 9.12 (2H, d, *J* = 2.1 Hz), 8.28 (2H, *J* = 2.1 Hz, s), 7.83 (2H, d, *J* = 7.9 Hz), 7.77–7.75 (2H, *m*), 7.65 (2H, dd, *J* = 7.8, 1.5 Hz), 7.60 (2H, d, *J* = 1.2 Hz), 7.40–7.36 (6H, m), 2.06–2.02 (8H, m, $CH_2C_5H_{11}$), 1.13–1.02 (24H, m, $C_2H_4(CH_2)_3CH_3$), 0.77 (12H, t, *J* = 6.8 Hz, CH_3), 0.70–0.61 (8H, m, $CH_2CH_2C_4H_9$).
^{13}C NMR (100MHz, $CDCl_3$): δ (ppm) 190.18 (CO), 161.71, 153.77 (CH), 152.08, 151.07, 142.18, 140.15, 138.50, 135.23, 130.02, 129.65 (CH), 127.72 (CH), 126.98 (CH), 125.95 (CH), 123.00 (CH), 121.27 (CH), 120.48 (CH), 120.11 (CH), 55.38 (C-9), 40.39, 31.49, 29.66, 23.79, 22.56, 13.99 (CH_3).
DEPT-135 ^{13}C NMR (100MHz, $CDCl_3$): δ (ppm) 161.73, 153.79 (CH), 152.09, 151.08, 142.18, 140.16, 138.51, 135.25, 130.03, 129.66 (CH), 127.72 (CH), 126.99 (CH), 125.95 (CH), 123.01 (CH), 121.28 (CH), 120.48 (CH), 120.11 (CH), 55.39 (C-9), 40.40 (CH_2), 31.49 (CH_2), 29.67 (CH_2), 23.79 (CH_2), 22.57 (CH_2), 14.00 (CH_3).
MS (ESI$^+$) *m/z*: 847.55 ([M+H]$^+$, 100%). Calcd. for $C_{61}H_{70}N_2O$: 846.55.

3,7-Bis(9,9-dioctyl-4,5-diazafluoren-2-yl)dibenzothiophene-*S,S*-dioxide (NSN)

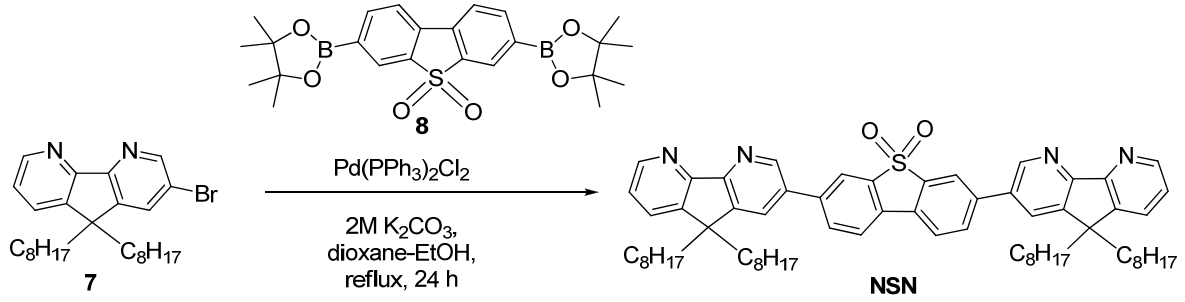

Under nitrogen, to a three-necked flask containing 2-bromo-9,9-dioctyl-4,5-diazafluorene (**7**) (402 mg, 0.854 mmol), 3,7-bis(4,4,5,5-tetramethyl-1,3,2-dioxaborolan-2-yl)dibenzothiophene-*S,S*-dioxide (**8**) (200 mg, 0.427 mmol), 2M aqueous K_2CO_3 (4 mL, 8 mmol), 1,4-dioxane (20 mL) and ethanol (2 mL) were added. The mixture was degassed with argon for 15 minutes before adding $Pd(PPh_3)_2Cl_2$ (10 mg, 0.014 mmol, 3 mol%) and then degassed for another 15 minutes. The mixture was stirred under reflux (oil bath, 115 °C) for 24 hours under nitrogen atmosphere. After cooling to room temperature, the solvent was evaporated under reduced pressure on a rotavapor. The residue was dissolved in ethyl acetate (100 mL), washed with water (2 × 50 mL), dried over anhydrous $MgSO_4$, filtered off and evaporated to afford the crude product (788 mg) as a brown oil. The crude product was purified by flash chromatography on silica gel eluting with PE:EA (gradient from 1:1 to 1:9) to afford pure oligomer **NSN** as a yellow solid (152 mg, 59%).

^{1}H NMR (400 MHz, $CDCl_3$): δ (ppm) 9.00 (2H, d, *J* = 2.0 Hz), 8.74 (2H, dd, *J* = 4.8, 1.2 Hz), 8.16 (2H, d, *J* = 0.8), 8.05–7.99 (4H, m), 7.95 (2H, d, *J* = 2.0 Hz), 7.76 (2H, dd, *J* = 7.6, 1.2 Hz), 7.33 (2H, dd, *J* = 7.6, 4.8 Hz), 2.10-2.06 (8H, m, $CH_2C_7H_{15}$), 1.25–0.98 (40H, m, $C_2H_4(CH_2)_5CH_3$), 0.81 (12H, t, *J* = 7.2 Hz, $C_7H_{14}CH_3$), 0.72–0.66 (8H, m, $CH_2CH_2C_6H_{13}$).

^{13}C NMR (100MHz, $CDCl_3$): δ (ppm) 159.01, 157.78, 149.88 (CH), 148.18 (CH), 145.64, 145.55, 141.17, 139.00, 133.65, 132.87 (CH), 130.79, 130.65 (CH), 128.69 (CH), 123.37 (CH), 122.52 (CH), 121.03 (CH), 51.66 (C-9), 39.31 (CH_2), 31.72 (CH_2), 29.90 (CH_2), 29.18 (CH_2), 29.14 (CH_2), 24.16 (CH_2), 22.58 (CH_2), 14.05 (CH_3).

DEPT-135 ^{13}C NMR (100 MHz, $CDCl_3$): δ (ppm) 159.01, 157.82, 149.91 (CH), 148.20 (CH), 145.61, 145.52, 141.19, 138.98, 133.63, 132.86 (CH), 130.76, 130.64 (CH), 128.66 (CH), 123.35 (CH), 122.51 (CH), 121.03 (CH), 51.66 (C-9), 39.35 (CH_2), 31.72 (CH_2), 29.18 (CH_2), 29.14 (CH_2), 24.16 (CH_2), 22.57 (CH_2), 14.05 (CH_3).

MS (ESI^+) *m/z*: 1020.42 ($[M+Na]^+$, 100%). Calcd. for $C_{66}H_{84}N_4O_2S$: 996.63.

2,7-Bis(dibenzothiophene-*S,S*-dioxide-3-yl)-4,5-diazfluorene (SNS)

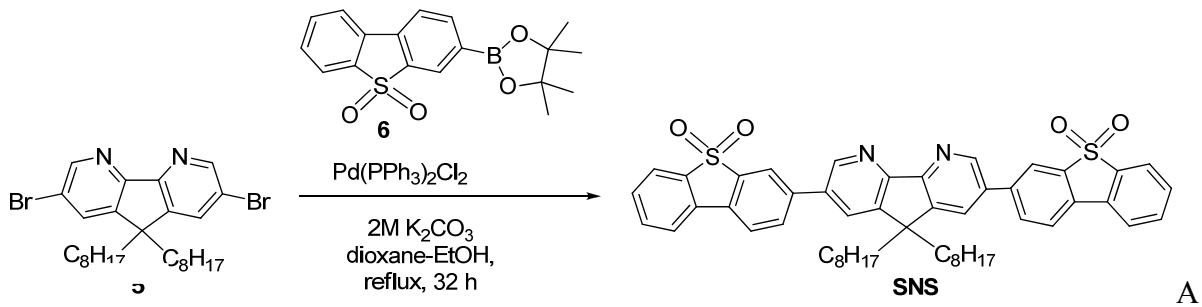

A three-necked flask (50 mL) was charged with 2,7-dibromo-9,9-dioctyl-4,5-diazafluorene (**5**) (150 mg, 0.272 mmol), 3-(4,4,5,5-tetramethyl-1,3,2-dioxaborolan-2-yl)dibenzothiophene-*S,S*-dioxide (**6**) (373 mg, 1.090 mmol), 2M aqueous K_2CO_3 (4 mL, 8 mmol), dioxane (20 mL) and ethanol (4 mL) and degassed with argon for 15 minutes. Then $Pd(PPh_3)_2Cl_2$ (6 mg, 0.008 mmol) was added and the mixture was degassed for another 15 minutes. The mixture was stirred under reflux (oil bath, 115 °C) for 32 hours under nitrogen atmosphere. After cooling to room temperature, the mixture was diluted with water (15 mL) and then extracted with DCM (2 × 100 mL). The combined DCM layers

were washed with water (2 × 20 mL), dried with anhydrous $MgSO_4$, filtered off and evaporated on a rotavapor to afford the crude product (580 mg) as a brown oil. The crude product was purified by flash chromatography on silica gel eluting with DCM:MeOH mixture (gradient ratio of 100:1 to 100:2) to afford pure oligomer **SNS** as an off yellow solid (60 mg, 26%).

^{1}H NMR (400 MHz, $CDCl_3$): δ (ppm) 9.03 (2H, d, J = 1.9 Hz), 8.15 (2H, d, J = 1.1 Hz), 8.00–7.95 (6H, m), 7.89 (4H, d, J = 8.0 Hz), 7.72 (2H, t, J = 7.5 Hz), 7.60 (2H, t, J = 7.6 Hz), 2.16–2.12 (4H, m, $CH_2C_7H_{15}$), 1.24–0.98 (20H, m, $C_2H_4(CH_2)_5CH_3$), 0.79 (6H, t, J = 6.0 Hz, $C_7H_{14}CH_3$), 0.78–0.69 (4H, m, $CH_2CH_2C_6H_{13}$).

^{13}CNMR (100MHz, $CDCl_3$): δ (ppm) 158.14, 148.50 (CH), 146.13, 140.72, 138.92, 137.92, 134.15, 134.12 (CH), 132.66 (CH), 131.22, 131.18, 130.68 (CH), 128.78 (CH), 122.41(CH), 122.34 (CH), 121.87 (CH), 120.91 (CH), 51.94, 39.39 (CH_2), 31.63 (CH_2), 29.92 (CH_2), 29.19 (CH_2), 29.16 (CH_2), 24.30 (CH_2), 22.57 (CH_2), 14.04 (CH_3).

DEPT-135 ^{13}C NMR (100MHz, $CDCl_3$): δ (ppm) 158.14, 148.50 (CH), 146.13, 140.73, 138.92, 137.92, 134.16, 134.12 (CH), 132.70 (CH), 131.19, 130.69 (CH), 128.79 (CH), 122.42 (CH), 122.33 (CH), 121.86 (CH), 120.92 (CH), 51.94, 39.39 (CH_2), 31.70 (CH_2), 29.92 (CH_2), 29.19 (CH_2), 29.17 (CH_2), 24.29 (CH_2), 22.57 (CH_2), 14.04 (CH_3).

MS (ESI$^+$) *m/z*: 843.39 ([M+Na]$^+$, 100%). Calcd. for $C_{51}H_{52}N_2O_4S_2$: 820.34.

References

1 (a) Y. Yang, Q. Pei, and A. J. Heeger, *J. Appl. Phys*., 1996, **79**, 934; (b) J. Stamplf, S. Tasch, G. Leising, and U. Scherf, *Synth. Met*., 1995, **71**, 2125–2128.

2 S. Hamai and F. Hirayama, *J. Phys. Chem.,* **1983**, *87*, 83–89.

3 C. Y. Huang, *Methods in Enzymology*, 1982, **87**, 509–525.

4 P. Job, *Annali di Chimica Applicata*, 1928, **9**, 113–203.

5 Gaussian 09, Revision A02, M. J. Frisch, G. W. Trucks, H. B. Schlegel, G. E. Scuseria, M. A. Robb, J. R. Cheeseman, G. Scalmani, V. Barone, B. Mennucci, G. A. Petersson, H. Nakatsuji, M. Caricato, X. Li, H. P. Hratchian, A. F. Izmaylov, J. Bloino, G. Zheng, J. L. Sonnenberg, M. Hada, M. Ehara, K. Toyota, R. Fukuda, J. Hasegawa, M. Ishida, T. Nakajima, Y. Honda, O. Kitao, H. Nakai, T. Vreven, J. A. Montgomery Jr., J. E. Peralta, F. Ogliaro, M. J. Bearpark, J. Heyd, E. N. Brothers, K. N. Kudin, V. N. Staroverov, R. Kobayashi, J. Normand, K. Raghavachari, A. P. Rendell, J. C. Burant, S. S. Iyengar, J. Tomasi, M. Cossi, N. Rega, N. J. Millam, M. Klene, J. E. Knox, J. B. Cross, V. Bakken, C. Adamo, J. Jaramillo, R. Gomperts, R. E. Stratmann, O. Yazyev, A. J. Austin, R. Cammi, C. Pomelli, J. W. Ochterski, R. L. Martin, K. Morokuma, V. G. Zakrzewski, G. A. Voth, P. Salvador, J. J. Dannenberg, S. Dapprich, A. D. Daniels, Ö. Farkas, J. B. Foresman, J. V. Ortiz, J. Cioslowski and D. J. Fox, Gaussian, Inc., Wallingford CT, 2009.

6 (a) A. D. Becke, *Phys. Rev. A*, 1988, **38**, 3098–3100. (b) A. D. Becke, *J. Chem. Phys.,* 1993, **98**, 5648–5652.

7 C. Lee, W. Yang and R. G. Parr, *Phys. Rev. B*, 1988, **37**, 785–789.

8 I. I. Perepichka, I. F. Perepichka, M. R. Bryce and L.-O. Pålsson, *Chem. Commun.,* 2005, 3397–3339.

9 (a) J. Mlochoski and Z. Szulc, *J. Prakt. Chem*., 1980, **322**, 971; (b) W.-J. Li, H.-M. Wu, Y.-B. Li, C.-P. Hu, M.-D. Yi, L.-H. Xie, L. Chen, J.-F. Zhao, X.-H. Zhao, N.-E. Shi, Y. Qian, C. Wang, W. Wei, and W. Huang, *Tetrahedron*, 2012, **68**, 8216–8221.

10 K. C. Moss, K. N. Bourdakos, V. Bhalla, K. T. Kamatekar, M. R. Bryce, M. A. Fox, H. L. Vaughan, F. B. Dias and A. P. Monkman, *J. Org. Chem.*, 2010, **75**, 6771–6781.

^{1}H NMR (400 MHz, $CDCl_3$) of FNF

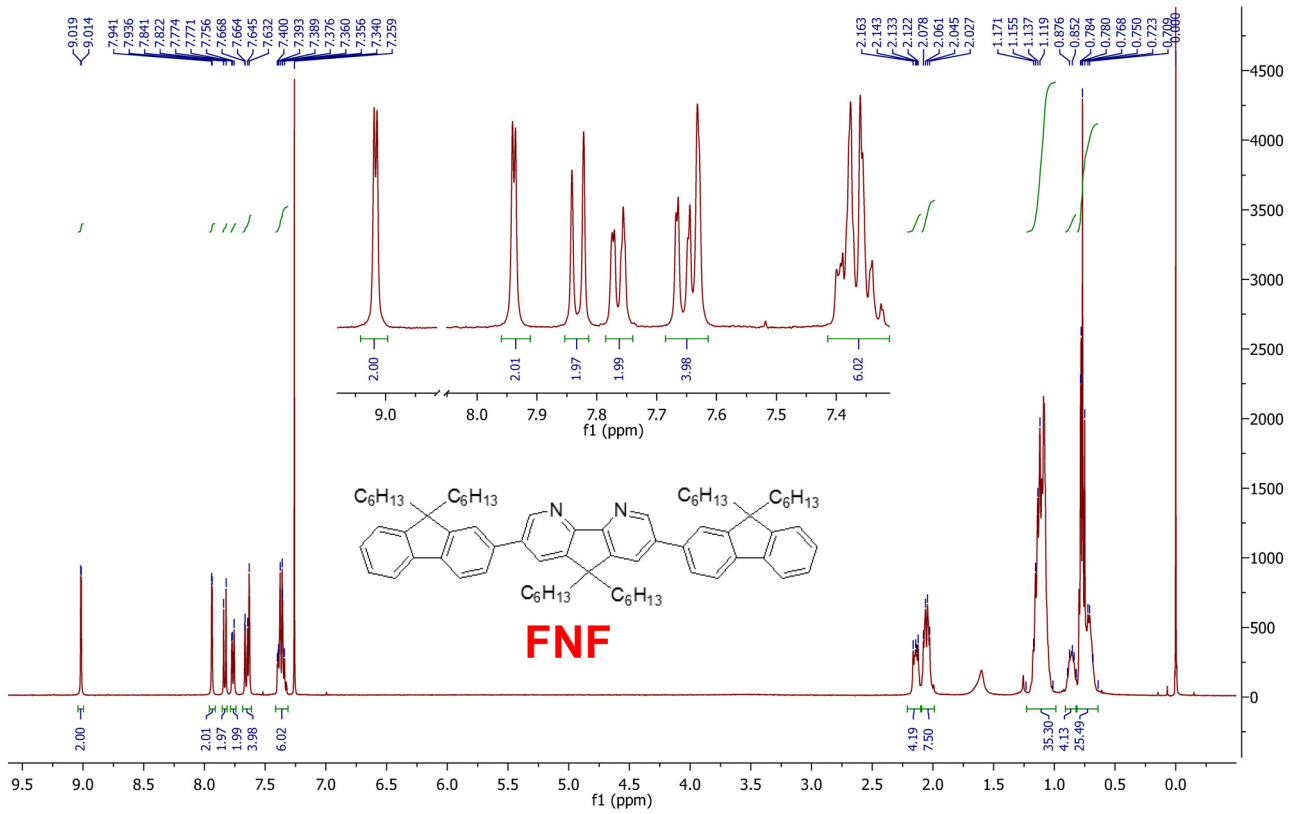

^{13}C NMR (100 MHz, $CDCl_3$) of FNF

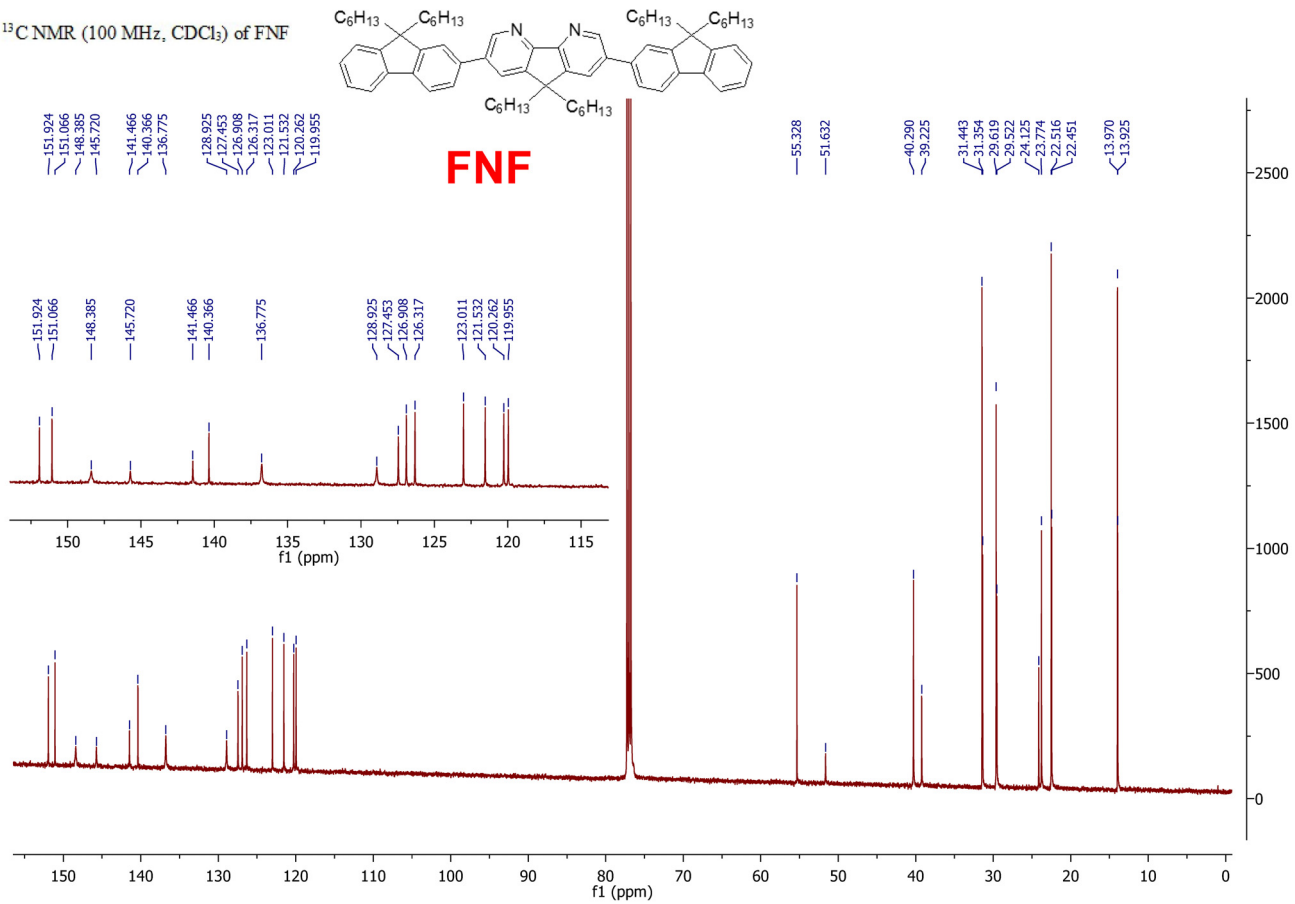

DEPTQ NMR (100MHz, $CDCl_3$) of FNF

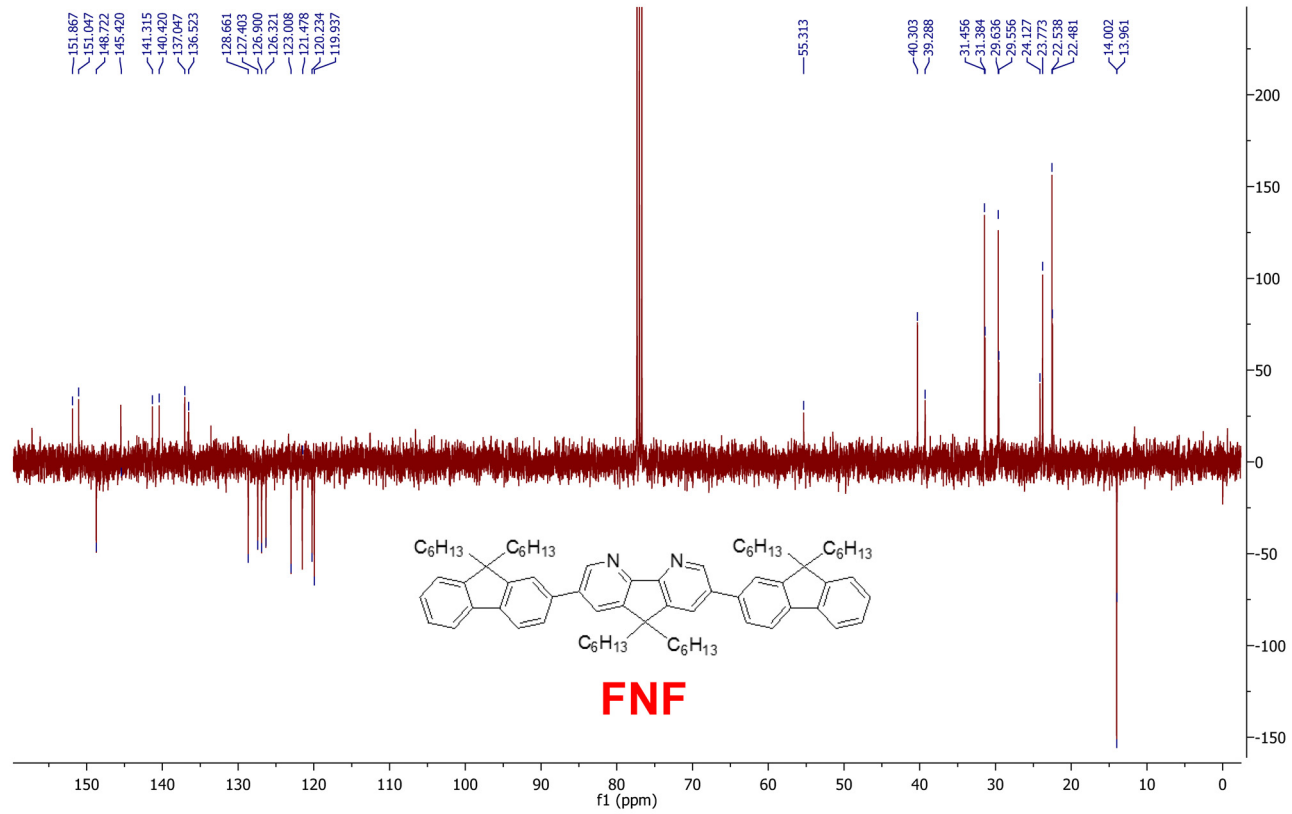

^{1}H NMR (400 MHz, $CDCl_3$) of FNoF

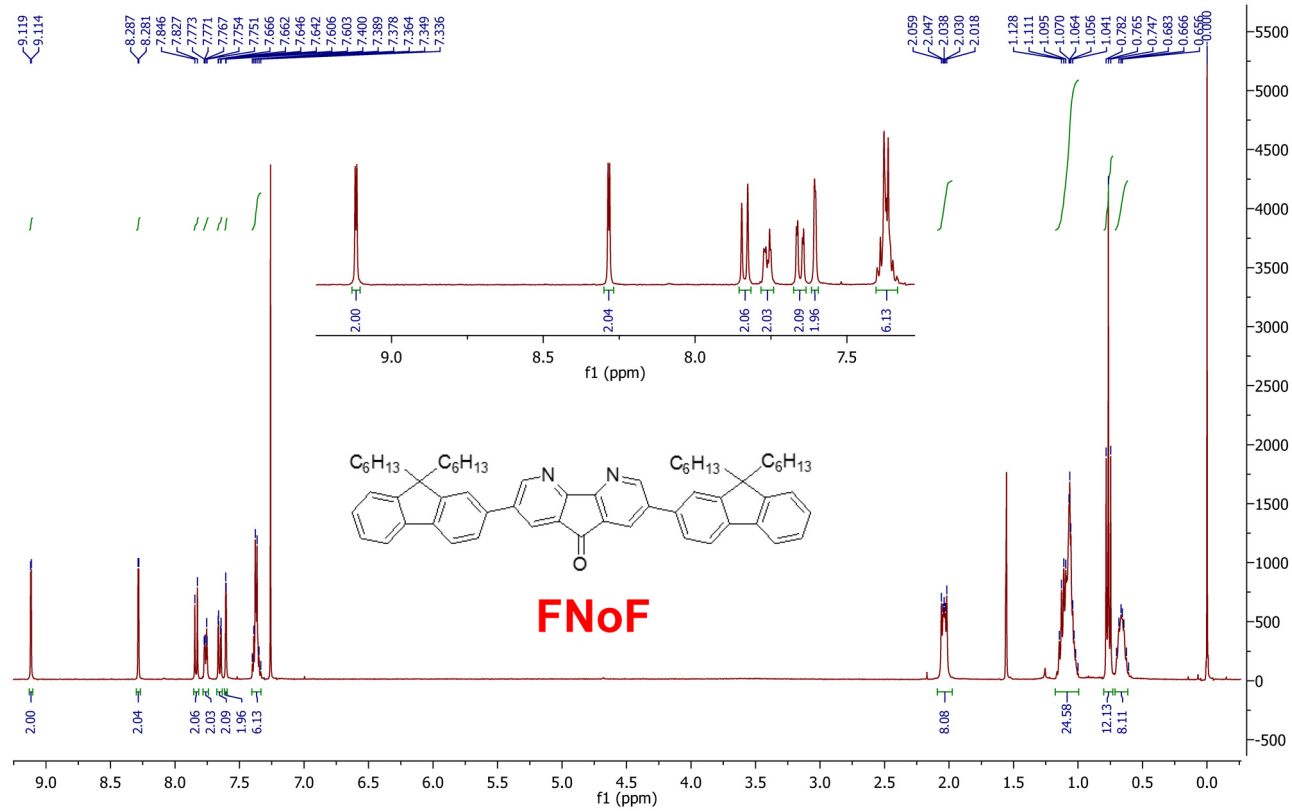

^{13}C NMR (100 MHz, $CDCl_3$) of FNoF

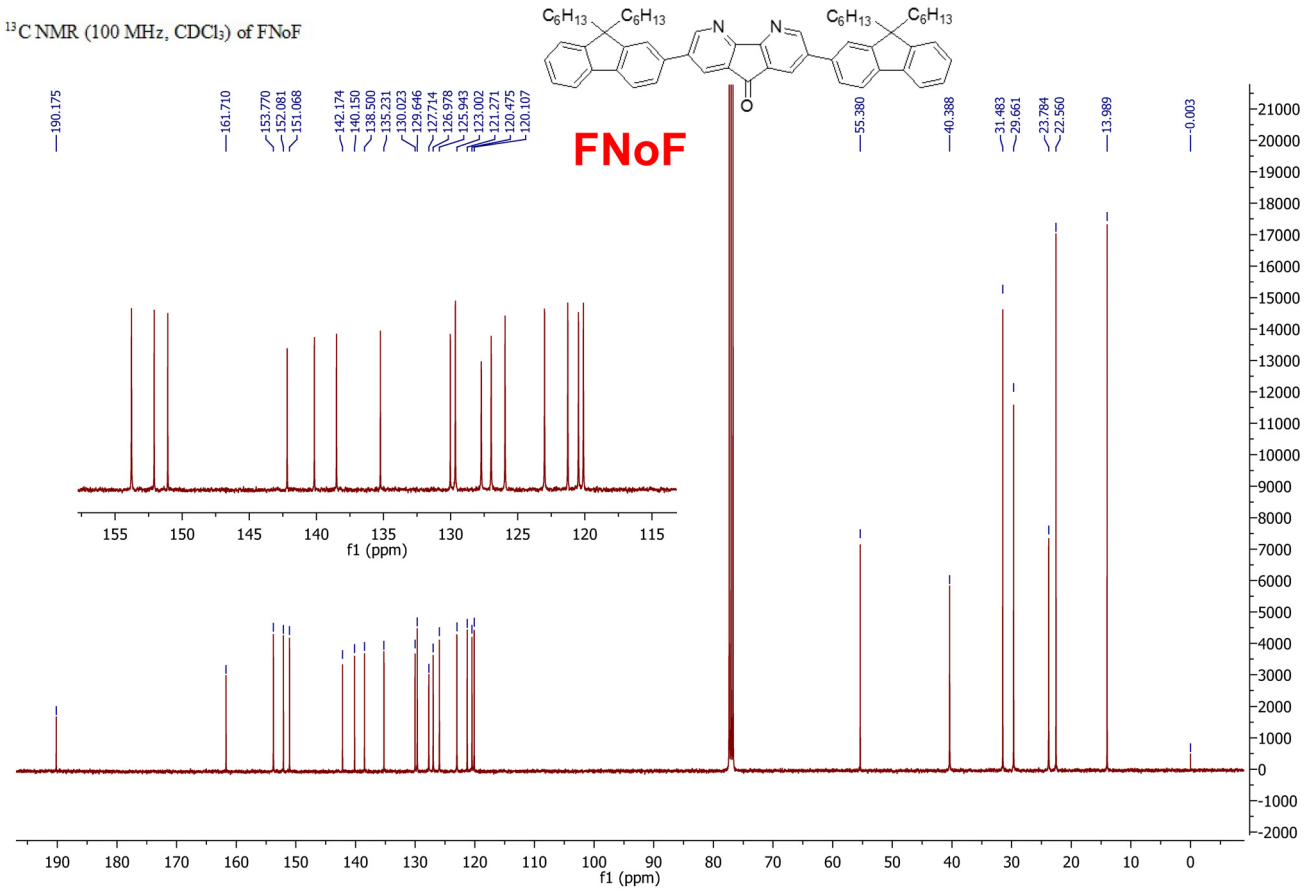

DEPTQ NMR (100MHz, $CDCl_3$) of FNoF

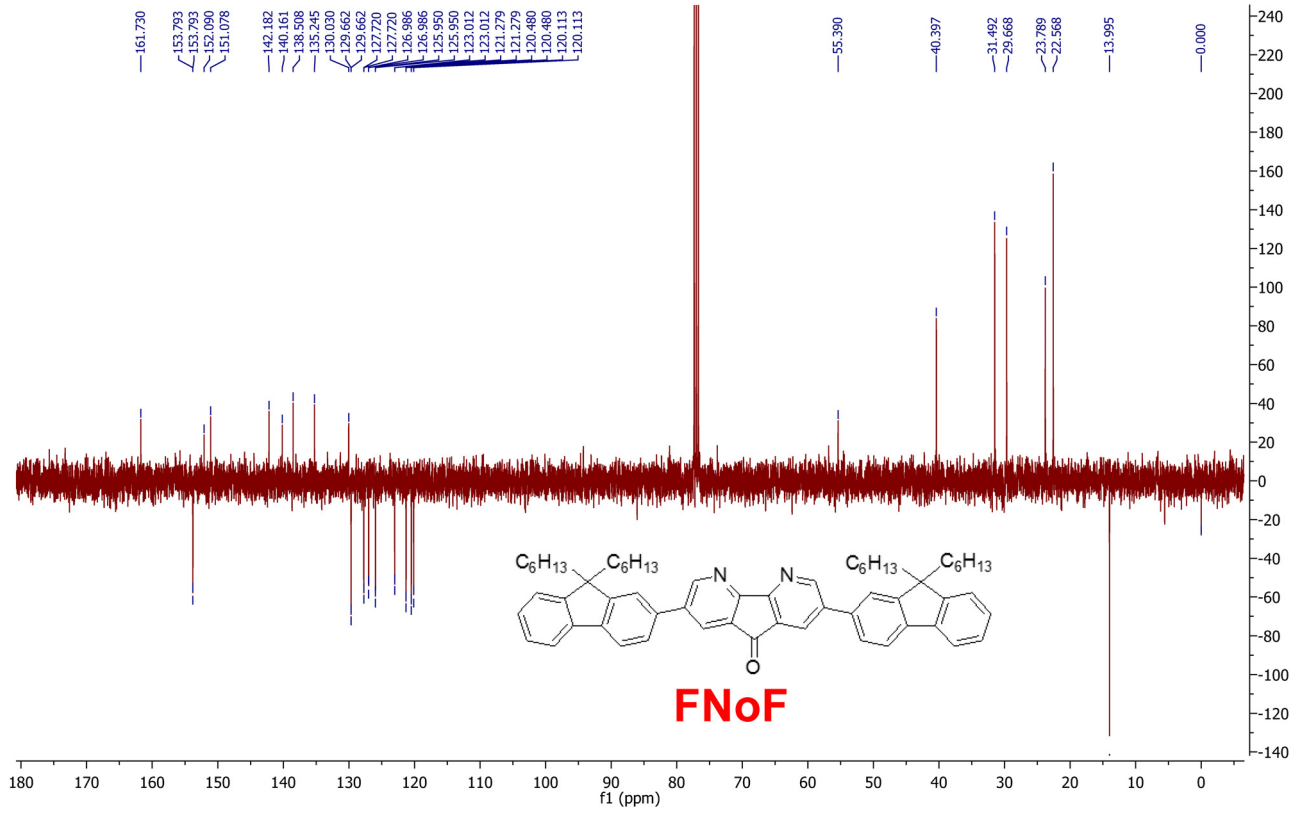

^{1}H NMR (400 MHz, $CDCl_3$) of FFNFF

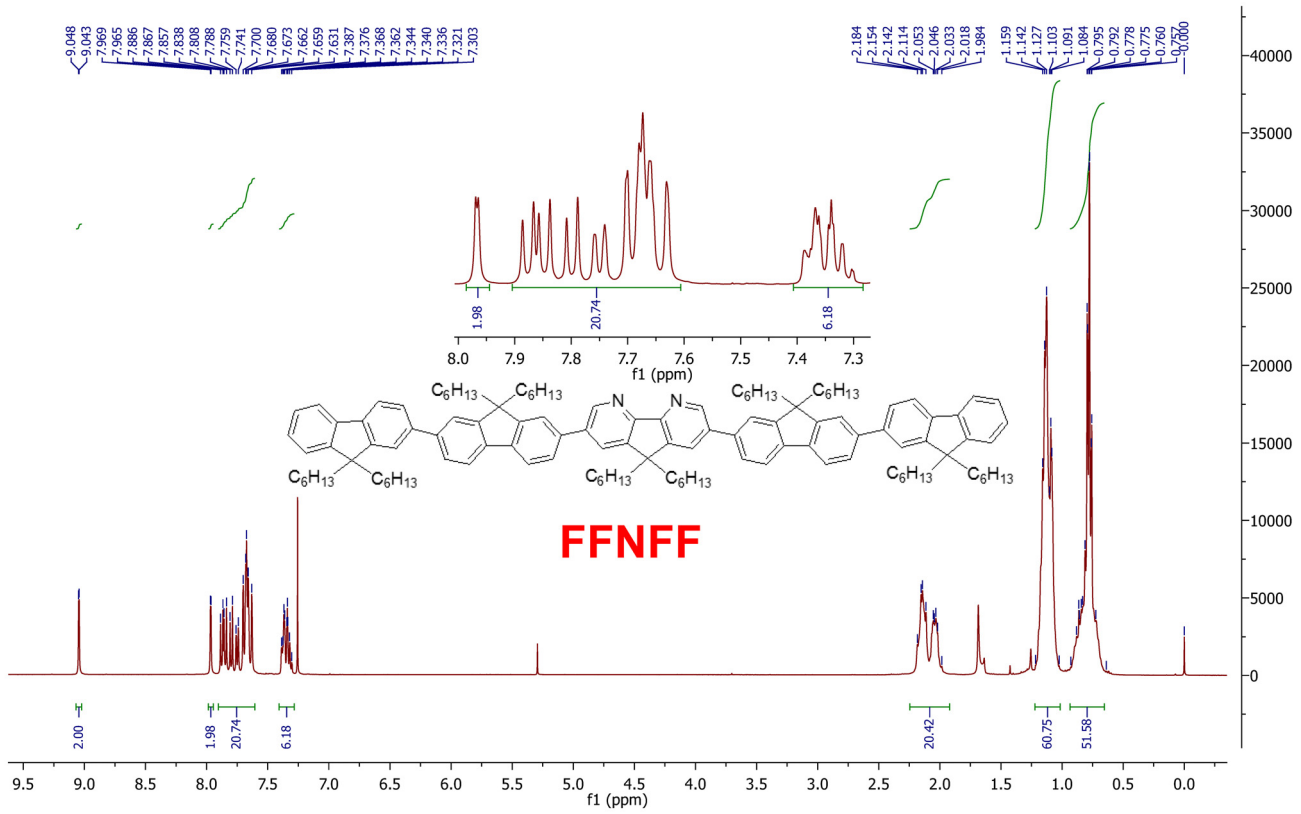

^{13}C NMR (101 MHz, $CDCl_3$) of FFNFF

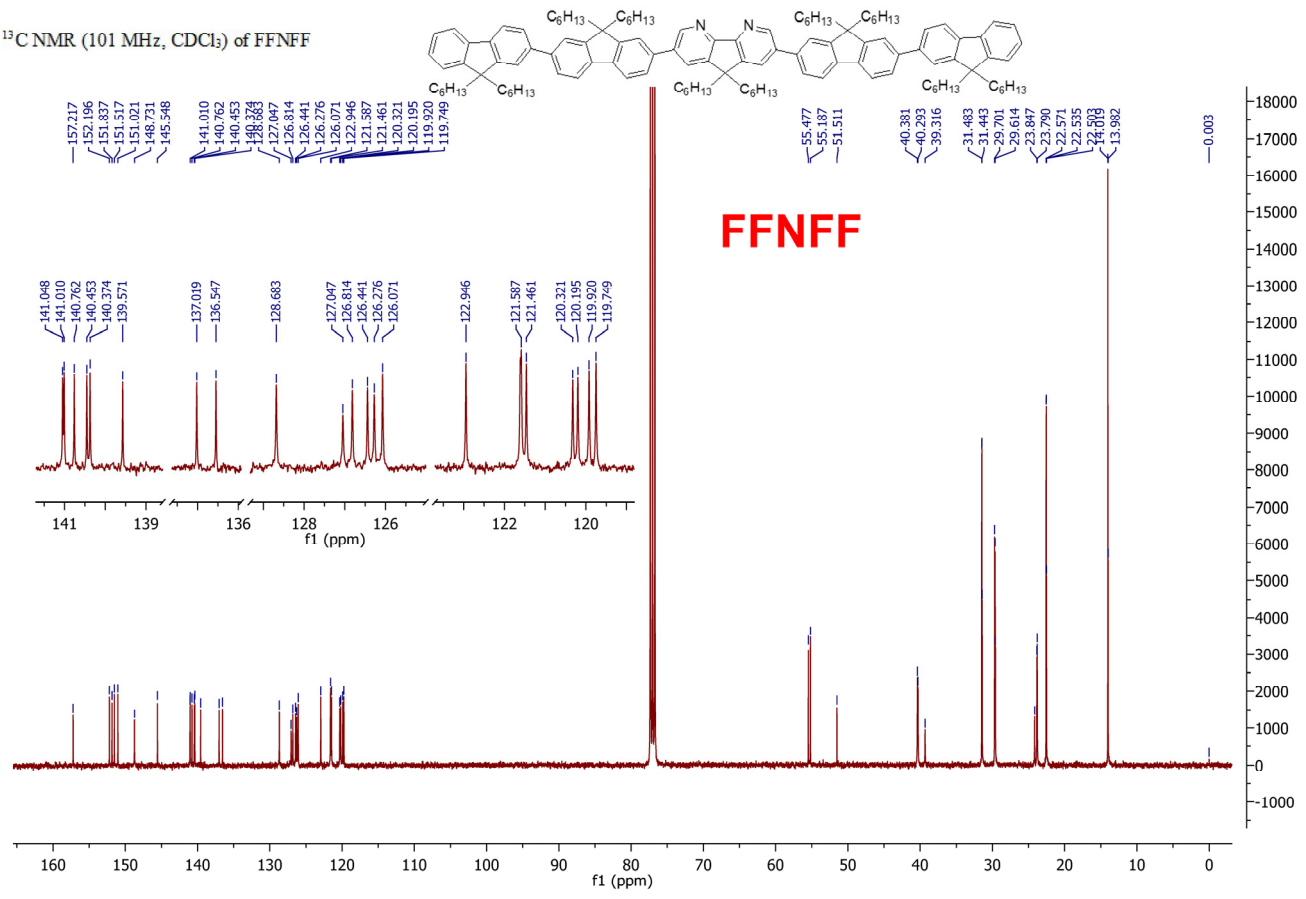

DEPTQ NMR (100MHz, $CDCl_3$) of FFNFF

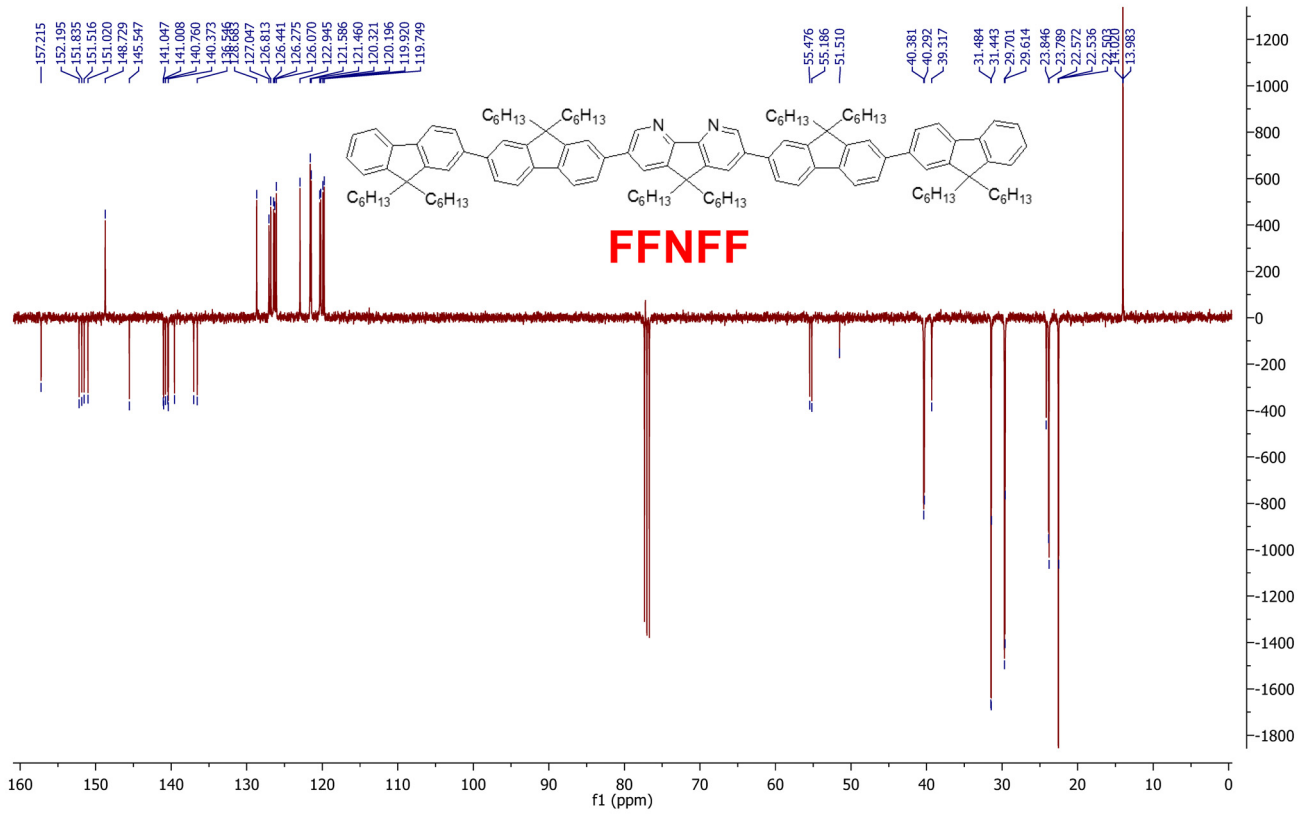

^1H NMR (400 MHz, $CDCl_3$) of NSN

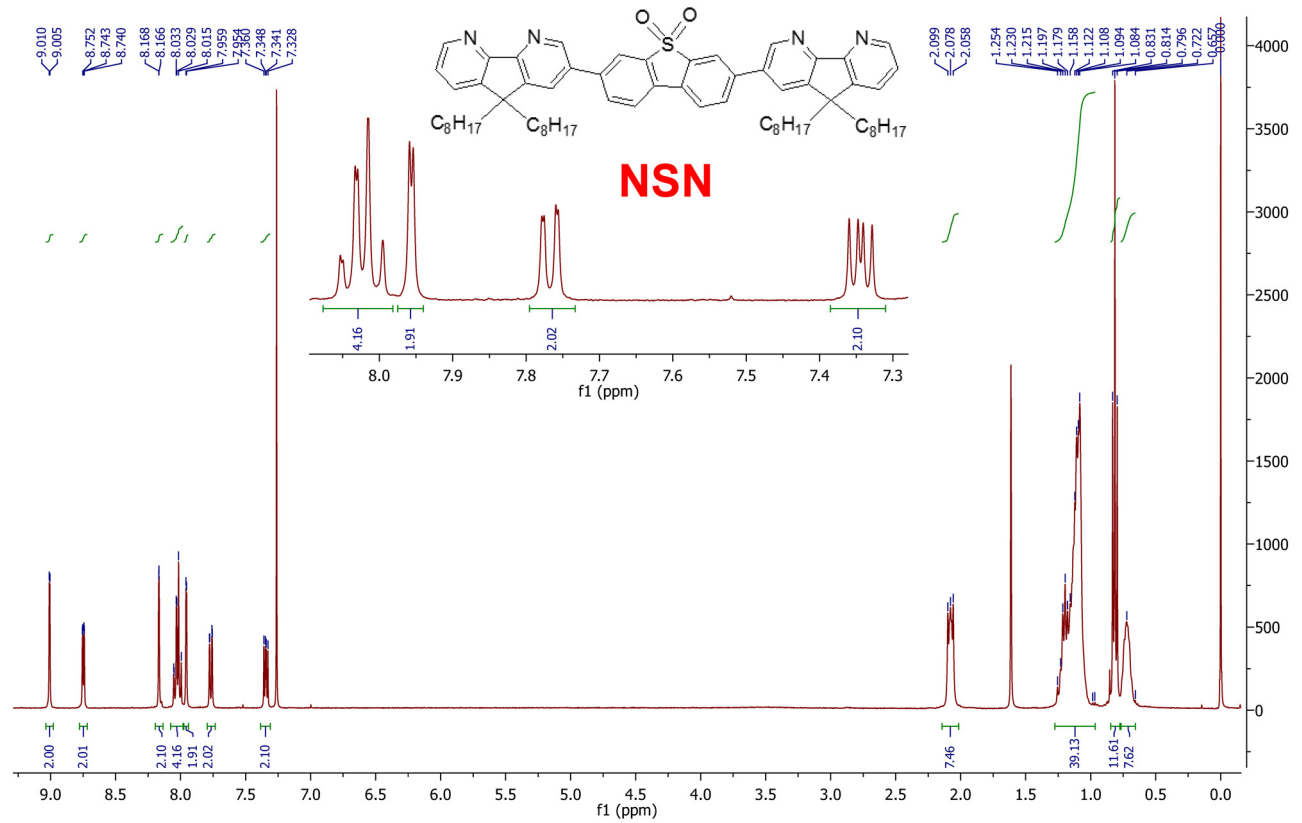

^{13}C NMR (101 MHz, $CDCl_3$) of NSN

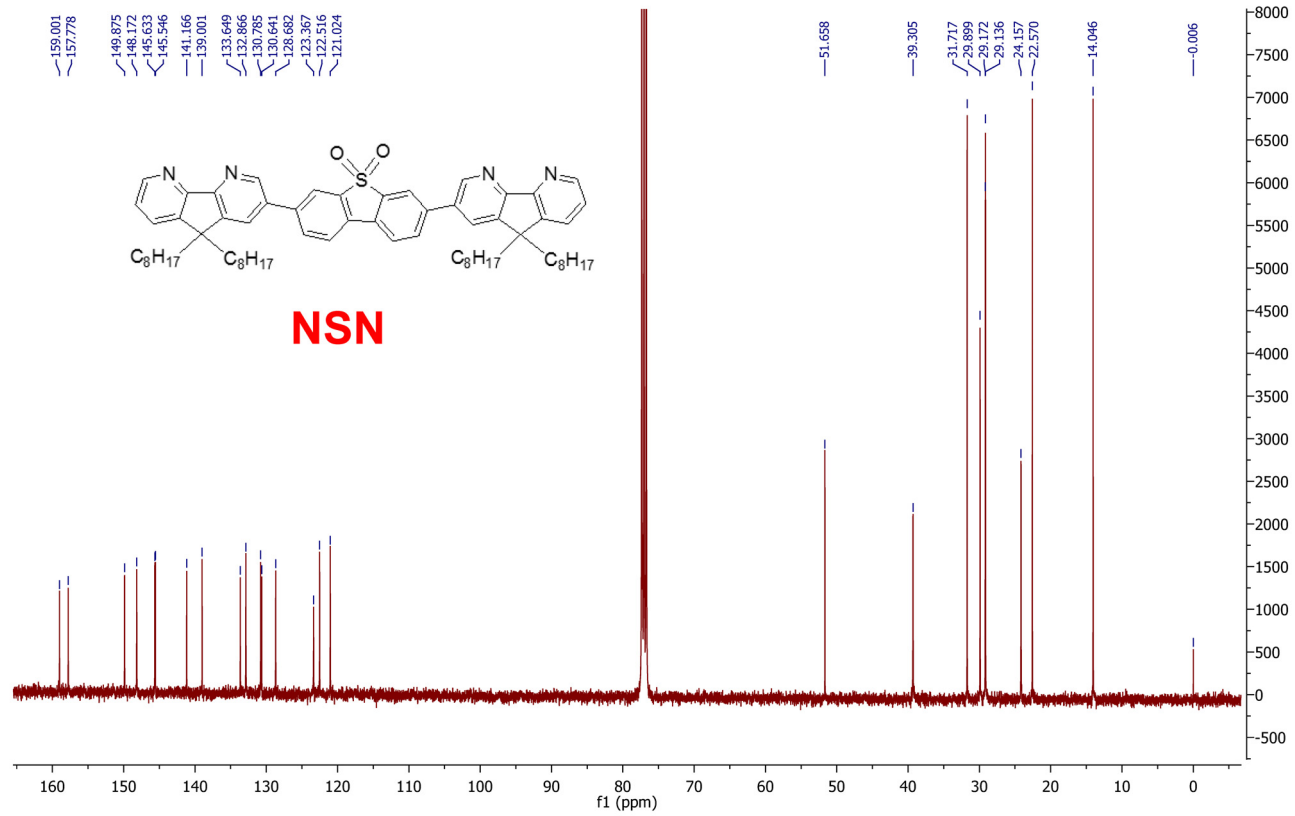

DEPTQ NMR (100MHz, $CDCl_3$) of NSN

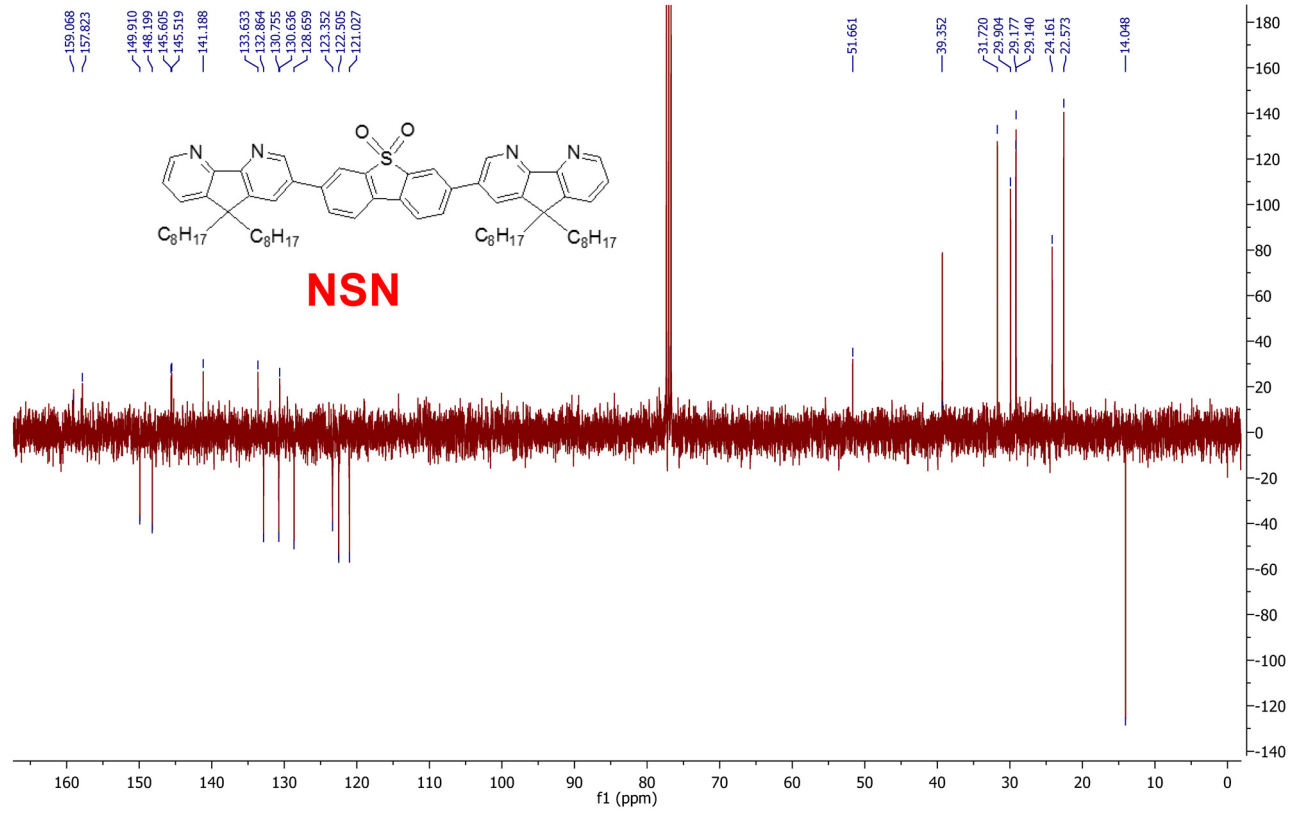

^{1}H NMR (400 MHz, $CDCl_3$) of SNS

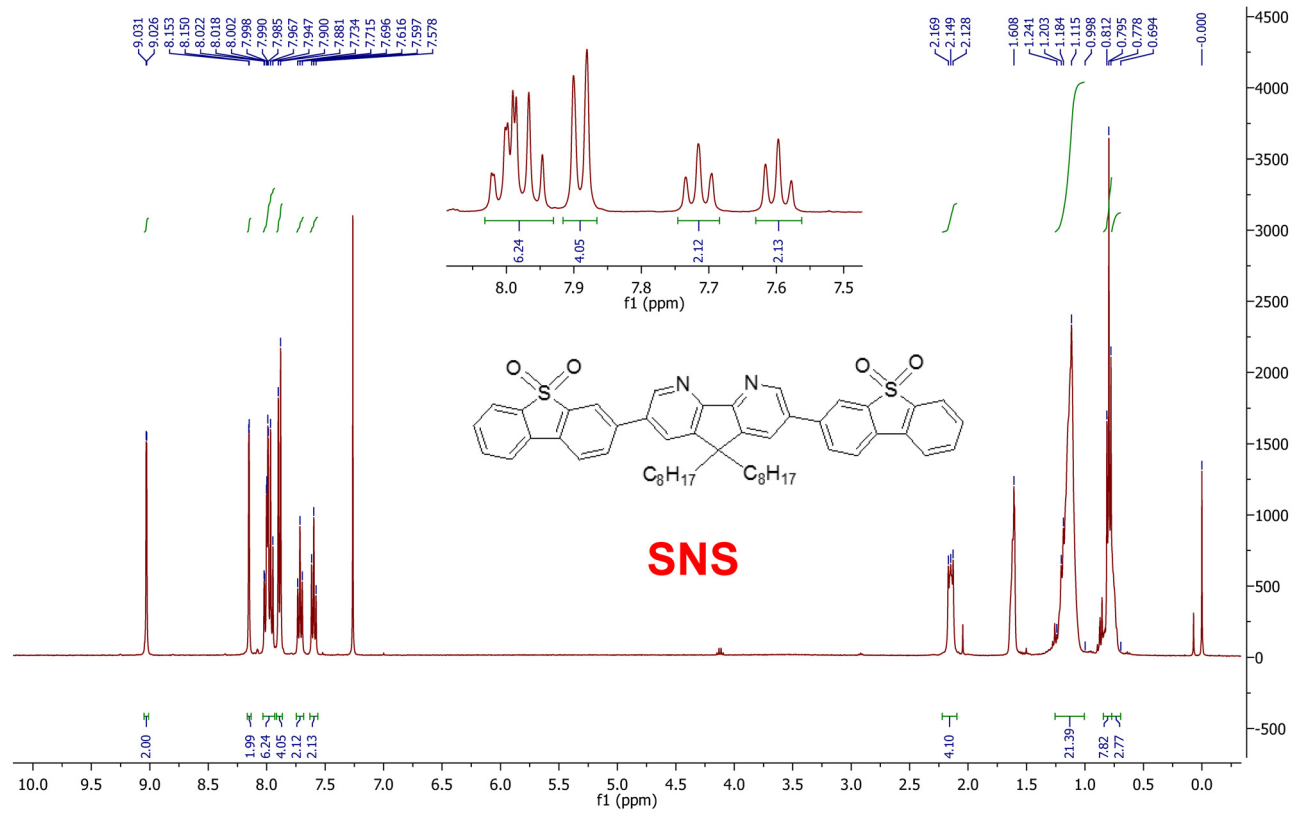

DEPTQ NMR (100MHz, $CDCl_3$) of SNS

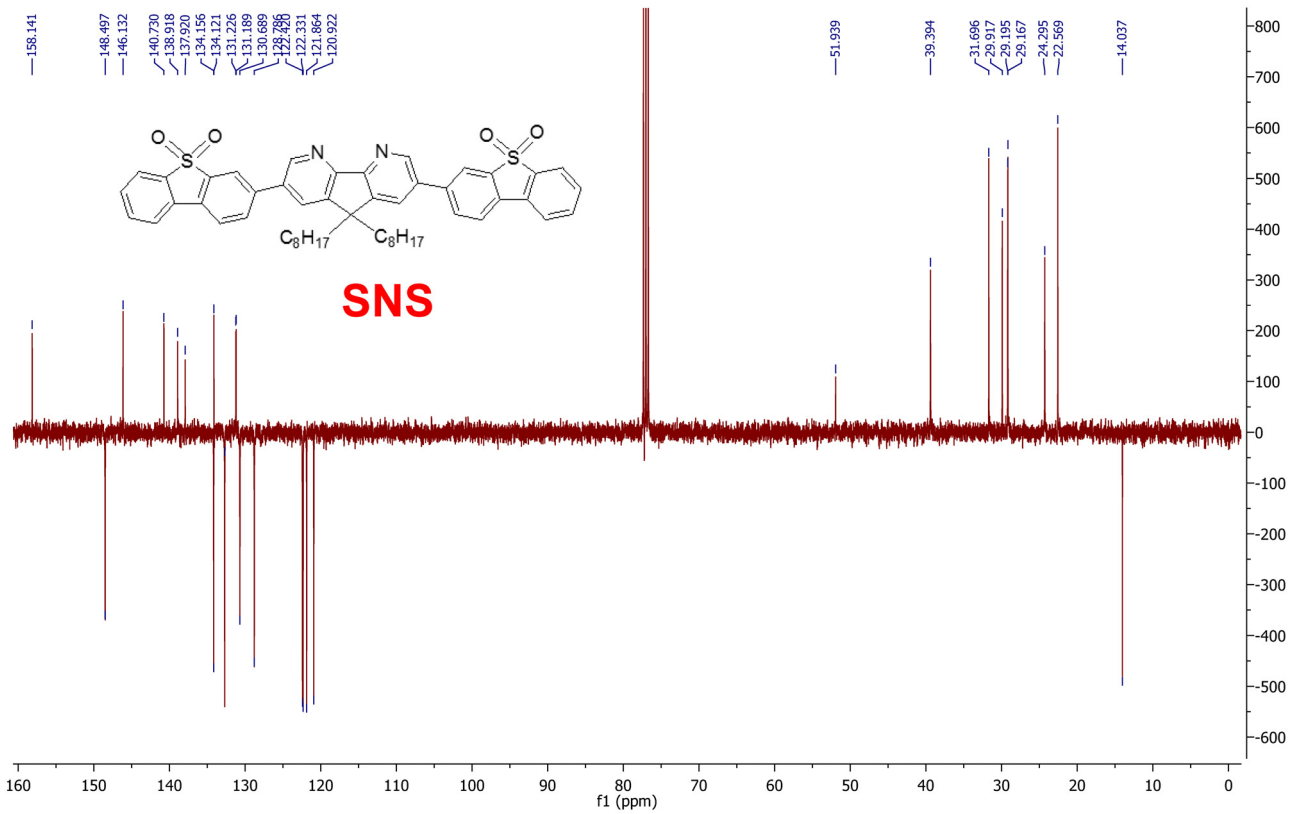

^{13}C NMR (101 MHz, $CDCl_3$) of SNS

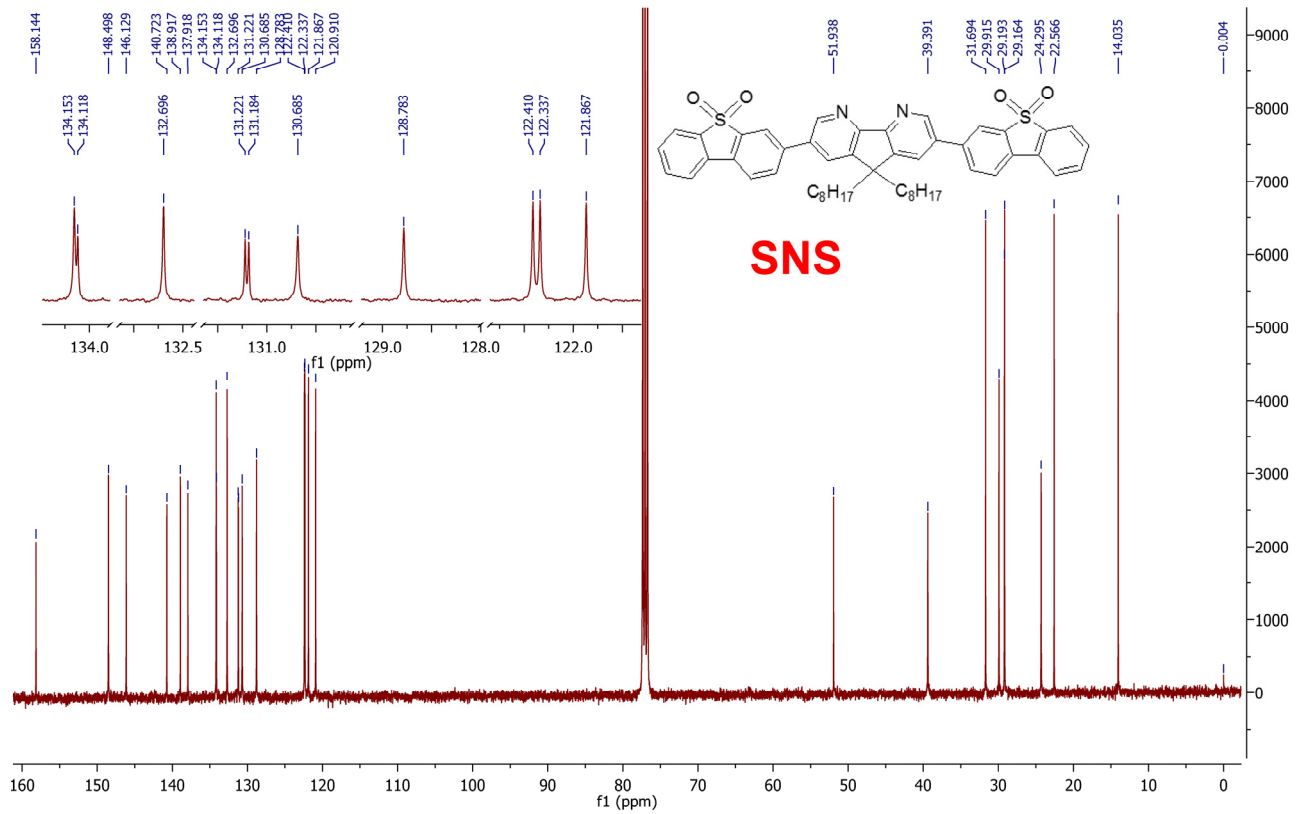

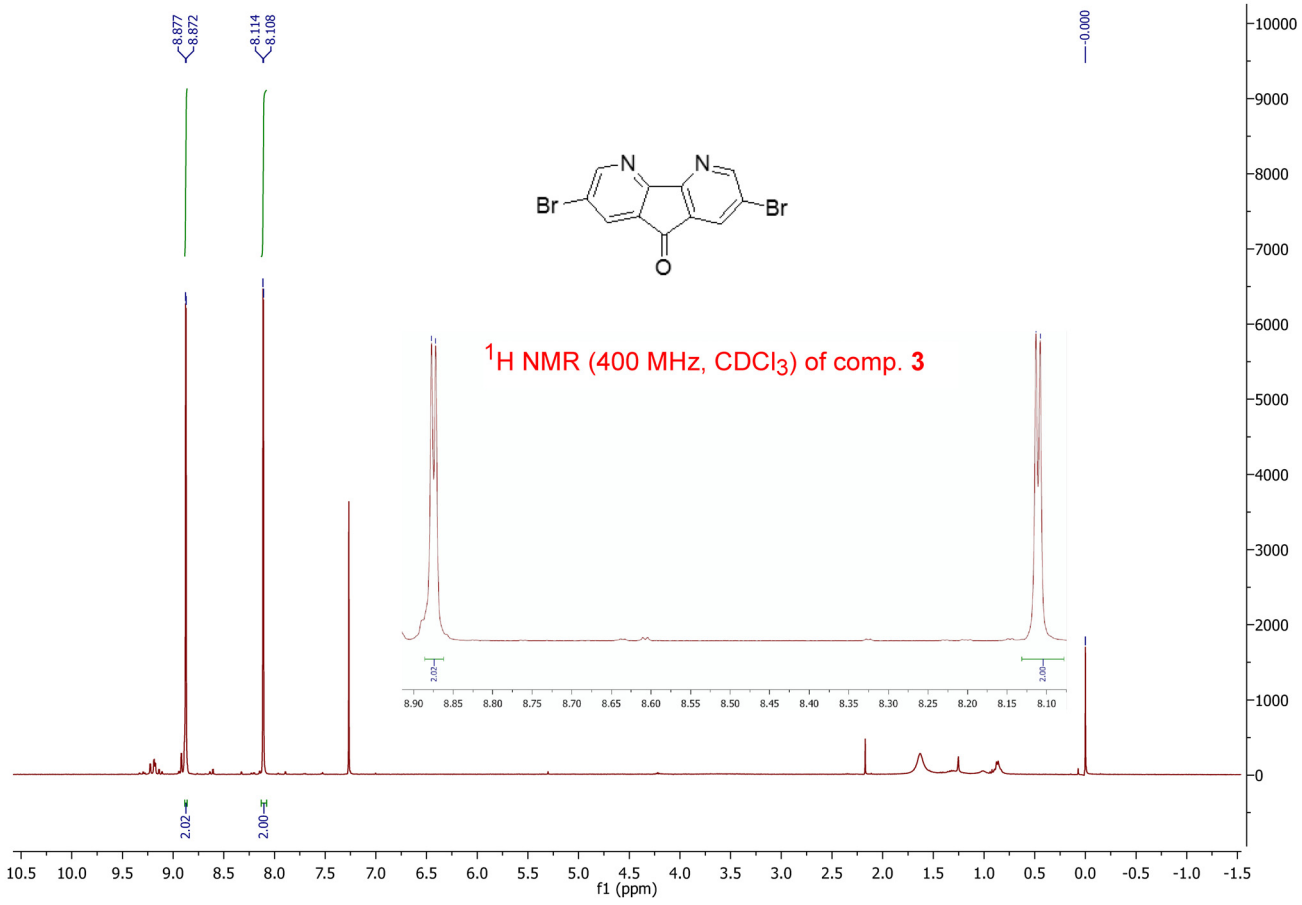

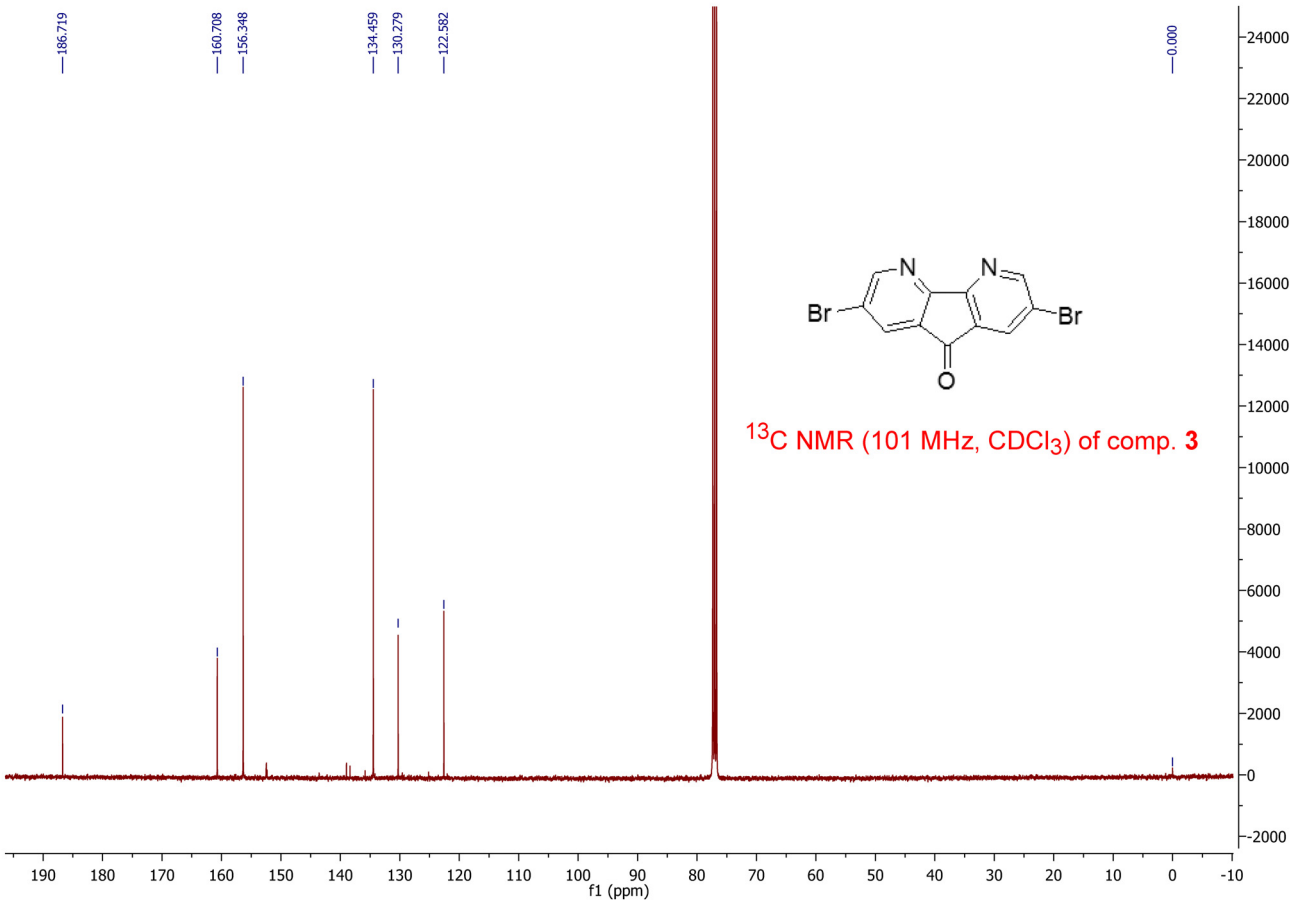

^{13}C NMR (101 MHz, $CDCl_3$) of comp. **3**

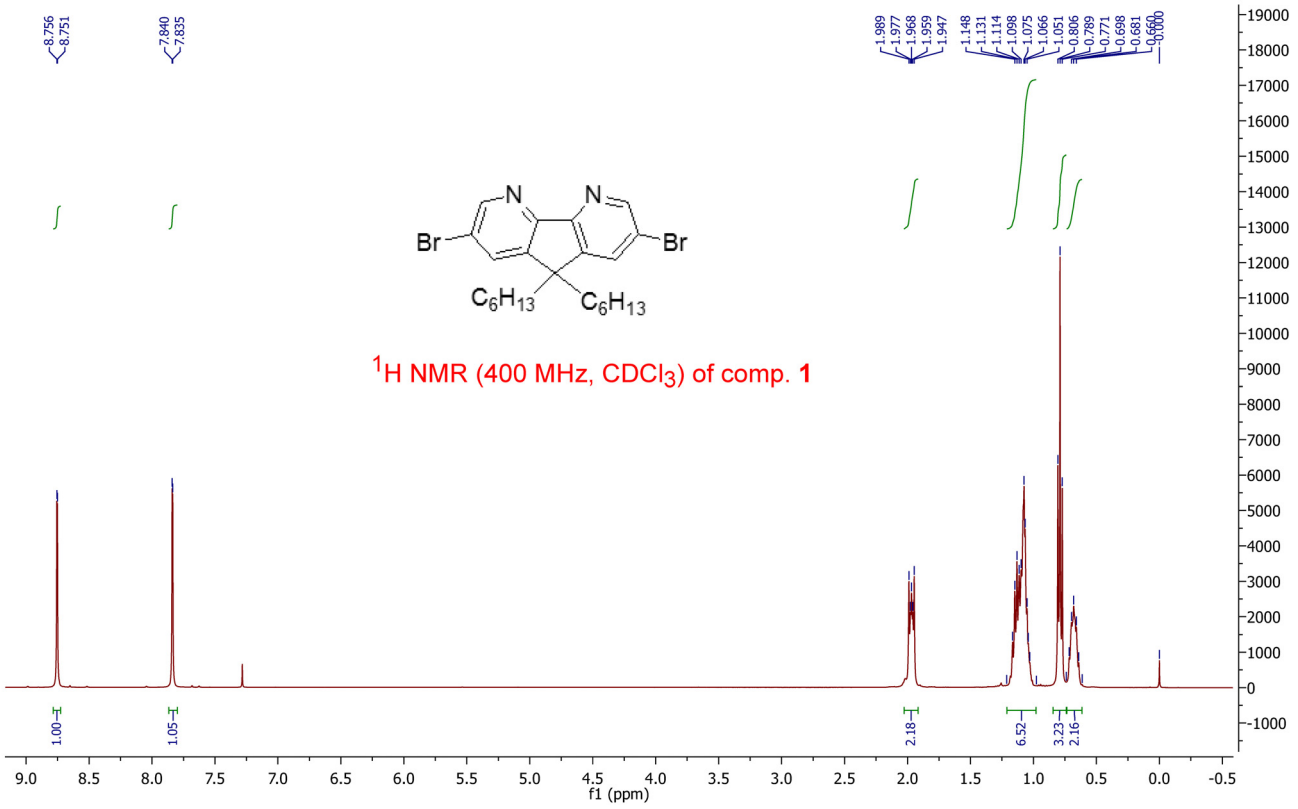

^{1}H NMR (400 MHz, $CDCl_3$) of comp. **1**

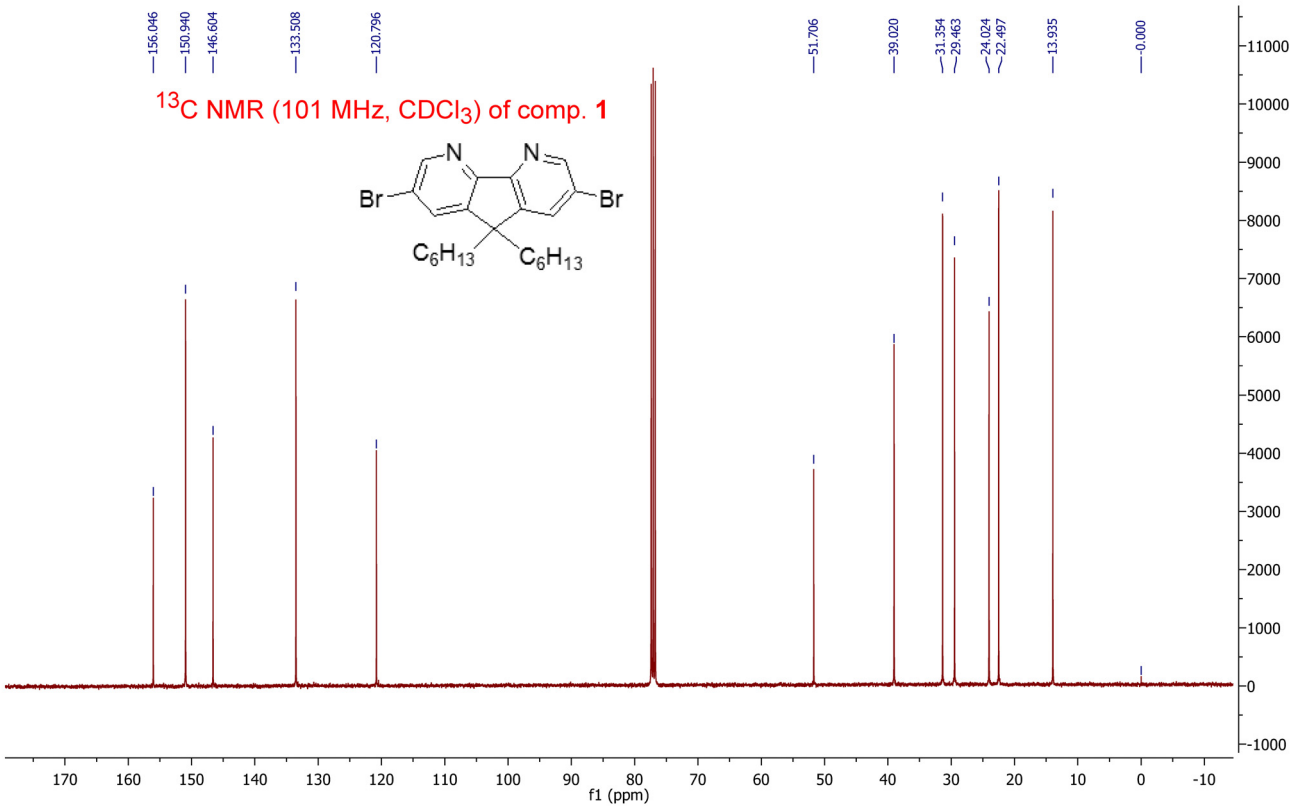
156.046
150.940
146.604
133.508
120.796
51.706
39.020
31.354
29.463
24.024
22.497
13.935
-0.000
^{13}C NMR (101 MHz, CDCl$_3$) of comp. **1**
Br
Br
N
N
C_6H_{13}
C_6H_{13}
f1 (ppm)

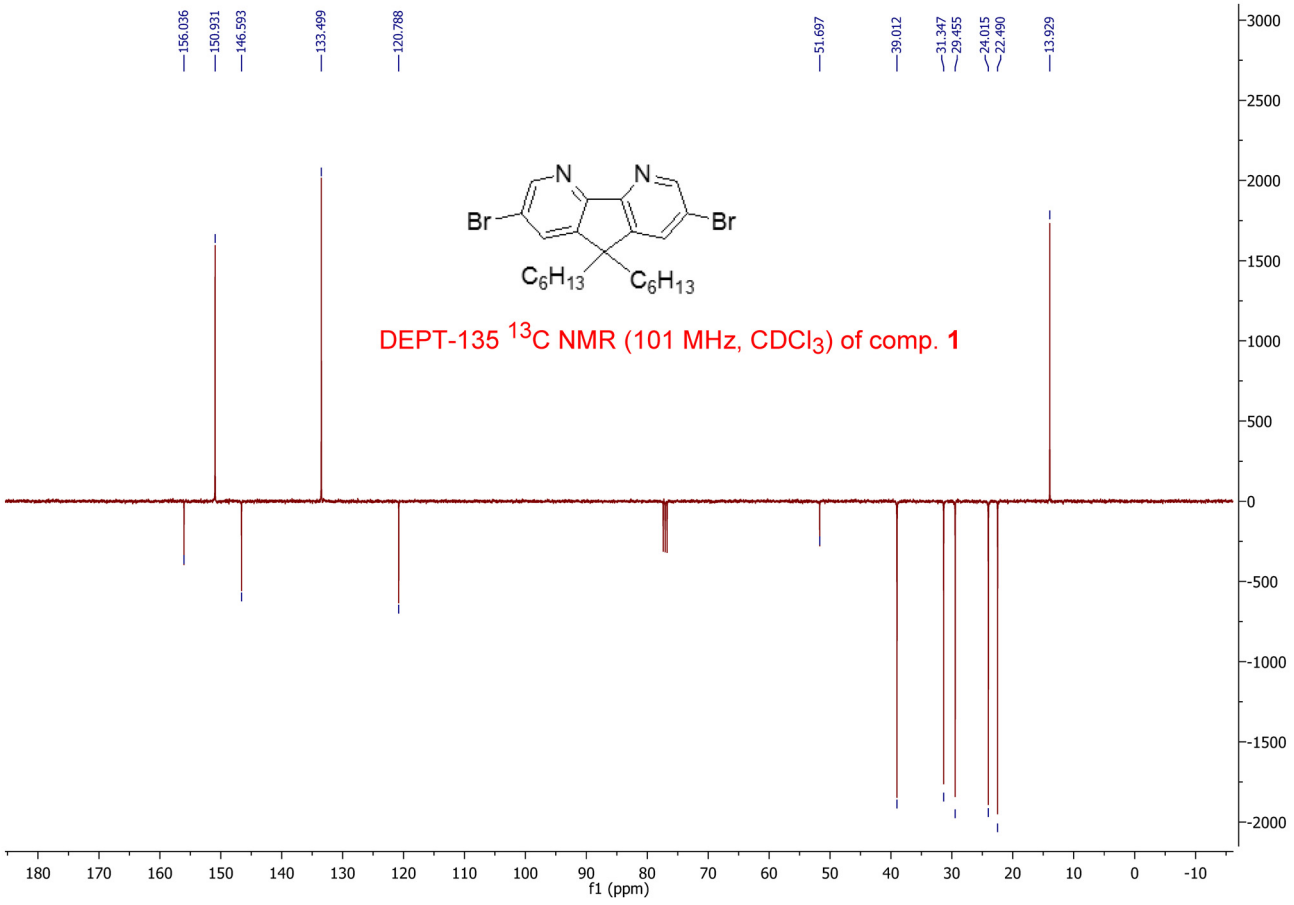
156.036
150.931
146.593
133.499
120.788
51.697
39.012
31.347
29.455
24.015
22.490
13.929
Br
Br
N
N
C_6H_{13}
C_6H_{13}
DEPT-135 ^{13}C NMR (101 MHz, CDCl$_3$) of comp. **1**
f1 (ppm)

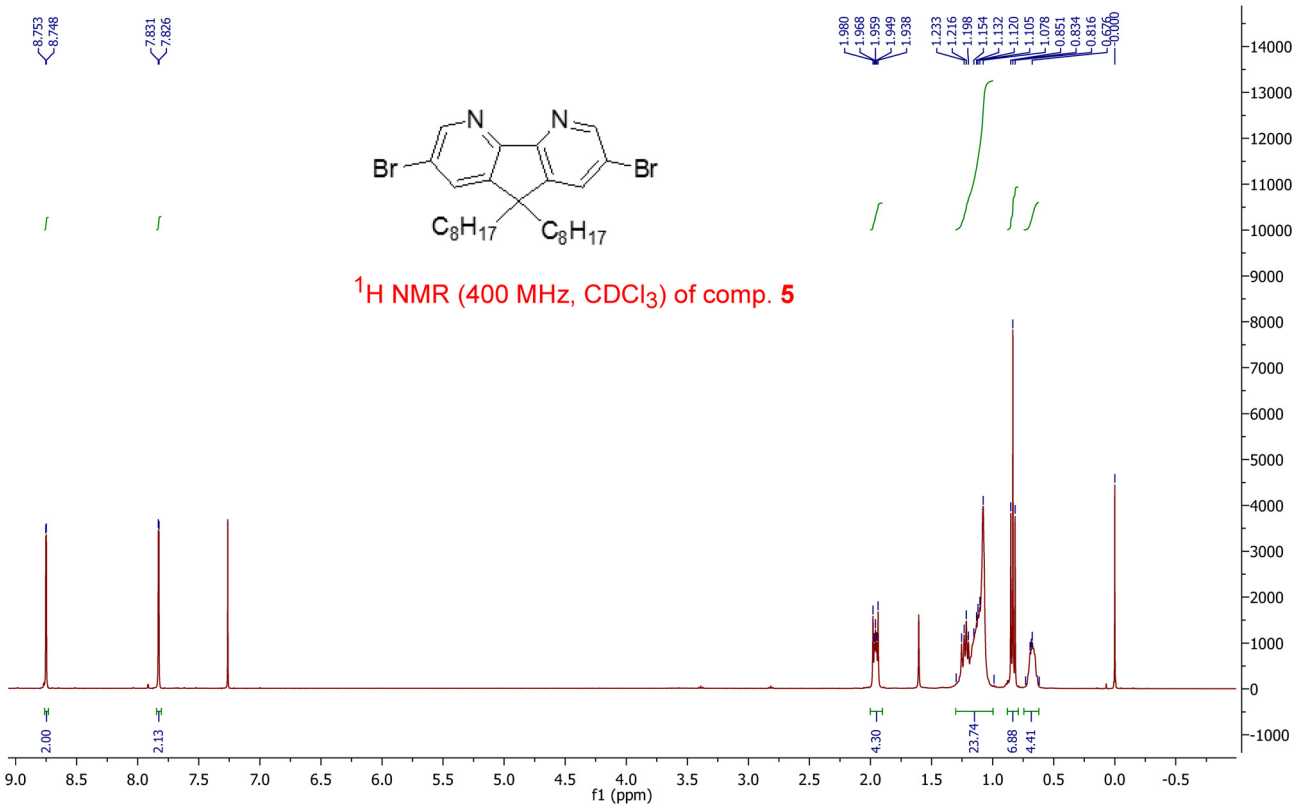

^{1}H NMR (400 MHz, $CDCl_3$) of comp. **5**

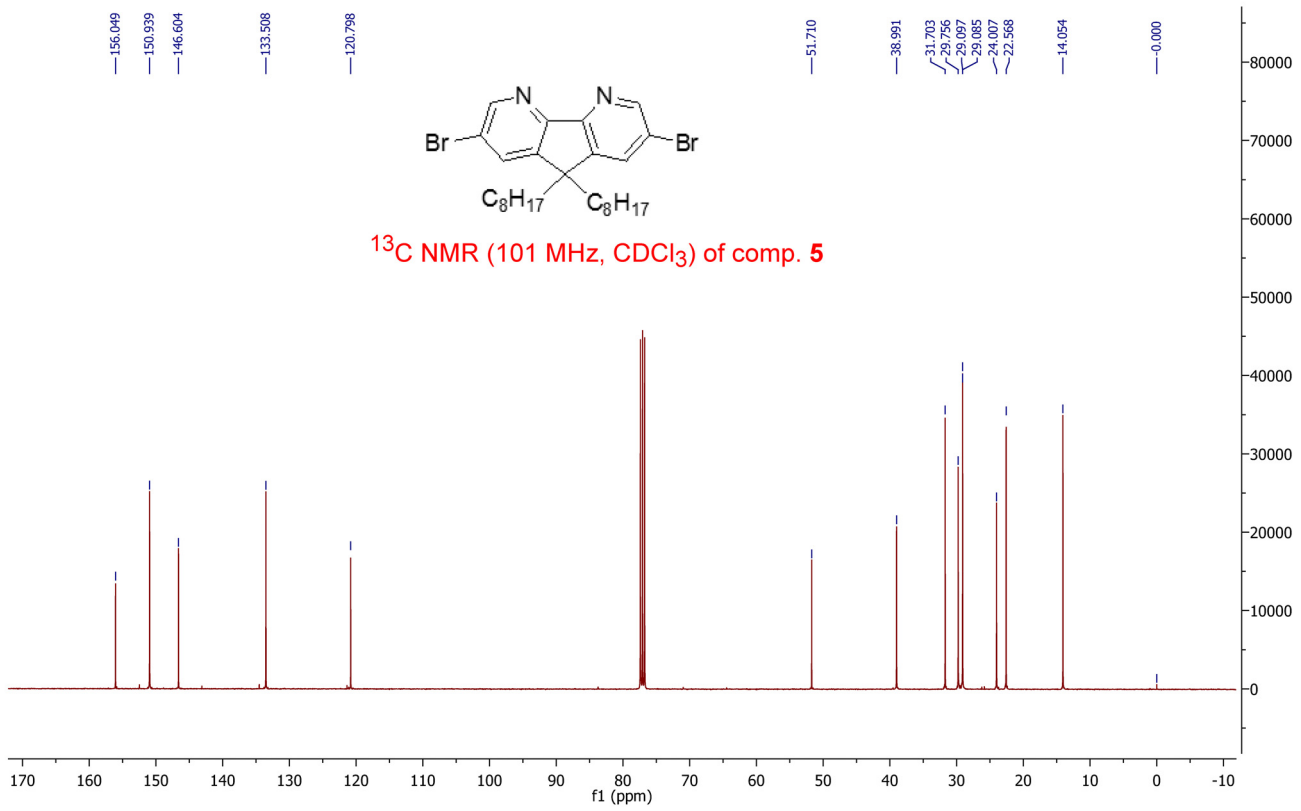

^{13}C NMR (101 MHz, $CDCl_3$) of comp. **5**

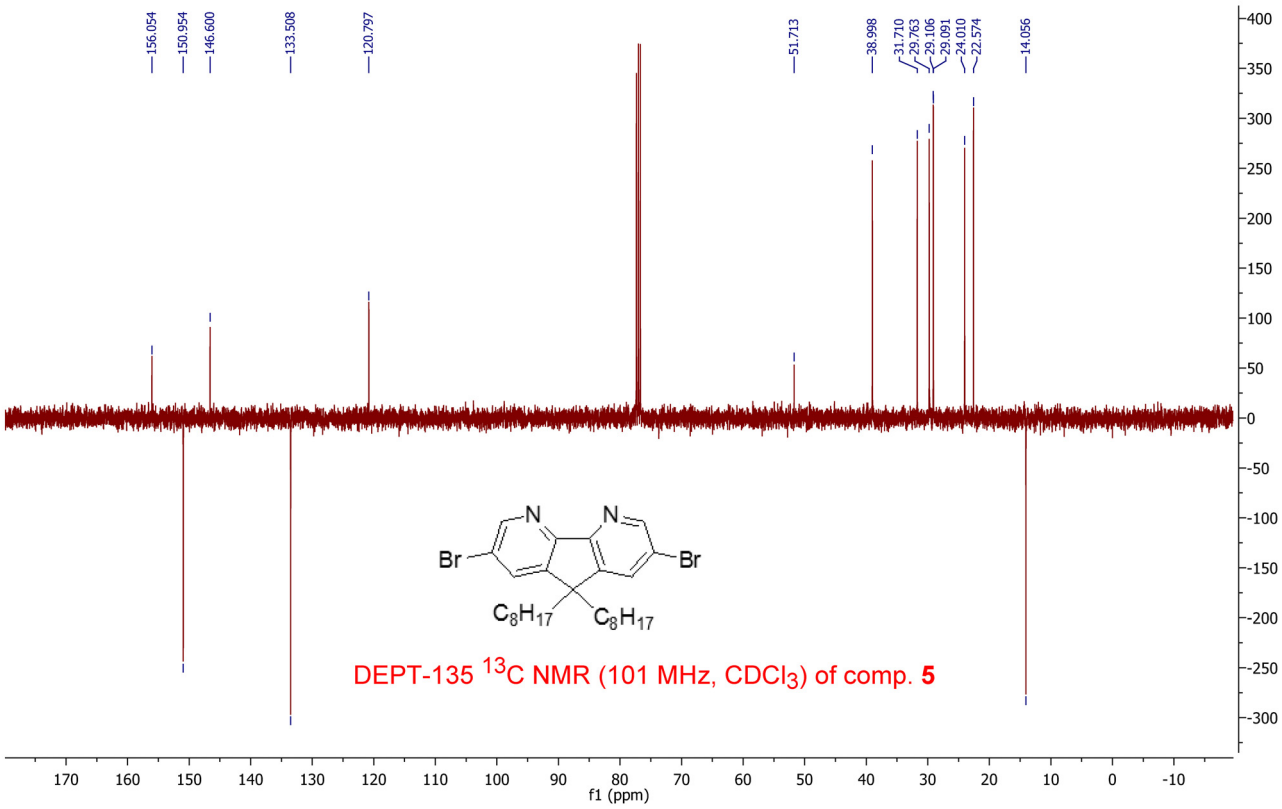

DEPT-135 ^{13}C NMR (101 MHz, $CDCl_3$) of comp. **5**

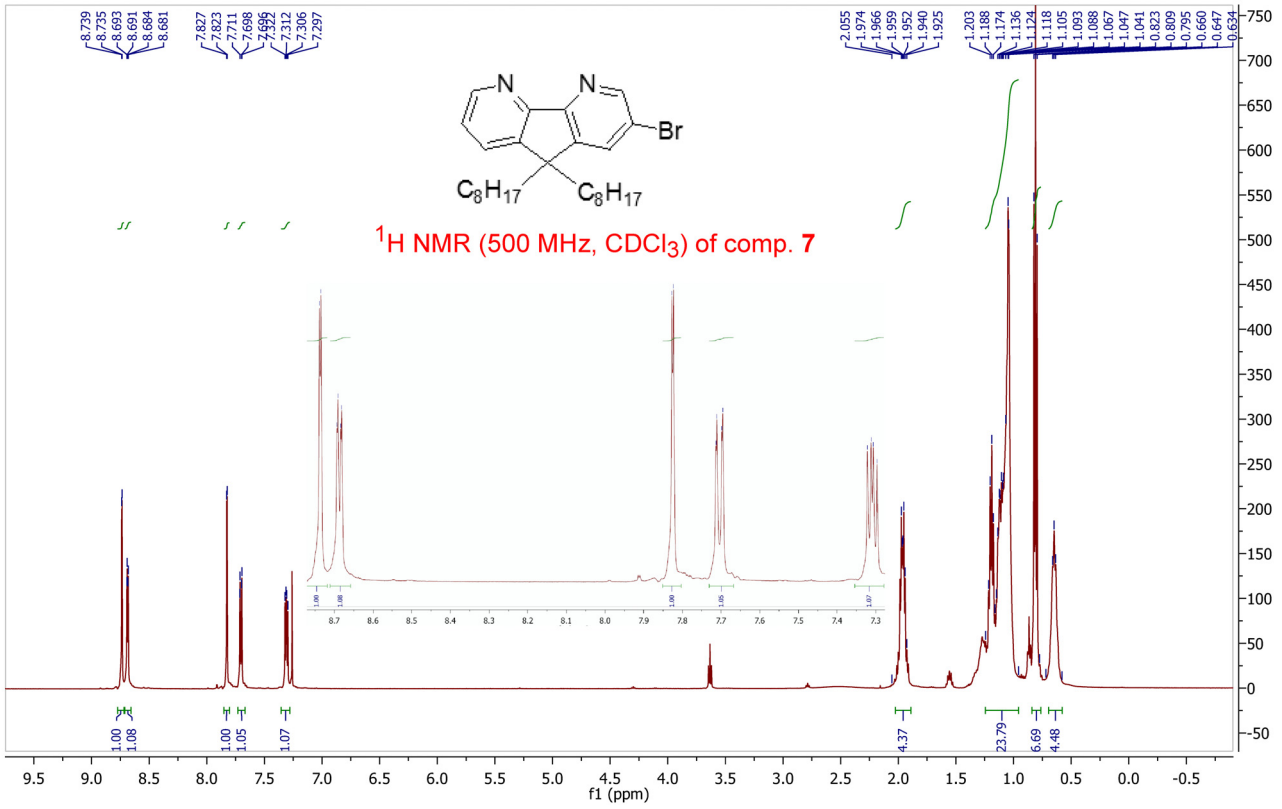

^{1}H NMR (500 MHz, $CDCl_3$) of comp. **7**

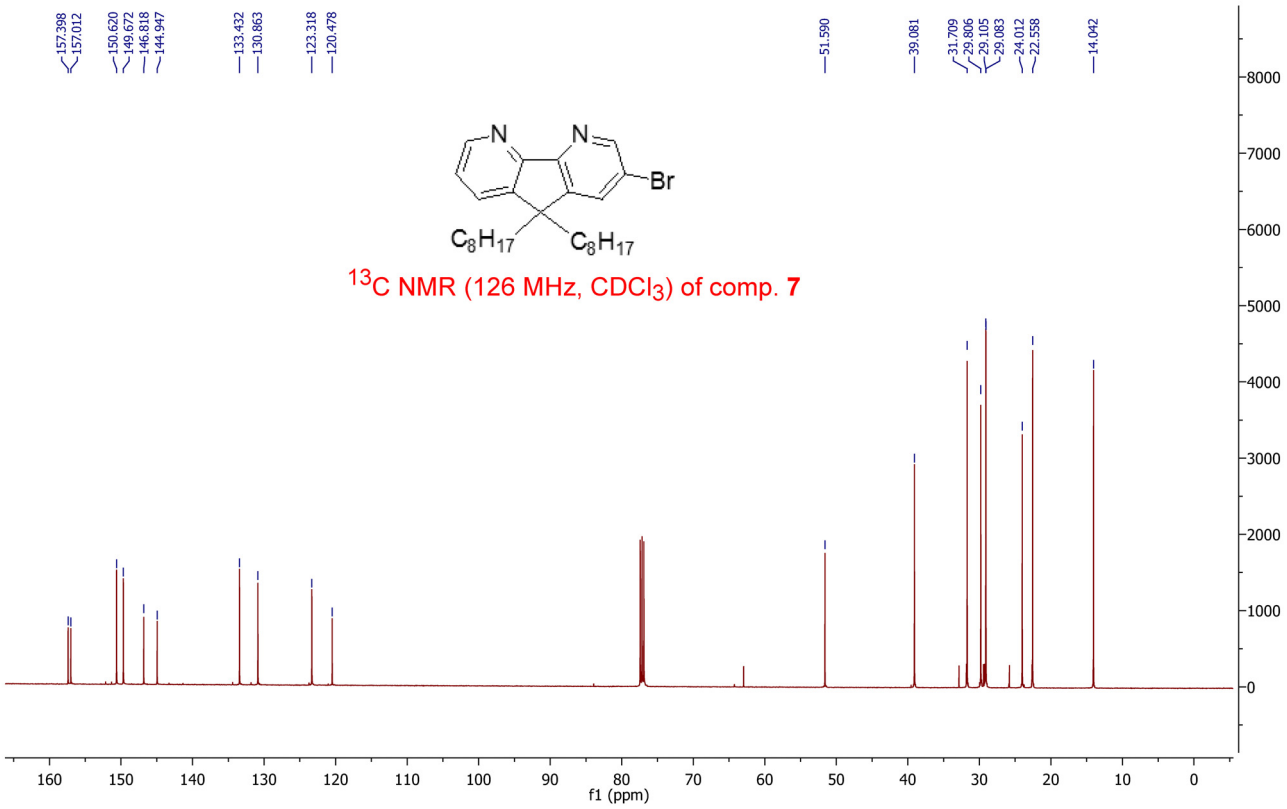
157.398
157.012
150.620
149.672
146.818
144.947
133.432
130.863
123.318
120.478
51.590
39.081
31.709
29.806
29.105
29.083
24.012
22.558
14.042
N
N
Br
C8H17
C8H17
13C NMR (126 MHz, CDCl3) of comp. 7
f1 (ppm)

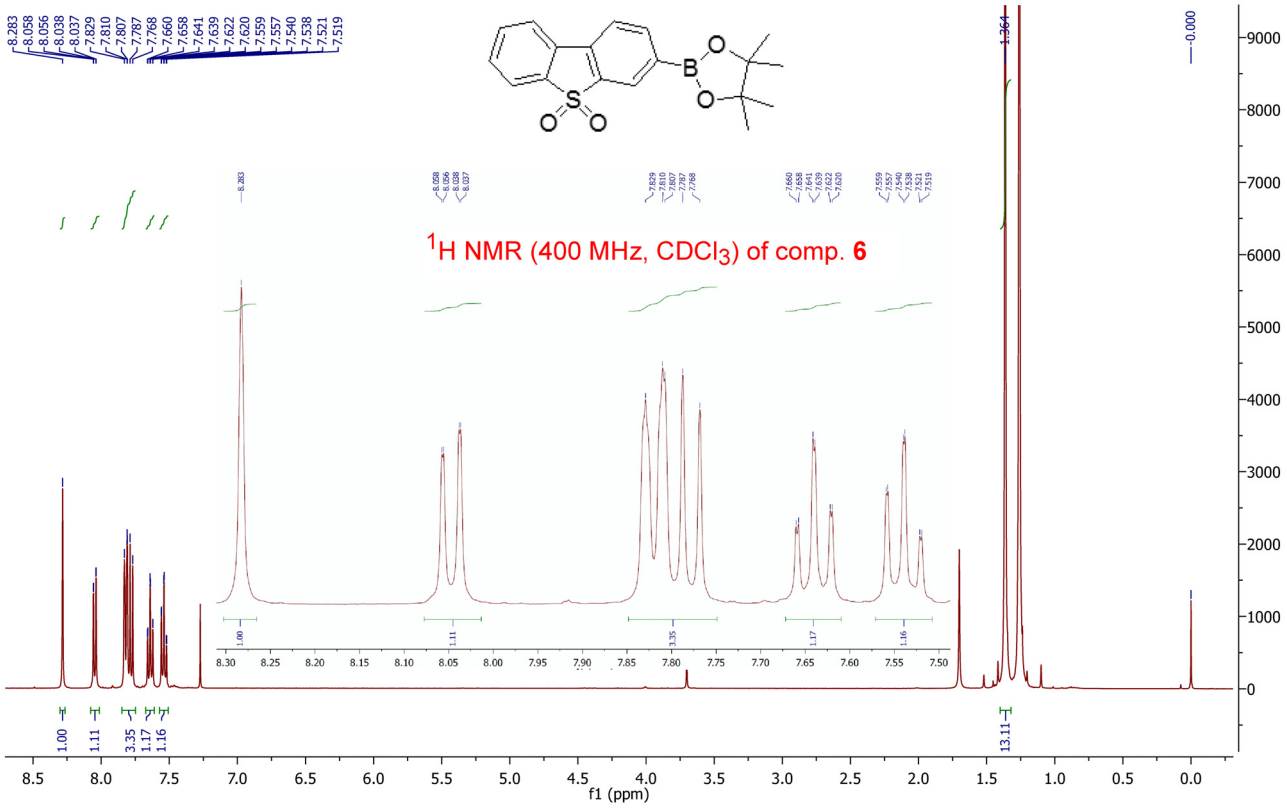
8.283
8.058
8.056
8.038
8.037
7.829
7.810
7.807
7.787
7.768
7.660
7.658
7.641
7.639
7.622
7.620
7.559
7.557
7.540
7.538
7.521
7.519
1.364
0.000
B
O
O
S
O
O
1H NMR (400 MHz, CDCl3) of comp. 6
1.00
1.11
3.35
1.17
1.16
13.11
f1 (ppm)

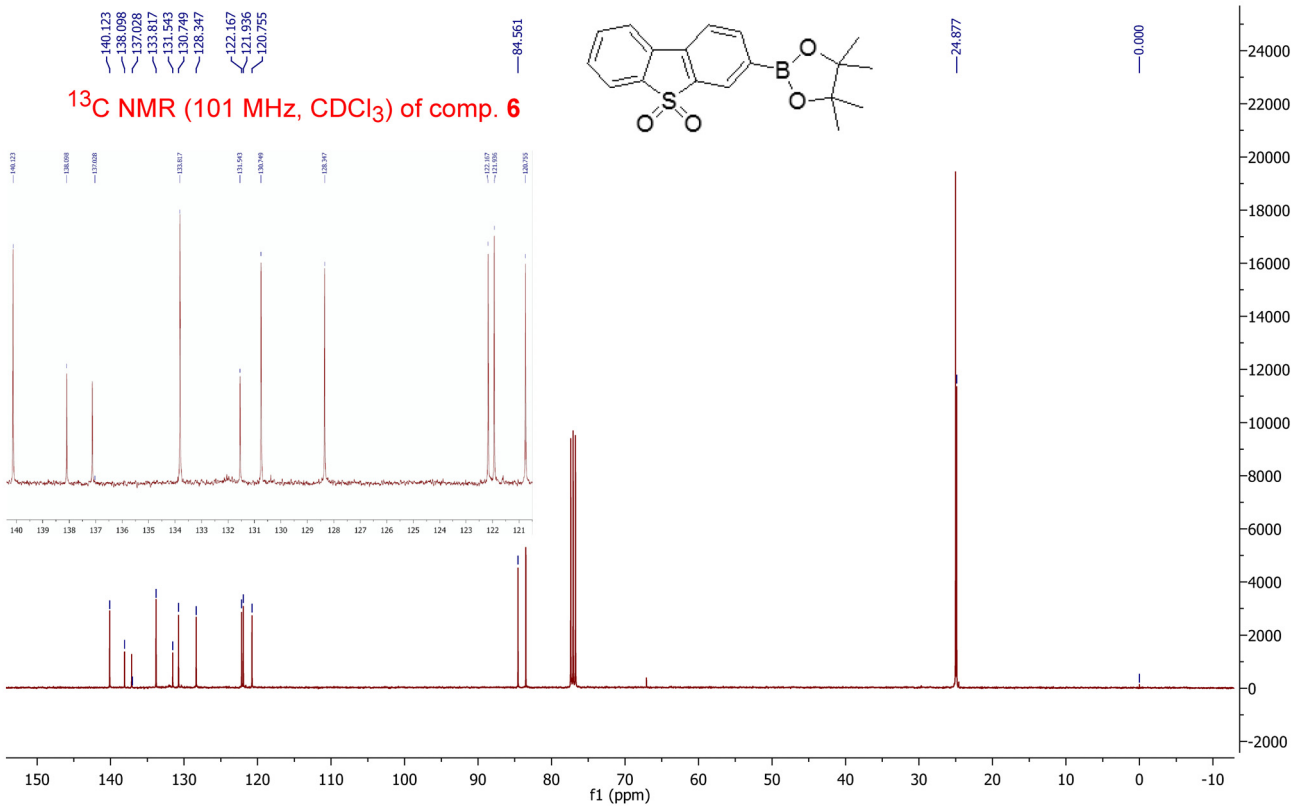

^{13}C NMR (101 MHz, $CDCl_3$) of comp. **6**

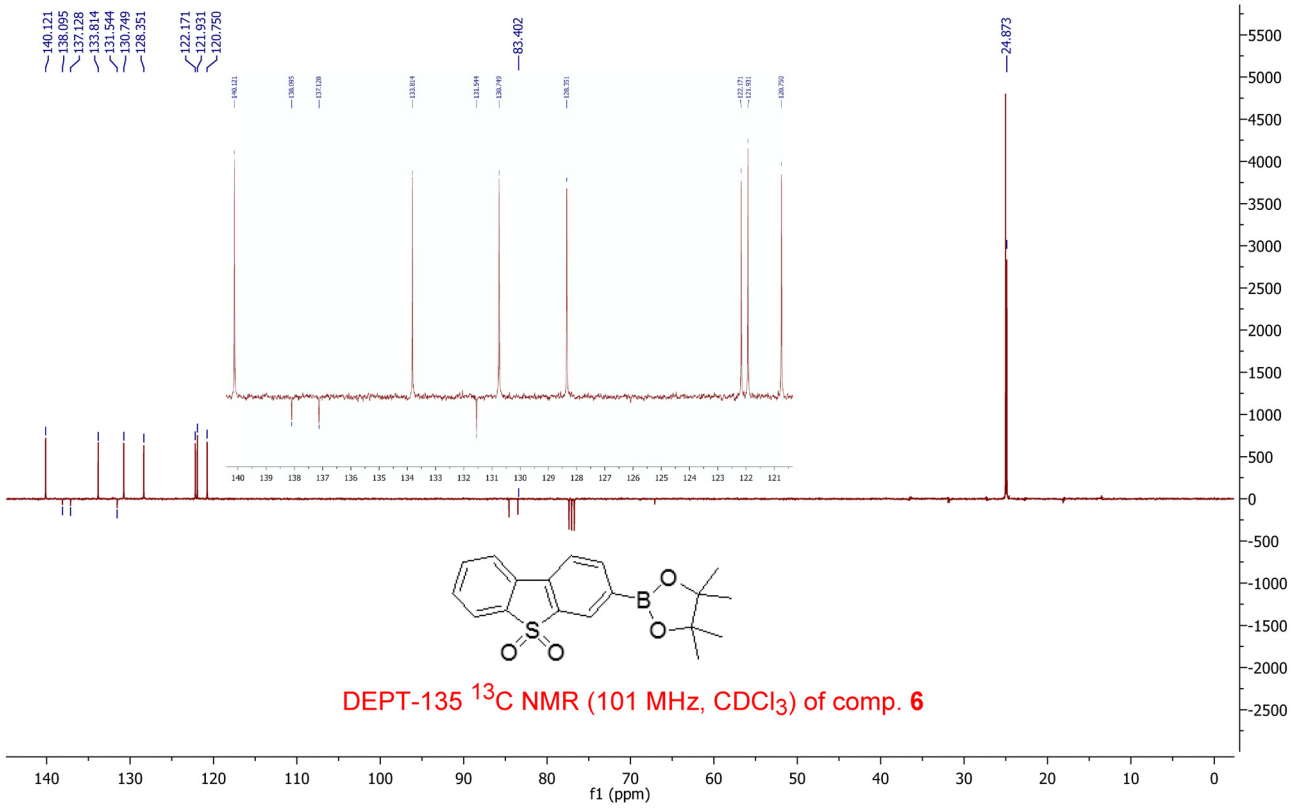

DEPT-135 ^{13}C NMR (101 MHz, $CDCl_3$) of comp. **6**

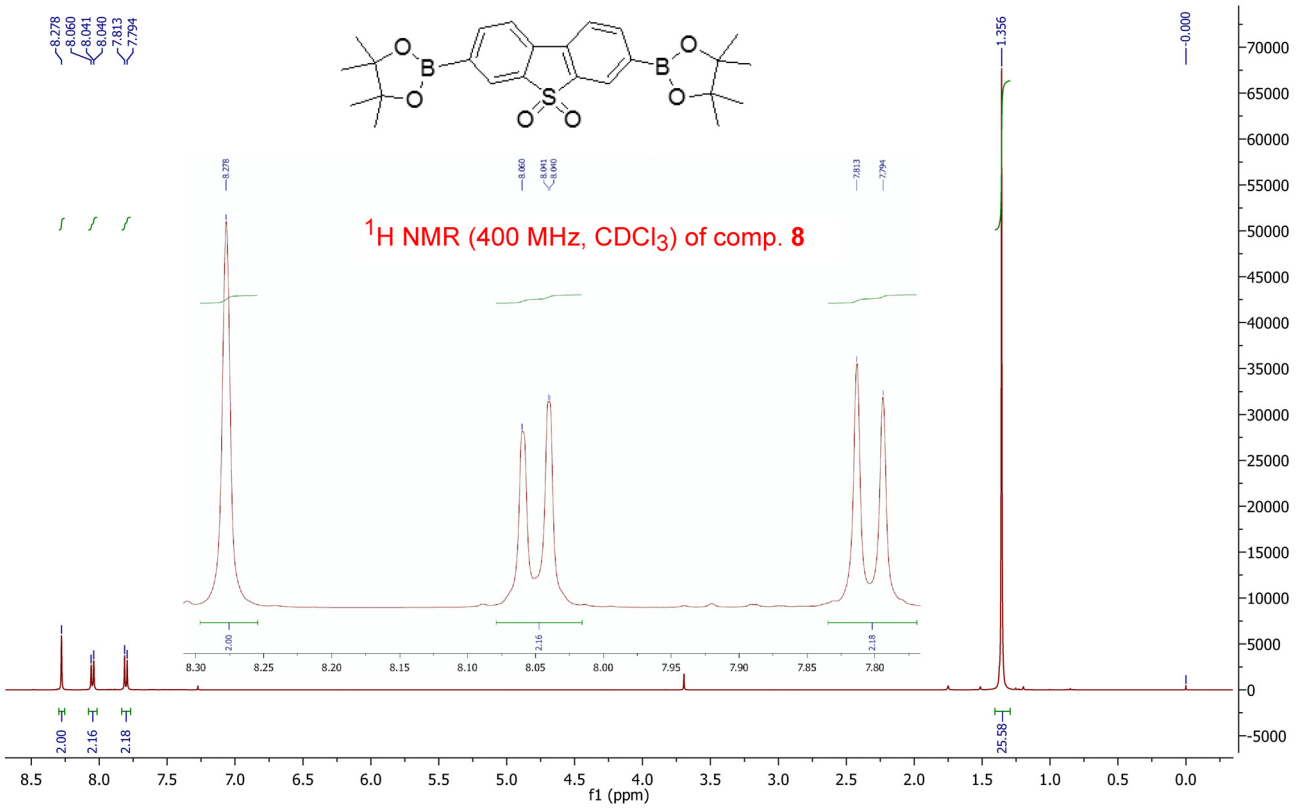

^{1}H NMR (400 MHz, $CDCl_3$) of comp. **8**

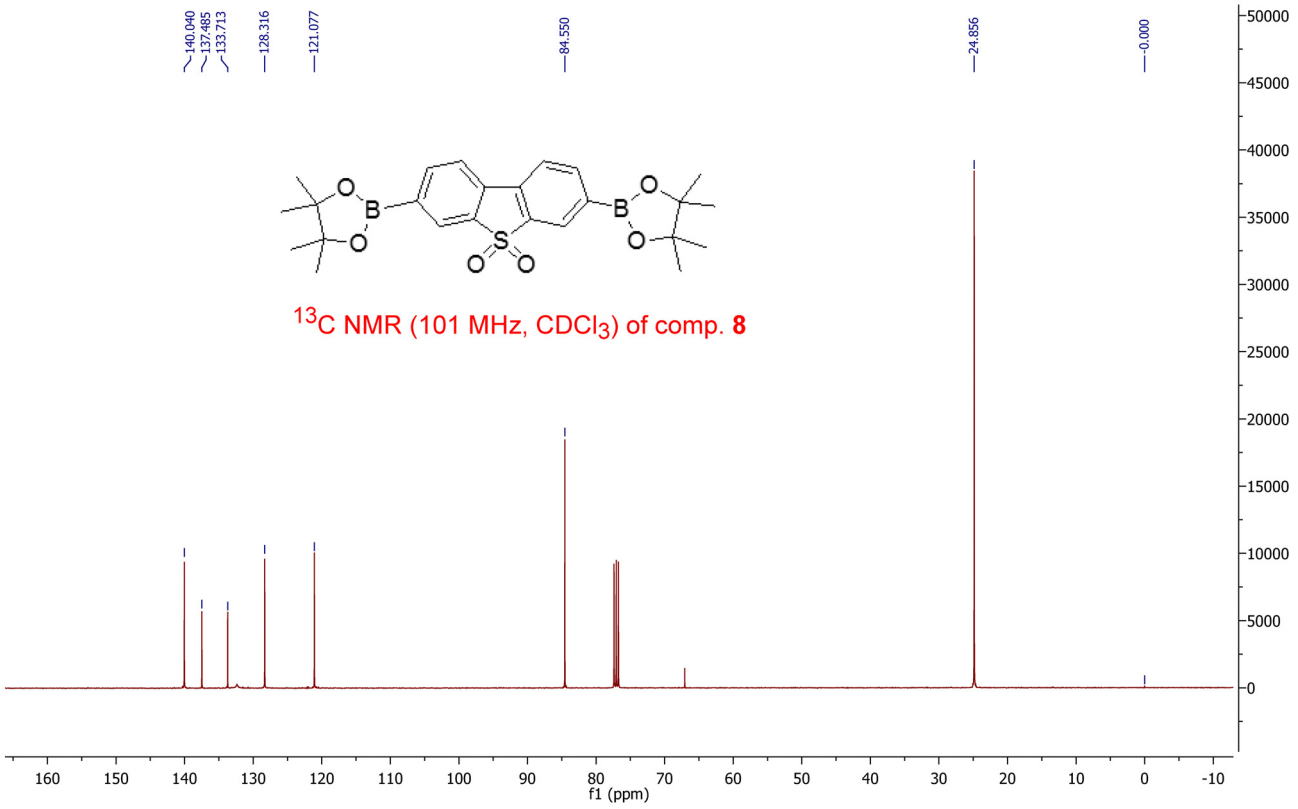

^{13}C NMR (101 MHz, $CDCl_3$) of comp. **8**

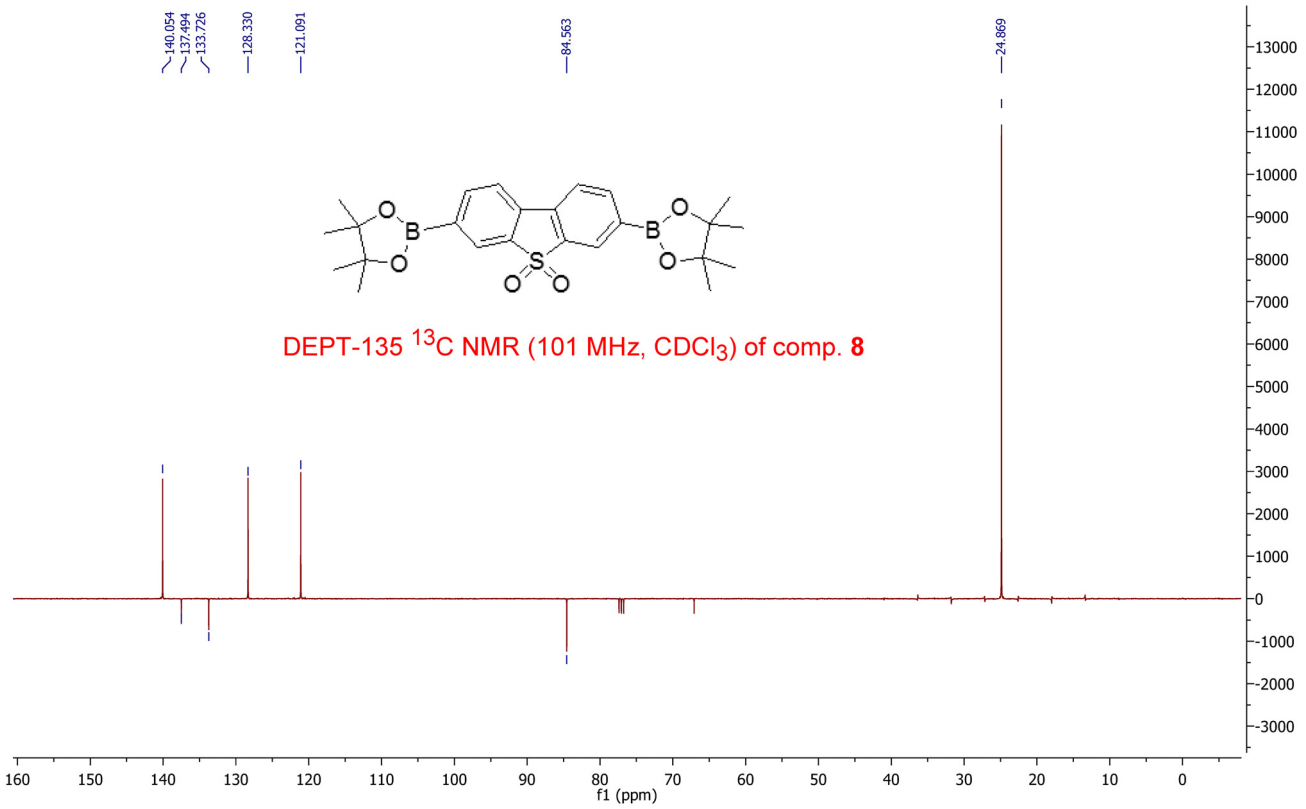

DEPT-135 ^{13}C NMR (101 MHz, $CDCl_3$) of comp. **8**

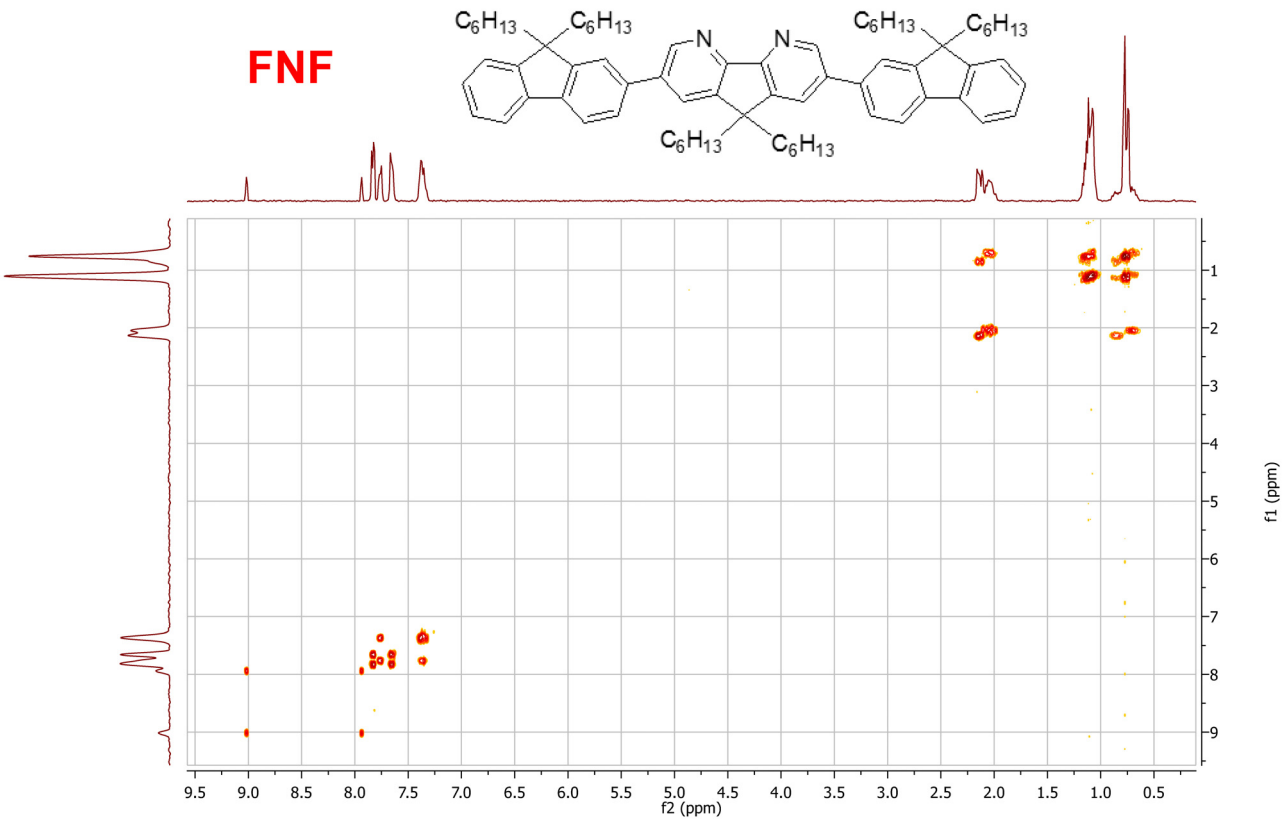

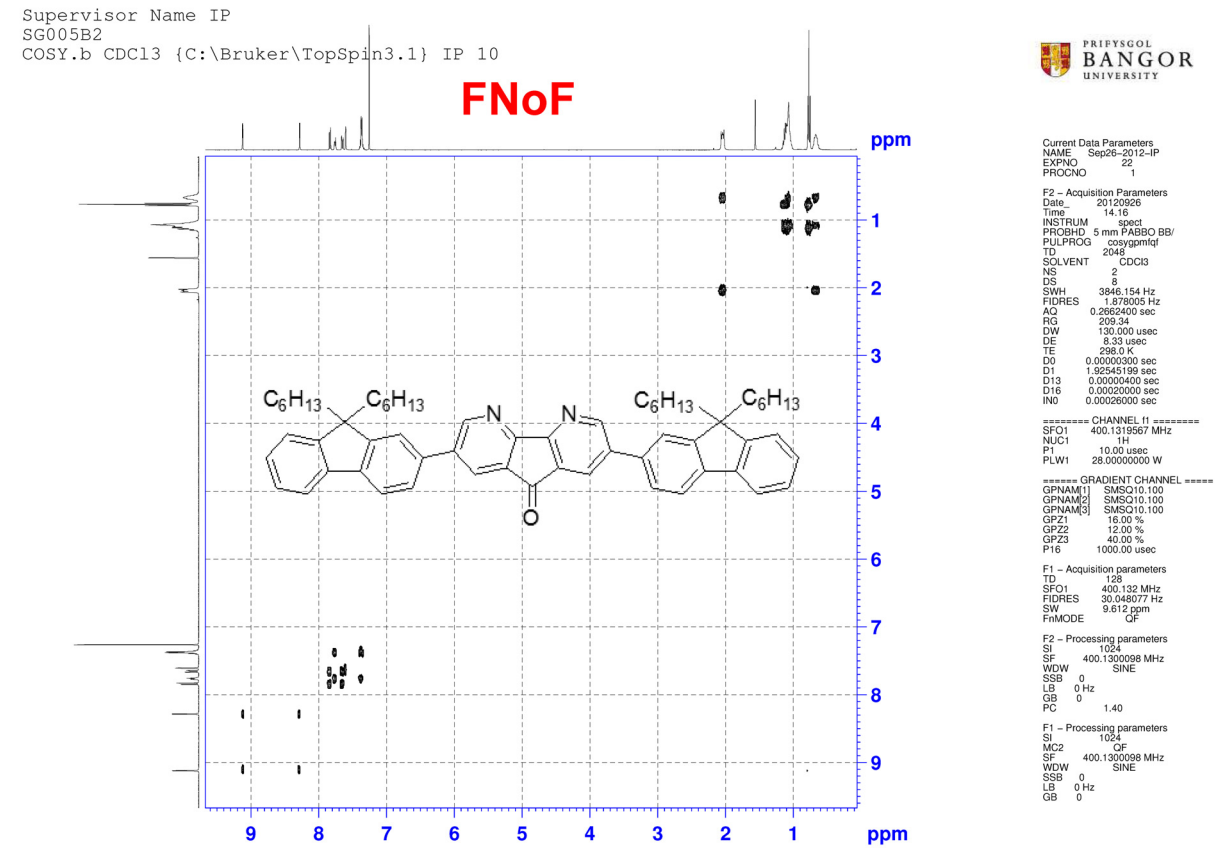
Supervisor Name IP
SG005B2
COSY.b CDCl3 {C:\Bruker\TopSpin3.1} IP 10
FNoF
PRIFYSGOL BANGOR UNIVERSITY
ppm
ppm
Current Data Parameters
NAME Sep26-2012-IP
EXPNO 22
PROCNO 1
F2 – Acquisition Parameters
Date_ 20120926
Time 14.16
INSTRUM spect
PROBHD 5 mm PABBO BB/
PULPROG cosygpmfqf
TD 2048
SOLVENT CDCl3
NS 2
DS 8
SWH 3846.154 Hz
FIDRES 1.878005 Hz
AQ 0.2662400 sec
RG 209.34
DW 130.000 usec
DE 8.33 usec
TE 298.0 K
D0 0.00000300 sec
D1 1.92545199 sec
D13 0.00000400 sec
D16 0.00020000 sec
IN0 0.00026000 sec
======== CHANNEL f1 ========
SFO1 400.1319567 MHz
NUC1 1H
P1 10.00 usec
PLW1 28.00000000 W
====== GRADIENT CHANNEL =====
GPNAM[1] SMSQ10.100
GPNAM[2] SMSQ10.100
GPNAM[3] SMSQ10.100
GPZ1 16.00 %
GPZ2 12.00 %
GPZ3 40.00 %
P16 1000.00 usec
F1 – Acquisition parameters
TD 128
SFO1 400.132 MHz
FIDRES 30.048077 Hz
SW 9.612 ppm
FnMODE QF
F2 – Processing parameters
SI 1024
SF 400.1300098 MHz
WDW SINE
SSB 0
LB 0 Hz
GB 0
PC 1.40
F1 – Processing parameters
SI 1024
MC2 QF
SF 400.1300098 MHz
WDW SINE
SSB 0
LB 0 Hz
GB 0

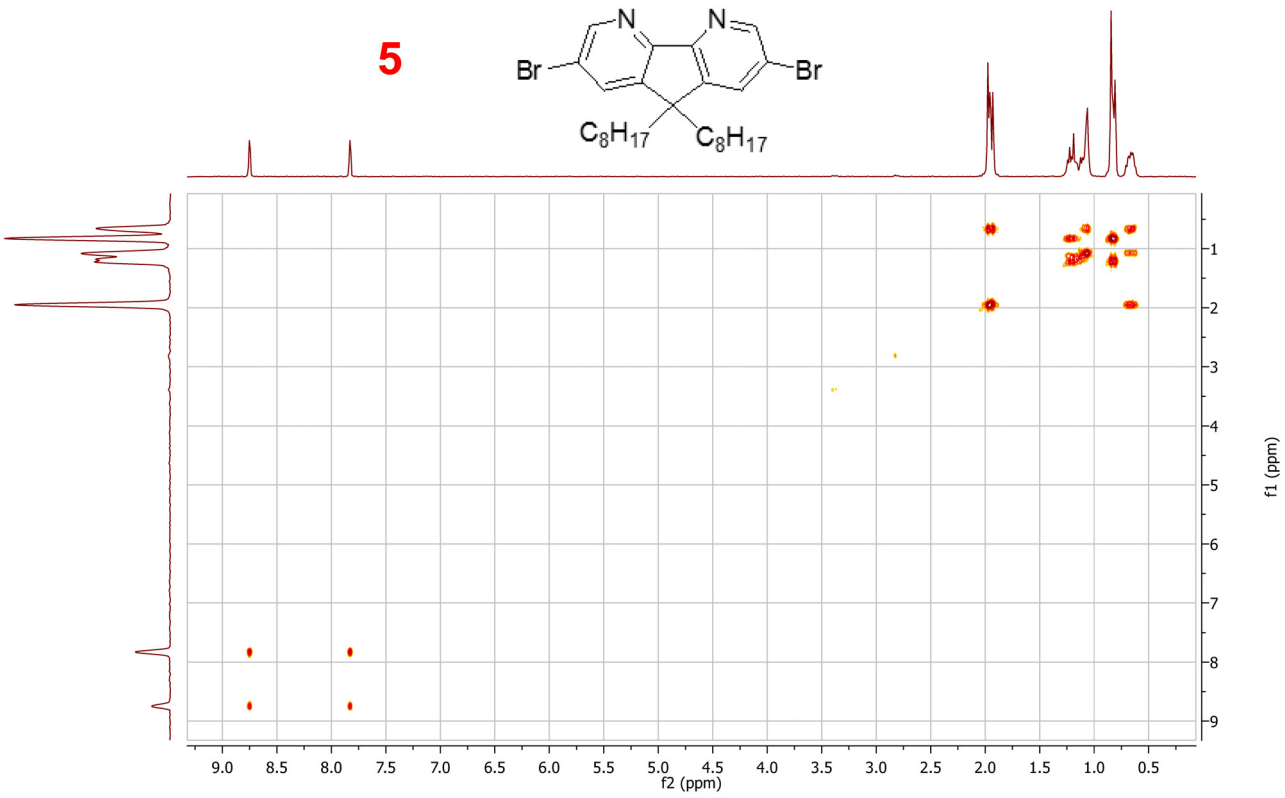
5
Br
Br
f2 (ppm)
f1 (ppm)

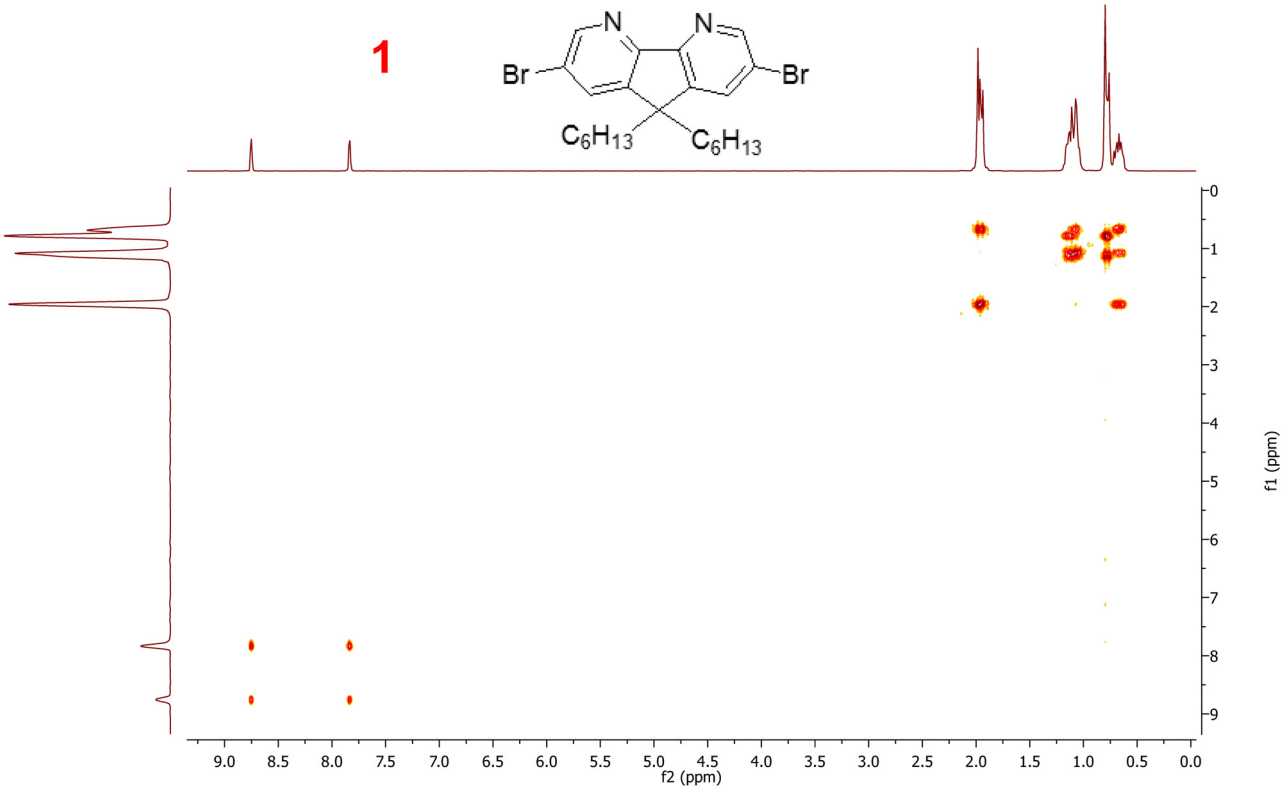
1
N
N
Br
Br
C6H13
C6H13
f2 (ppm)
f1 (ppm)

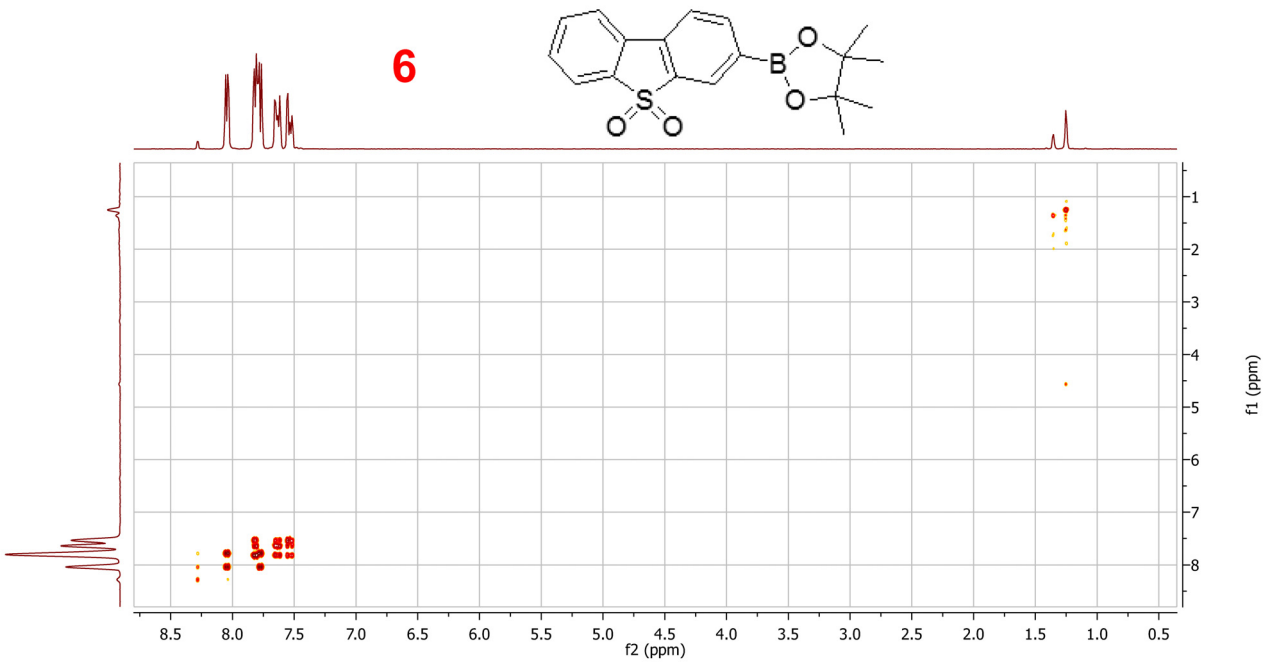
6
B
O
O
S
O
O
f2 (ppm)
f1 (ppm)

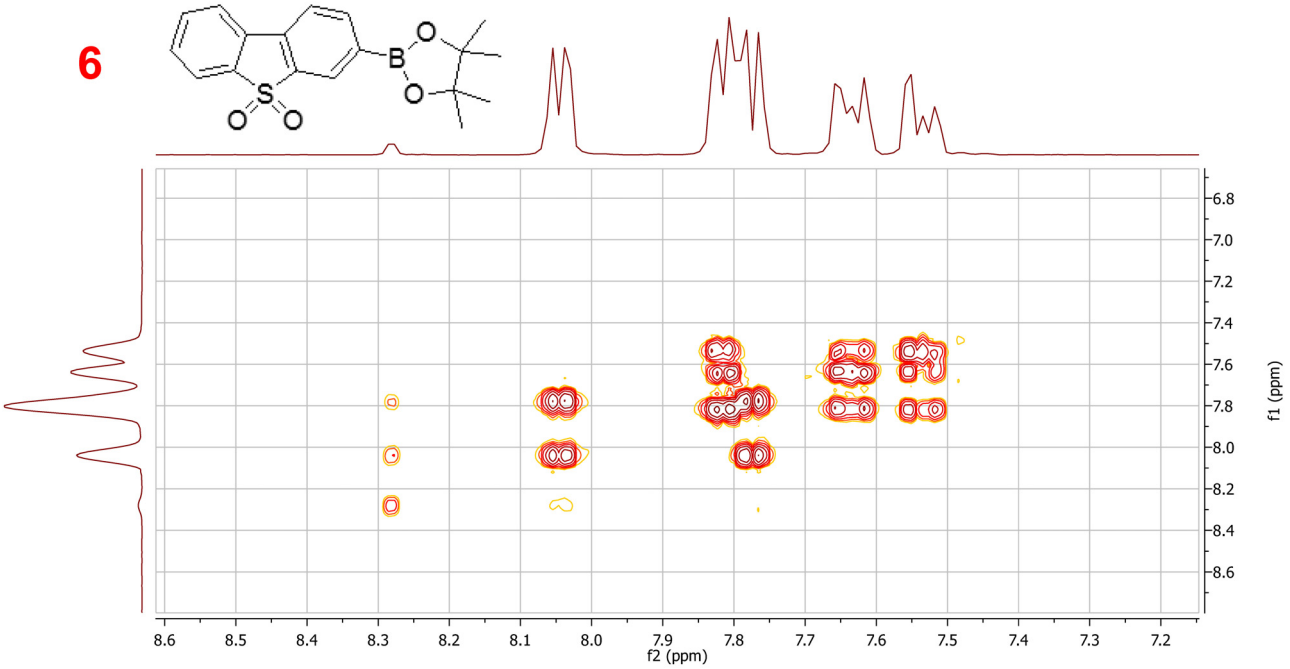
6
f2 (ppm)
f1 (ppm)

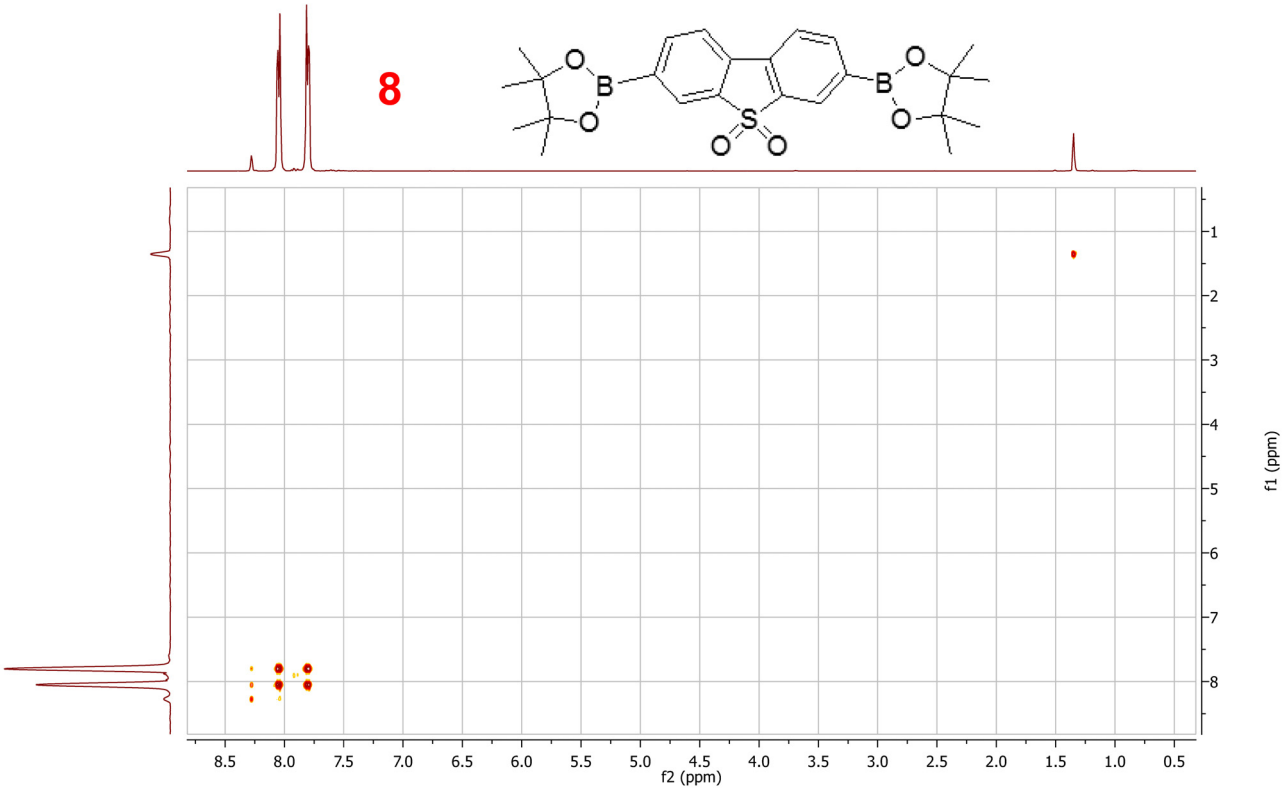
8
f2 (ppm)
f1 (ppm)

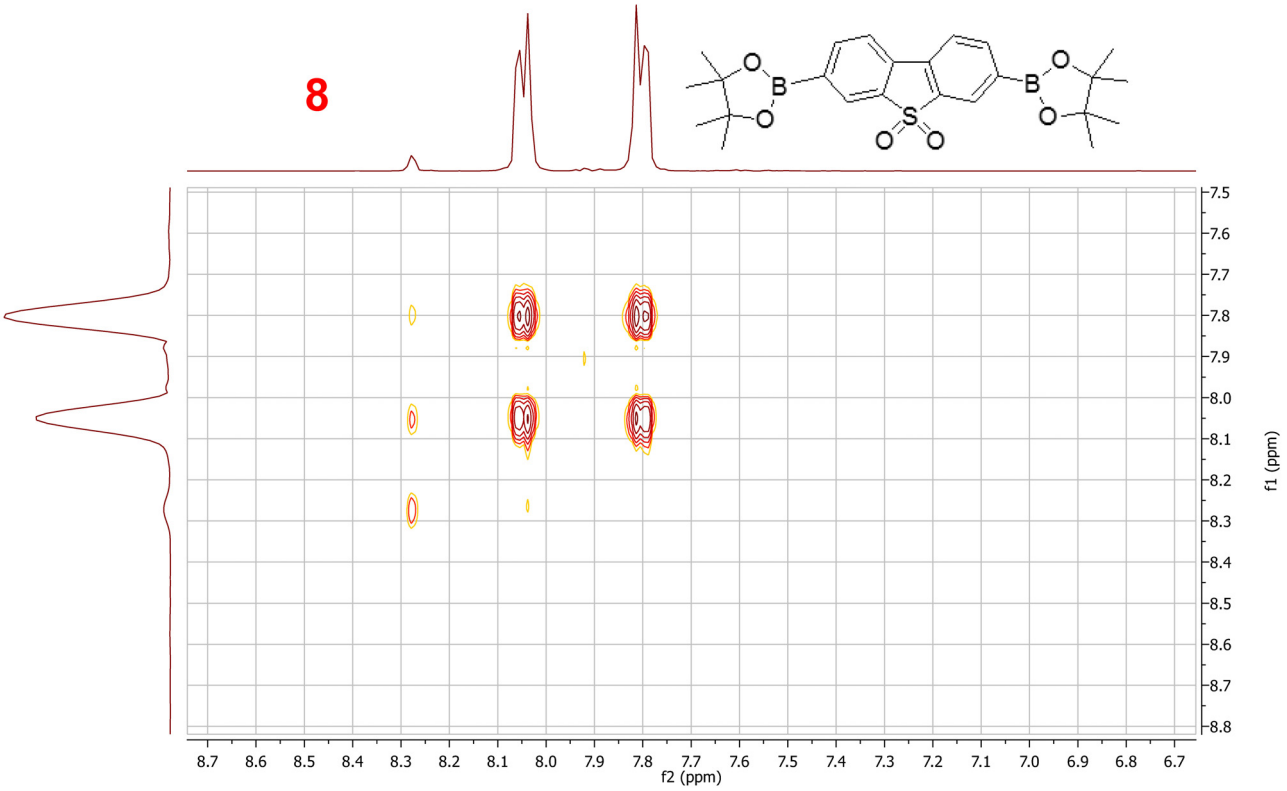
8
B
O
O
S
O
O
B
O
O
7.5
7.6
7.7
7.8
7.9
8.0
8.1
8.2
8.3
8.4
8.5
8.6
8.7
8.8
f1 (ppm)
8.7 8.6 8.5 8.4 8.3 8.2 8.1 8.0 7.9 7.8 7.7 7.6 7.5 7.4 7.3 7.2 7.1 7.0 6.9 6.8 6.7
f2 (ppm)

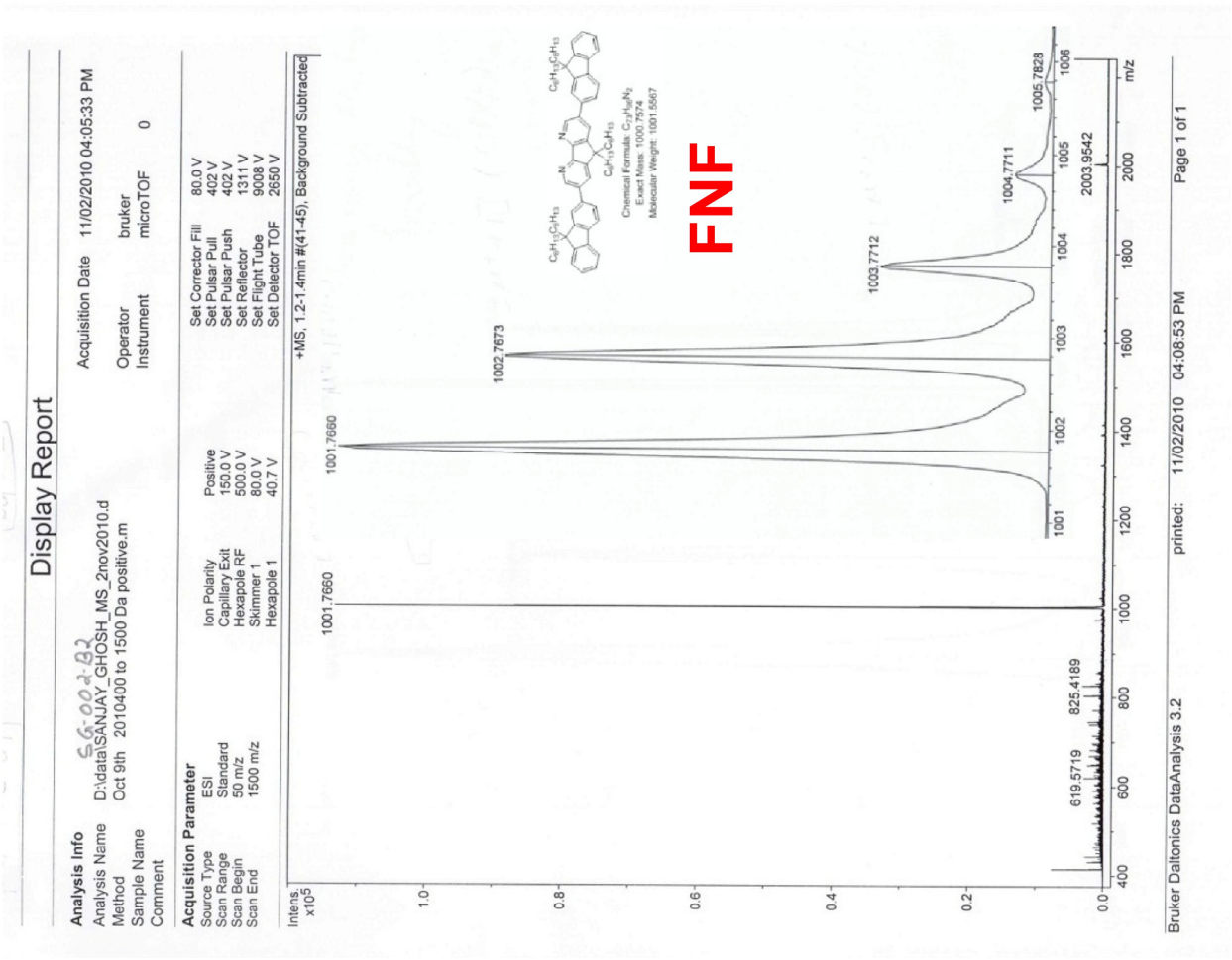
Display Report
Analysis Info
Analysis Name D:\data\SANJAY_GHOSH_MS_2nov2010.d
Method Oct 9th 2010400 to 1500 Da positive.m
Sample Name
Comment
Acquisition Date 11/02/2010 04:05:33 PM
Operator bruker
Instrument microTOF 0
Acquisition Parameter
Source Type ESI
Scan Range Standard
Scan Begin 50 m/z
Scan End 1500 m/z
Ion Polarity Positive
Capillary Exit 150.0 V
Hexapole RF 500.0 V
Skimmer 1 80.0 V
Hexapole 1 40.7 V
Set Corrector Fill 80.0 V
Set Pulsar Pull 402 V
Set Pulsar Push 402 V
Set Reflector 1311 V
Set Flight Tube 9008 V
Set Detector TOF 2650 V
+MS, 1.2-1.4min #(41-45), Background Subtracted
1001.7660
1002.7673
1003.7712
1004.7711
1005.7828
2003.9542
619.5719
825.4189
Chemical Formula: C72H70N2
Exact Mass: 1000.7574
Molecular Weight: 1001.5567
FNF
Bruker Daltonics DataAnalysis 3.2
printed: 11/02/2010 04:08:53 PM
Page 1 of 1

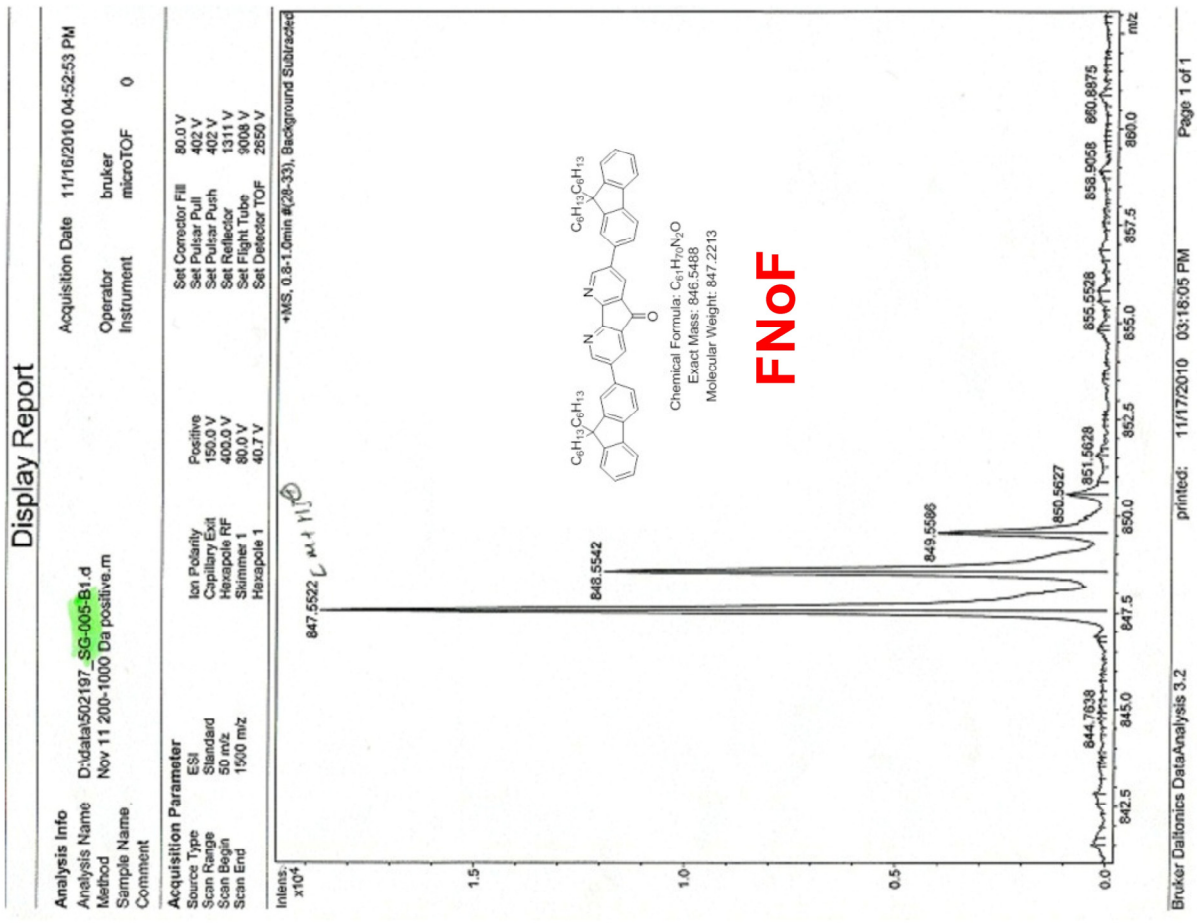
Display Report
Analysis Info
Analysis Name D:\data\502197_SG-005-B1.d
Method Nov 11 200-1000 Da positive.m
Sample Name
Comment
Acquisition Date 11/16/2010 04:52:53 PM
Operator bruker
Instrument microTOF 0
Acquisition Parameter
Source Type ESI
Scan Range Standard
Scan Begin 50 m/z
Scan End 1500 m/z
Ion Polarity Positive
Capillary Exit 150.0 V
Hexapole RF 400.0 V
Skimmer 1 80.0 V
Hexapole 1 40.7 V
Set Corrector Fill 80.0 V
Set Pulsar Pull 402 V
Set Pulsar Push 402 V
Set Reflector 1311 V
Set Flight Tube 9008 V
Set Detector TOF 2650 V
+MS, 0.8-1.0min #(28-33), Background Subtracted
847.5522
848.5542
849.5586
850.5627
851.5628
844.7638
855.5528
858.9058
860.8875
Chemical Formula: C61H70N2O
Exact Mass: 846.5488
Molecular Weight: 847.2213
FNoF
Bruker Daltonics DataAnalysis 3.2
printed: 11/17/2010 03:18:05 PM
Page 1 of 1

Display Report

Analysis Info

Analysis Name	800610_SG-145-l.d	Acquisition Date	16/04/2013 14:54:11
Method	DJW_300 to 2000da Apr 2012.m	Operator	bruker
Sample Name		Instrument	microTOF
Comment	Tetraalanine		

Acquisition Parameter					
Source Type	ESI	Ion Polarity	Positive	Set Corrector Fill	80.0 V
Scan Range	Standard	Capillary Exit	150.0 V	Set Pulsar Pull	402 V
Scan Begin	50 m/z	Hexapole RF	100.0 V	Set Pulsar Push	402 V
Scan End	3000 m/z	Skimmer 1	100.0 V	Set Reflector	1311 V
		Hexapole 1	39.5 V	Set Flight Tube	9008 V
				Set Detector TOF	2900 V

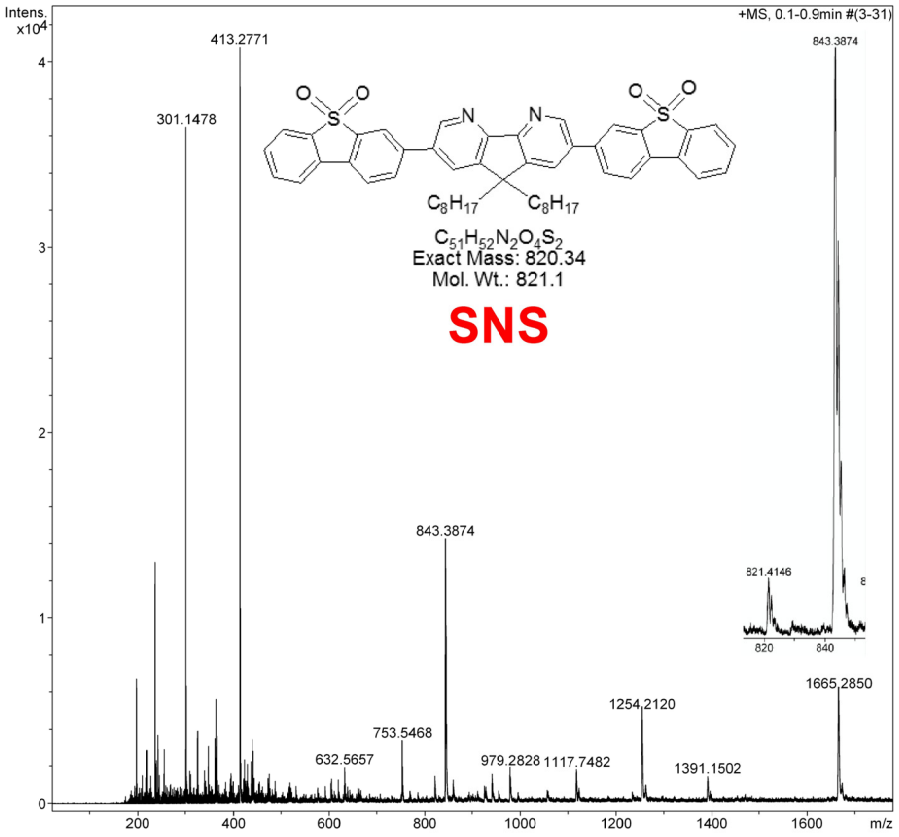

Bruker Daltonics DataAnalysis 3.2 printed: 23/04/2013 14:35:41 Page 1 of 1

Display Report

Analysis Info

Analysis Name	800611_SG-146-C.d	Acquisition Date	16/04/2013 14:58:02
Method	DJW_300 to 2000da Apr 2012.m	Operator	bruker
Sample Name		Instrument	microTOF
Comment	Tetraalanine		

Acquisition Parameter					
Source Type	ESI	Ion Polarity	Positive	Set Corrector Fill	80.0 V
Scan Range	Standard	Capillary Exit	150.0 V	Set Pulsar Pull	402 V
Scan Begin	50 m/z	Hexapole RF	100.0 V	Set Pulsar Push	402 V
Scan End	3000 m/z	Skimmer 1	100.0 V	Set Reflector	1311 V
		Hexapole 1	39.5 V	Set Flight Tube	9008 V
				Set Detector TOF	2900 V

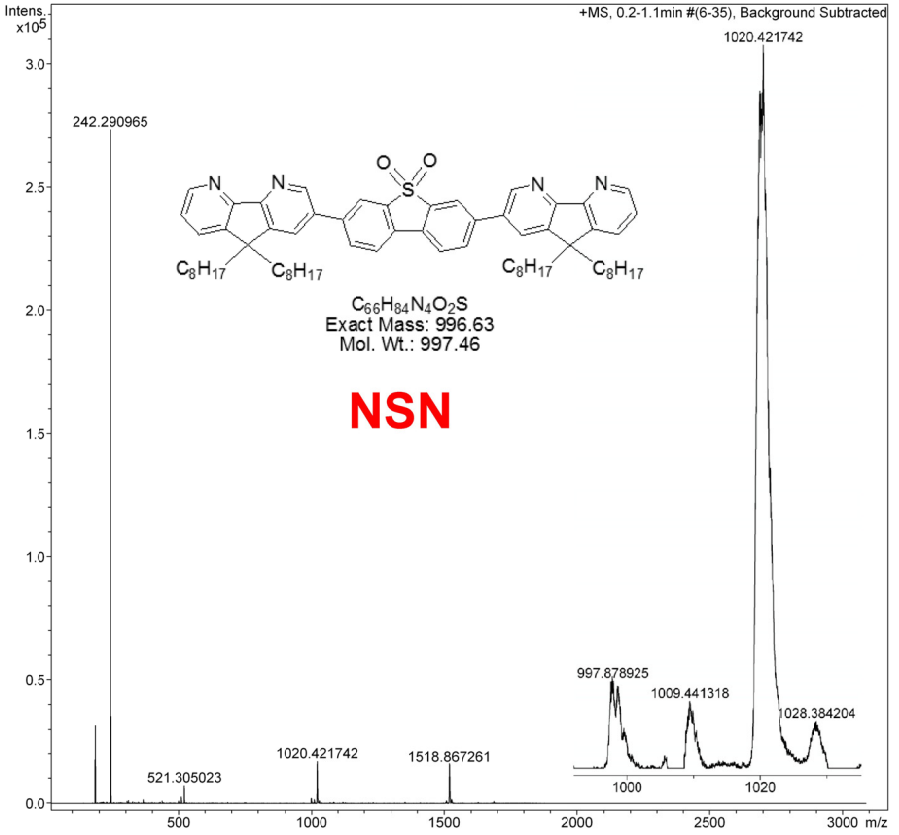

Bruker Daltonics DataAnalysis 3.2 printed: 23/04/2013 14:47:28 Page 1 of 1

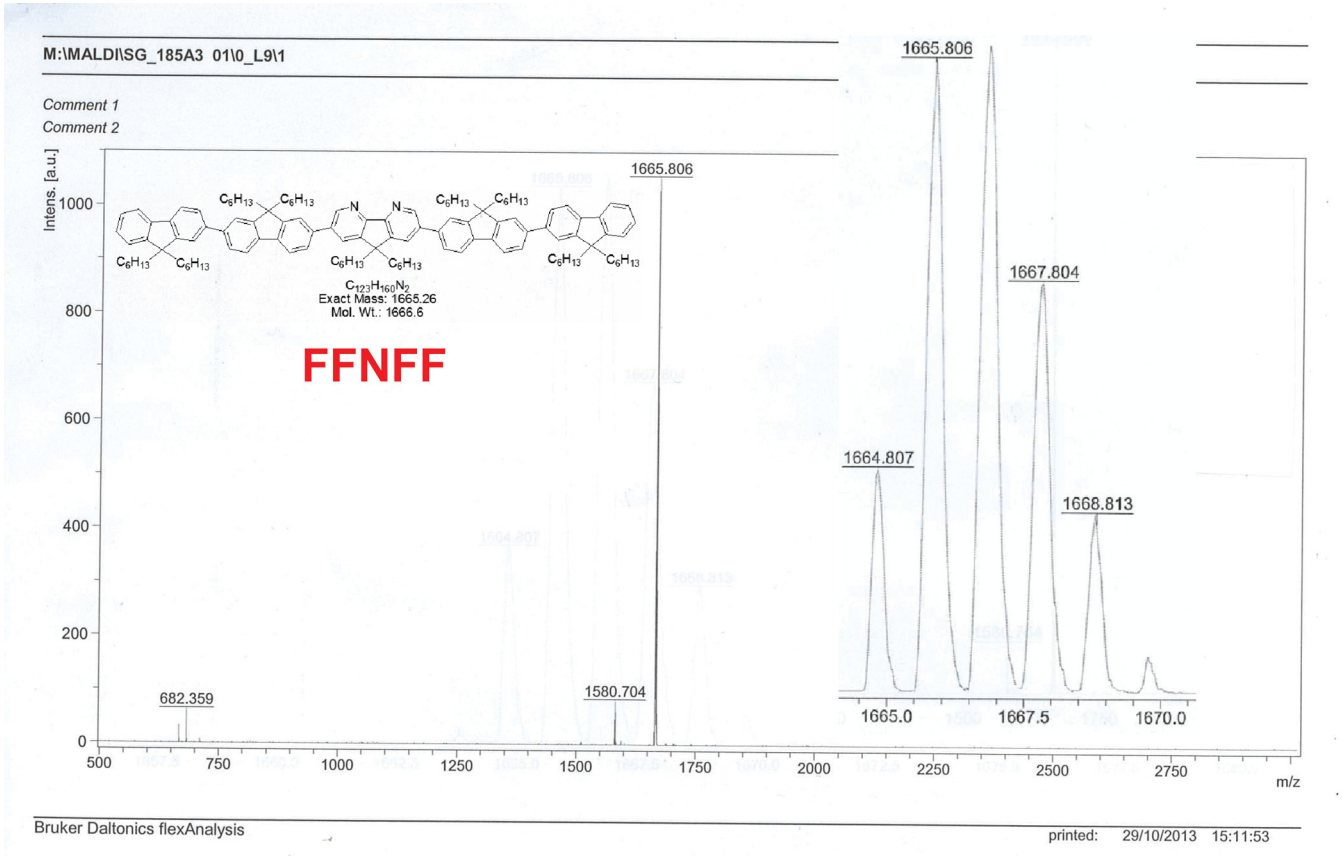
M:\MALDI\SG_185A3 01\0_L9\1
Comment 1
Comment 2
Intens. [a.u.]
1665.806
1667.804
1664.807
1668.813
682.359
1580.704
$C_{123}H_{160}N_2$
Exact Mass: 1665.26
Mol. Wt.: 1666.6
FFNFF
m/z
Bruker Daltonics flexAnalysis
printed: 29/10/2013 15:11:53

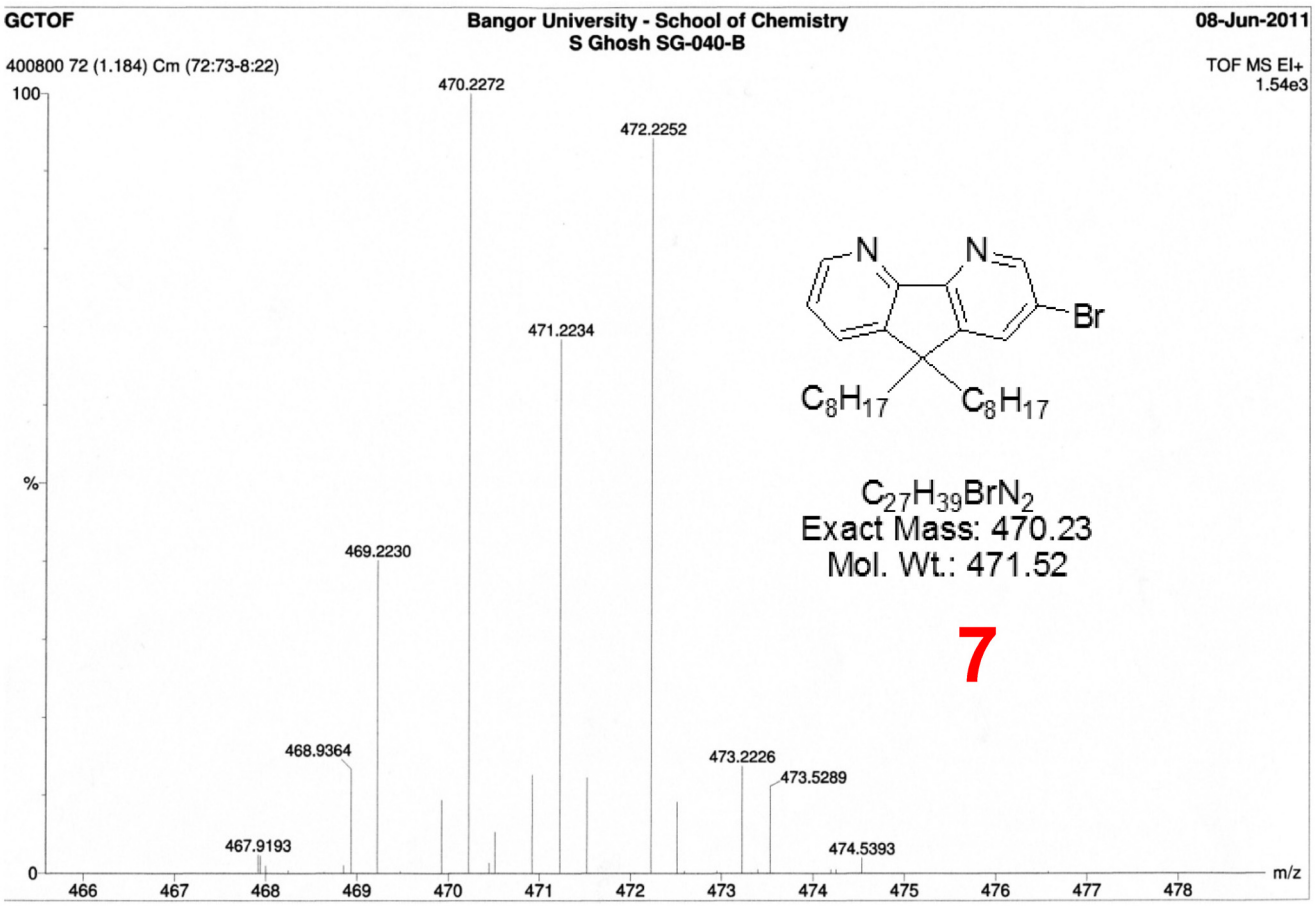
GCTOF
Bangor University - School of Chemistry
S Ghosh SG-040-B
08-Jun-2011
400800 72 (1.184) Cm (72:73-8:22)
TOF MS EI+
1.54e3
470.2272
472.2252
471.2234
469.2230
468.9364
467.9193
473.2226
473.5289
474.5393
%
m/z
$C_{27}H_{39}BrN_2$
Exact Mass: 470.23
Mol. Wt.: 471.52
7

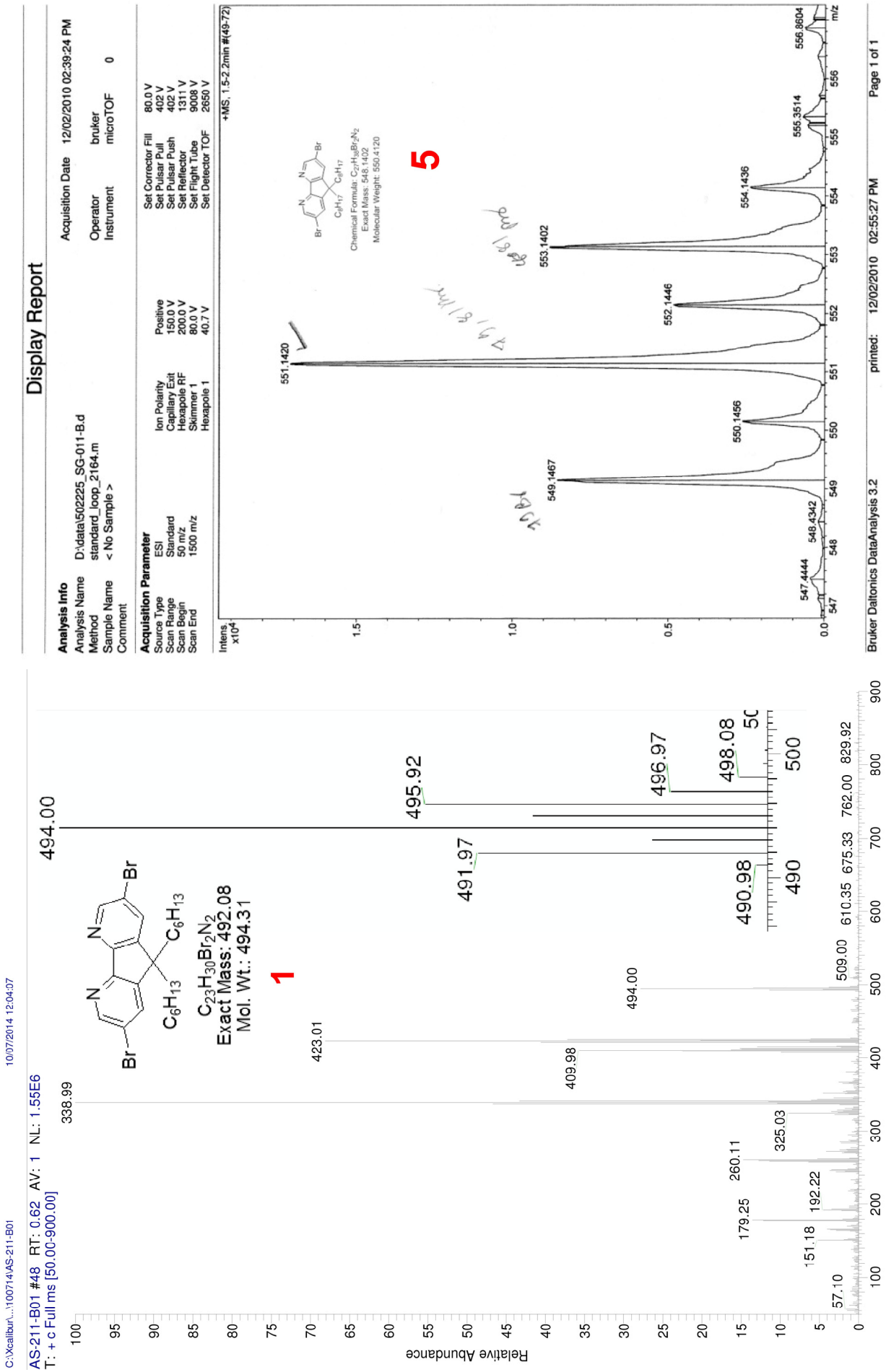
Display Report
Analysis Info
Analysis Name D:\data\502225_SG-011-B.d
Method standard_loop_2164.m
Sample Name < No Sample >
Comment
Acquisition Date 12/02/2010 02:39:24 PM
Operator bruker
Instrument microTOF 0
Acquisition Parameter
Source Type ESI
Scan Range Standard
Scan Begin 50 m/z
Scan End 1500 m/z
Ion Polarity Positive
Capillary Exit 150.0 V
Hexapole RF 200.0 V
Skimmer 1 80.0 V
Hexapole 1 40.7 V
Set Corrector Fill 80.0 V
Set Pulsar Pull 402 V
Set Pulsar Push 402 V
Set Reflector 1311 V
Set Flight Tube 9008 V
Set Detector TOF 2650 V
+MS, 1.5-2.2min #(49-72)
5
Chemical Formula: C27H38Br2N2
Exact Mass: 548.1402
Molecular Weight: 550.4120
551.1420
549.1467
550.1456
552.1446
553.1402
554.1436
555.3514
556.8604
547.4444
548.4342
Intens x10^4
m/z
Bruker Daltonics DataAnalysis 3.2 printed: 12/02/2010 02:55:27 PM Page 1 of 1
C:\Xcalibur\...\100714\AS-211-B01 10/07/2014 12:04:07
AS-211-B01 #48 RT: 0.62 AV: 1 NL: 1.55E6
T: + c Full ms [50.00-900.00]
1
Exact Mass: 492.08
Mol. Wt.: 494.31
494.00
495.92
491.97
496.97
498.08
490.98
338.99
423.01
409.98
494.00
509.00
610.35
675.33
762.00
829.92
260.11
325.03
179.25
192.22
151.18
57.10
Relative Abundance
m/z

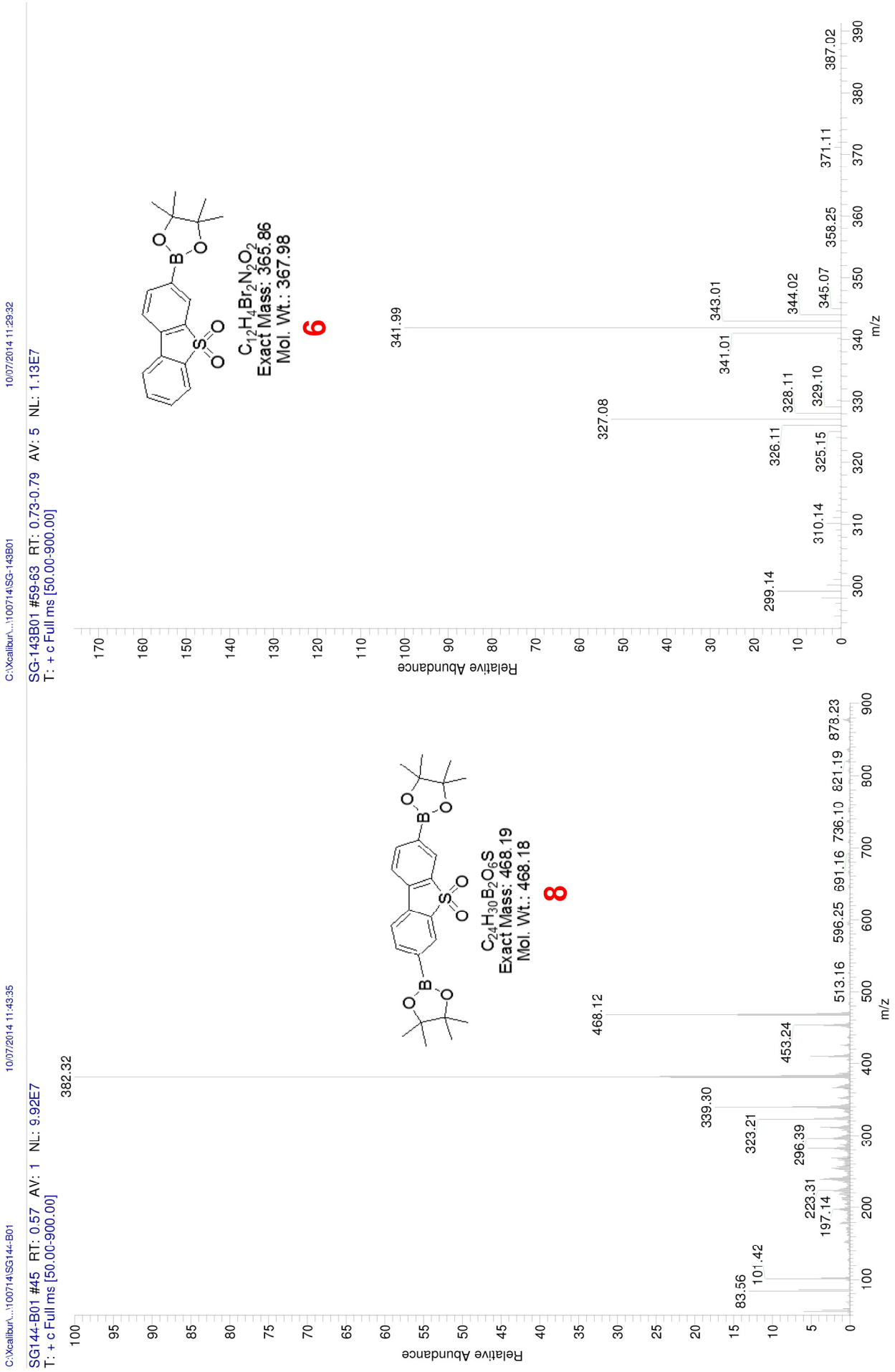
C:\Xcalibur\...\100714\SG144-B01
10/07/2014 11:43:35
SG144-B01 #45 RT: 0.57 AV: 1 NL: 9.92E7
T: + c Full ms [50.00-900.00]
Relative Abundance
m/z
382.32
339.30
323.21
296.39
223.31
197.14
101.42
83.56
453.24
468.12
513.16
596.25
691.16
736.10
821.19
878.23
C24H30B2O6S
Exact Mass: 468.19
Mol. Wt.: 468.18
8
C:\Xcalibur\...\100714\SG-143B01
10/07/2014 11:29:32
SG-143B01 #59-63 RT: 0.73-0.79 AV: 5 NL: 1.13E7
T: + c Full ms [50.00-900.00]
Relative Abundance
m/z
341.99
299.14
310.14
325.15
326.11
327.08
328.11
329.10
341.01
343.01
344.02
345.07
358.25
371.11
387.02
C12H4Br2N2O2
Exact Mass: 365.86
Mol. Wt.: 367.98
6